The University Of Sheffield.

Advanced functional MRI

By:

Shwan Kaka

A thesis submitted in partial fulfilment of the requirements for the degree of Doctor of Philosophy

The University of Sheffield
Faculty of Medicine, Dentistry and Health
(Medical School)

April, 2015

Abstract

Functional Magnetic Resonance Imaging (fMRI) has been widely used to study the responses of the somatosensory cortex, motor cortex and associated neuronal activity in the human cerebral cortex. fMRI is a non-invasive and indirect method for mapping brain activity through measurement of the hemodynamic responses associated with electrical neuronal activity and the neural activity leads directly to changes in blood flow, blood volume and the cerebral metabolic rate of oxygen consumption. Non-invasive neuroimaging technologies such as functional MRI have both advantages, such as good spatial resolution, and disadvantages, such as poor temporal resolution. Some of the disadvantages have been alleviated by incorporating other techniques such as optical spectroscopy or electroencephalography (EEG) which are also non-invasive. All these techniques are sensitive to the vascular response of neuronal activity but in addition we are now investigating the existence of a weak direct electromagnetic effect with advanced fMRI. This neuronal current effect which gives rise to main magnetic field modulation should provide additional information for studying nerve characteristics.

In this thesis, methods for fMRI mapping of responses from phantoms, the median nerve, the visual system, the motor sensory cortex and the thalamus are optimised and subsequently quantified.

The experimental results strongly support the main hypothesis of the thesis and suggest that the generated magnetic field due to ionic current can be detected by present generation MRI using specific experimental designs and stimulation paradigms.

Overall our results show that ionic currents in subjects can generate percentage signal changes in MRI up to 0.1± 0.01% corresponding to mean magnetic axonal fields of 0.7± 0.1nT with a Signal to Noise Ratio (SNR) of 3:1.

The responses of the median nerve, motor sensory cortex and thalamus were detected using transcutaneous electrical nerve stimulation (TENS) and the visual cortex using strobe light stimulation in the range of frequencies 2.1 Hz to 4.1 Hz. All these measurements were acquired at 1.5T. Fast fMRI experiments using TENS and finger tapping were also acquired

simultaneously. In addition, real and imaginary finger tapping experiments were performed in the motor sensory cortex at 3T.

Our results imply that axonal fields that are generated due to action potentials can generate effects on MRI sensitive enough to directly detect neuronal activity using advanced fMRI, although sensitivity is still not fully adequate for clinical use.

Acknowledgement

I would like to express my deepest gratitude towards my supervisor Professor **Martyn Paley** for giving me an opportunity to work in the field of Advanced functional Magnetic Resonance Imaging. He has helped not only support and guide me, but also my developments as a person and as a researcher throughout the duration of my Ph.D.

I would like to thank Prof. Paul Griffiths, my second supervisor, for giving me this opportunity to work with him. I am also extremely indebted to Prof. Jim Wild who provided me the impetus and guidance during study, Dilshad Haleem for giving me Matlab references. I also sincerely thank my department of cardiovascular science staff for the guidance and helpful suggestion during my study.

I gratefully acknowledge the sponsorship of the Human Capacity Development Program of the **Kurdistan Regional Government**. Thank you very much to the volunteers who participated in the experiments we have carried out under ethical permission from the University.

Finally, I am deeply grateful my dad **Kareem Kaka** who is always supporting me and motivating me from the first day when I started my school, my lovely wife **Marya** that she covered my time with our kids **Heaven**, **Nastya**, and **Zhoobin** to provide a suitable and comfortable study environment, and my brother **Saman Kaka** for always supporting and calling me from home.

Conference Presentations and Publications

1 S Kaka, M Paley, "Fast Functional magnetic resonance imaging mapping of motor sensory cortex function using transcutaneous electrical nerve stimulation (TENS) of the median nerve" P49, 19th Annual Meeting BC-ISMRM, York, Sept 2013.

2 S Kaka, M Paley, "Investigating possible fMRI responses in the median nerve during wrist stimulation by Transcutaneous Electrical Nerve Stimulation (TENS)" 3031, Joint Annual Meeting ISMRM-ESMRMB, Milan Italy, 10-16 May 2014.

3 S Kaka, M Paley, "Fast fMRI Measurements during Motor-Sensory Cortex Activation Using TENS Stimulation of the Median Nerve" 11, ISMRM Workshop on Functional MRI: Emerging Techniques & New Interpretations, 22-25 June 2014, Charleston, SC, USA.

4 S Kaka, M Paley, "Motor Cortex Responses to Real and Imaginary Finger Tapping Using Fast fMRI at 3T" 12, ISMRM Workshop on Functional MRI: Emerging Techniques & New Interpretations, 22-25 June 2014, Charleston, SC, USA.

5 S Kaka, M Paley, "Possible fast fMRI responses in the visual cortex at high stimulation frequencies" 13, ISMRM Workshop on Functional MRI: Emerging Techniques & New Interpretations, 22-25 June 2014, Charleston, SC, USA.

6 M Paley, S Kaka et al. "Advanced fMRI and the Brain Computer Interface." Brain-Computer Interfaces. Springer International Publishing, 2015. 185-213.

Contents

List of Figures

Abbreviations and Symbols

A	Ampere
$\Delta S/S_{eq}$	Percentage signal change
μ_o	Permeability of free space
1D	One dimensional
2D	Two dimensional
3D	Three dimensional
AP	Action Potential
B_{cg}	Conductive gel magnetic field
BOLD	Blood Oxygen Level Dependent
C	Speed of light
CAT	Computed Axial Tomography
CBF	Cerebral Blood Flow
CBV	Cerebral Blood Volume
$CMRO_2$	Cerebral Metabolic Rate of Oxygen
CMRglu	Cerebral Metabolic Rate of glucose
CT	Computed Tomography
DND	Direct Neuronal Detection
ΔE	Is the energy difference between the spin states
EEG	Electroencephalography
EPI	Echo Planar Imaging
f	Frequency
FFT	Fast Fourier Transform

FID	Free Induction Decay
fMRI	functional Magnetic Resonance Imaging
FT	Fourier Transform
γ	Gyromagnetic ratio
GE	Gradient Echo
Gf	Frequency encode gradient
Gphi	Phase encode gradient
GRACE	Ghost Reconstructed Alternating Current Estimation
Gs	Slice selection gradient
Hz	Hertz
I	current
K	Potassium
k	Is Boltzmann's constant, 1.3805x10-23 J/Kelvin
MEG	Magnetoencephalography
Ml	Longitudinal magnetisation
mm	millimetre
MRI	Magnetic Resonance Imaging
Mt	Transverse magnetisation
n	nano
Na	Sodium atom
NaCl	Sodium chloride
N-	The number of spins in the upper energy level
N+	The number of spins in the lower energy level
ncMRI	neuronal current MRI
NMR	Nuclear Magnetic Resonance

nT nano Tesla

Ω Ohm

PCA Principal Component Analysis

PET Positron Emission Tomography

r The distance from the magnetic source

RF Radio Frequency

ROI Region of Interest

SE Spin Echo

S_{eq} Fully relaxed equilibrium signal

SNR Signal to Noise Ratio

SPECT Single Photon Emission Computed Tomography

SQUID Superconducting quantum interference devices

T Tesla

T1 Longitudinal relaxation time

T2 Transverse relaxation time

T2* transverse relaxation time with inhomogeneous T2 effect

TE Time to Echo

TENS Transcutaneous Electric Nerve Stimulator

TR Repetition Time

V volt

λ Wavelength

π The ratio of the circumference to the diameter of a circle

ω_o Larmor frequency

Chapter 1: Introduction

1.1 Introduction

Brain activity research is playing an increasingly important role in the field of neuroscience. Neural and brain activity are the most fascinating and complex processes in the human body. Investigation and development of functional medical imaging systems has been a popular research area but there are a number of intense debates about the role of functional imaging. Development of new functional imaging methods such as fMRI (functional Magnetic Resonance Imaging), PET (Positron Emission Tomography), SPECT (Single Photon Emission Computed Tomography), MEG (Magnetoencephalography) and EEG (Electroencephalogram) have allowed study of the changes associated with specific functions in the brain, in-vivo. It is now possible to map neural activity non-invasively by measuring differences with the subject carrying out a specific task and comparing with control periods (without tasks).

These new tools are used by neurophysiologists, cognitive psychologists, cognitive scientists and other researchers interested in brain function (Landini, Positano et al. 2005). Obtaining information on regional haemodynamics has been useful for both physiological research and clinical assessment. In 1920 the first measurements of brain electrical currents were performed by Hans Berger (Millett 2001, Jacks and Miller 2003). There are now many published studies using EEG for brain functional mapping (Cook, O'Hara et al. 1998), studying the visual areas and retinotopic organization (George, Aine et al. 1995), memorizing tasks (Gevins, Smith et al. 1997) and combination with other brain activity measurement tools to gain high spatio-temporal resolution (Dale and Sereno 1993, Tamura, Hoshi et al. 1997, Sharon, Hamalainen et al. 2007). Optical methods are widely used in medicine as well to measure optical properties of tissues. In addition, optical spectroscopy can measure both intracellular and intravascular activities (Villringer and Chance 1997). Hill and Keynes reported a small change in the nerve, which had less opacity because of scattering of the light. This change happened during nerve stimulation (Hill and Keynes 1949).

The next stage was the development of use of radioactive materials in nuclear medicine for functional brain imaging using PET and SPECT. This method has been widely used to

investigate uptake of glucose labelled substances (Blake, Johnson et al. 2003) using in vivo measurements to image molecular interactions during biological activities and protein function (Phelps 2000, Sharma, Luker et al. 2002), brain functional activity during movement and control by feedback from the visual cortex, basal ganglia and the cerebellum (Fukuyama, Ouchi et al. 1997).

There is also now widespread use of magnetic resonance imaging (MRI) for functional mapping of the human brain. MRI is based on a nuclear phenomenon which depends on the magnetic moment of nuclei when placed in an external magnetic field (Rabi, Millman et al. 1938). MRI was invented in 1973 independently by Lauterbur in the USA (Lauterbur 1973) and Mansfield in the UK (McRobbie 2003). About 20 years ago functional MRI (fMRI) was developed and is now the best tool for detection of brain activity and is also clinically applicable. Complex tasks and challenges can be presented to subjects within the magnet and the response of the brain measured. fMRI has become a powerful tool to study both brain function and structure (McClure, York et al. 2004). It has also been used for direct neuronal detection , for example, in the optic nerve using axonal magnetic fields (Xiong, Fox et al. 2003, Konn, Leach et al. 2004, Chow, Cook et al. 2007, Chow, Dagens et al. 2008, Paley, Chow et al. 2009, Xue, Chen et al. 2009) and other research studies. However, each imaging modality has its own advantages and disadvantages. fMRI provides high spatial but inferior temporal resolution relative to other methods (Detre and Floyd 2001).

In 1990 BOLD, (Blood-oxygen-level dependent) contrast was discovered by Seiji Ogawa. It was a novel principle, studied in animal images at high magnetic field strength and involving changes in transverse relaxation times dependent on the oxygenation level of blood. This study found additional advantages of fMRI for measuring neural activation, depending on both blood volume and flow (Ogawa, Lee et al. 1990). The first successful human fMRI studies were published by John W. Belliveau in 1991 using the BOLD method. These tasks involved visual stimulation and measurement of increased blood volume in the primary visual cortex (Belliveau, Kennedy et al. 1991). The activity is detected due to the oxygenation in the blood flowing in the whole brain and the region of interest (Mulert and Lemieux 2010).

In visual stimulation paradigms, the modulation produced depends on the details of the visual pattern presented to the eye. Attempts have previously been made to measure the effects of the action potentials generated by the ganglion cells and travelling through the optic nerve using MRI in so-called direct neuronal detection (DND) experiments (Singh 1994, Kamei, Iramina et al. 1999, Xiong, Fox et al. 2003, Paley, Chow et al. 2009). DND would have a major advantage over use of the BOLD effect as it is a direct electromagnetic effect which can be seen in real-time. In comparison the BOLD effect relies on the haemodynamic response which takes 1 to 2 seconds, and typically rises to a peak at about 5 seconds after the stimulus in humans and so cannot reflect underlying neural activity accurately. Despite all the challenges in the previous studies for direct neuronal detection, the potential accuracy and efficiency for detection of brain neural activities has motivated us to further investigation. In this study, advanced functional MRI (Fast fMRI) neuroimaging will form the topic of this thesis. Before presenting this in more detail, competing and complementary neuroimaging methods will be briefly reviewed.

1.2 Neuroimaging Techniques

Imaging techniques are the processes used to create images of the human body for clinical purposes or for researchers to view activity or problems within the human brain. Imaging is performed without having to perform invasive neurosurgery. Therefore, it allows doctors and researchers to view activity or problems that are not visible to the human eye. Neuroimaging techniques are used in both anatomical and functional imaging of the brain (Brouns, Raf, et al 2009) and are also used to diagnose metabolic diseases. In this section, the most used functional techniques relevant to the scope of this thesis are presented. These techniques can be broadly categorized as follows;

1.3 Electroencephalography (EEG)

Electroencephalography (EEG) is a medical imaging technique that measures brain activity through electrical effects. It is a noninvasive, functional brain imaging method, which is also used for research. Attempts to understand brain activity led to the discovery of EEG, more than a century ago. It became a subject of intense interest through recording and analysing electrical activity using electrodes on the scalp.

Richard Caton is credited with the invention of the EEG in 1875. He observed the EEG from the exposed brains of animals. As with most inventions, there are often parallel paths of development in progress. The German neurologist Hans Berger recorded the first human EEG in 1924(Teplan 2002, Haas 2003). His first recording of the brain's electrical activity from the scalp was in 1929. Berger discovered that the brain can generate weak electric currents, which depend on brain activity and which can be measured without opening the skull. This report was confirmed by Adrian (Niedermeyer and Da Silva 2005). It provided a new tool for both neurologic and psychiatric diagnosis at the same time (Tudor, Tudor et al. 2005). However, it took quite a while before it became an accepted method to measure brain function in both health and disease from its first invention in 1875 (Mulert and Lemieux 2010). The many current applications of electroencephalography are based on Berger's initial work. After Adrian and Mathews confirmative demonstration, this method became of wide interest in 1934. Through analysing the EEG, they found regular oscillations at about 10 to 12 Hz which they called the alpha rhythm and which was generated in the occipital lobes. Then later Berger observed the reaction alpha rhythms with more precise amplifiers. Progress increased rapidly from Berger's work in 1934, when Fischer and Lowenbach and then a year later Gibbs and Davis published the first epileptic form spike demonstrations and reported the classic pattern of absence of seizures respectively (Zifkin and Avanzini 2009). In 1945 the demand for EEG recordings was growing rapidly for both clinical and neurology research. In 1950, Gray Walter developed an adjunct to EEG called EEG topography which makes recordings with large numbers of electrodes, and which allowed mapping brain electrical activity from measurements taken across the surface of the skull. In addition, they showed that brain rhythms change according to the mental task demanded. In the 1980s EEG was more popular, especially for psychiatry. However, the neurologists did not always agree with the findings of EEG. It remains a good tool for researchers (Vinhas, Oliveira et al. 2008). The EEG technique is a neurophysiologic measurement; it can measure complex brain electrical processing activity and detect changes within a millisecond by recordings from the scalp, which means it is non-invasive. It cannot measure current through the brain but can detect the difference voltages. From the EEG, the electrical activities produced by the brain are distinguished by frequency band and amplitude. The brain waves which can be differentiated are in five

major bands with a frequency range of 1-30 Hz and an amplitude range of 20-100μV (Muthuswamy and Thakor 1998, Belo, Coito et al. 2011, Romo Vázquez, Vélez-Pérez et al. 2011) : beta (β) (13 Hz and above), Alpha (α) (7–13 Hz), delta (δ) (0.5 – 4Hz), theta (θ) (4 – 8Hz) and gamma rhythm (γ) (30-100 Hz). Gamma waves have been recorded from depth EEG of epileptic patients (Lachaux, George et al. 2005). These bands are divided dependent on the brain tasks and activity which are dependent on the level of consciousness. By analysing these waves, researchers have been studying brain activity through a direct measurement of neural activity with very high temporal resolution but relatively low spatial resolution due to the distance from the source of the activity.

1.4 Magnetoencephalography (MEG)

MEG is a functional neuroimaging technique used to measure the magnetic fields in the brain via very sensitive magnetometers called SQUIDs (superconducting quantum interference devices). MEG is a direct measure of brain function with very high temporal resolution; it provides a recording of magnetic fields produced by transient currents occurring during brain activity.

In 1968, David Cohen measured the first signals using just a copper coil. These coils were sensitive enough for detecting weak magnetic fields. However, the measurement was noisy even though he used a magnetically shielded room (Cohen 1968). After SQUID detectors were introduced in 1970 (Cohen 1972), fields lower than 0.5×10^{-12} T could be measured in the same range of frequency as in the EEG. Then, the signal was improved compared to EEG by using multiple sensors covering most of the head.

MEG is completely non-invasive, and it records the magnetic field outside the head unaffected by both brain tissue and the skull. The transient currents generated by a set of active neurons produces a magnetic field oriented in an orthogonal direction in accordance with Maxwell's equations. Therefore, MEG is sensitive to the perpendicular current flows within the scalp and does not require the electrodes that are used in the EEG. It produces slightly more accurate spatial localization of neural activity than EEG. Overall though, it produces quite poor resolution images, like EEG, using a complex inverse model of the originating dipoles. Thus, MEG is often used together with sequential MRI to show the

location of the dipoles overlaying the brain's structure. Many studies have used such a combination of MEG with MRI to show precisely which areas of the brain were activated during tasks (Dale and Sereno 1993, Zotev, Matlashov et al. 2008).

1.5 Positron Emission Tomography (PET)

PET is used for nuclear medicine imaging and is a non-invasive functional imaging technique (although it does require radioactivity to be introduced into the body) that produces a three-dimensional image or map of how organs and tissues function within the body. Introduced in the 1970s, it was the first clinical technology to measure physiological functioning in the brains of normal human volunteers which were activated undertaking specific tasks. The positron emission tomography concept was first introduced by David E. Kuhl, Luke Chapman and Roy Edwards in the late 1950s, and the first PET scanner was built in 1961 by James Robertson and his associates using single images (Zhang 2015). The first appearance of papers reporting PET in functional imaging studies using active and control experiments was in 1984 (Mintun, Raichle et al. 1984).

This system works by detecting gamma rays that are emitted by a positron-emitting radionuclide (tracer) after injection of a small amount into a peripheral vein. Many types of tracers are used such as; oxygen-15, fluorine-18, carbon-11, or nitrogen-13. This tracer explores changes during activation indirectly through blood flow and metabolism. Therefore, it detects the relative changes in response over time due to specific tasks. The PET technique is the most expensive and has lower spatial resolution (2-3mm at best) than fMRI but has higher spatial resolution than SPECT. In addition, it has poor temporal resolution due to the distance travelled before the positron eventually meets an electron through the tissue.

1.6 Single Photon Emission Computed Tomography (SPECT)

SPECT is another type of nuclear imaging method that is used for anatomy and function providing a means of examining regional cerebral blood flow and metabolism in a Region Of Interest (ROI) during both control and active conditions. Like PET, it uses radioactive material to assess the physiologic properties of organ systems in vivo. The most widely

material used is technetium-99m– labeled hexamethylpropyleneamine oxime (^{99m}Tc-HMPAO).

Sensitive detectors, which are the main part of the system are responsible for collecting photons that are emitted by the subject. Estimation of the photon energy and the interaction position are primary variables that dictate the performance of a SPECT image reconstruction. The complex reconstruction process influences the spatial resolution, which is lower than both PET and MRI. In addition, it has lower temporal resolution (figure1.6). SPECT has the lowest spatial resolution of the imaging technologies that are used for functional mapping of the human brain, but is used commonly due to the relatively low cost of scanning.

1.7 Magnetic Resonance Imaging (MRI)

MRI or magnetic resonance imaging is a noninvasive technology used for medical diagnosis. It is currently the most important device used for high quality, three dimensional imaging. In 1946, nuclear magnetic measurements were made accurately by Edward Mills Purcell and Felix Bloch independently, who simultaneously published works on nuclear magnetic resonance in materials and the principles of NMR (Geva 2006). After 10 years from this discovery, Odeblad and Lindstrom attempted to use NMR in medicine by analyzing spectral line widths (Odeblad and Lindstrom 1955, Andrä and Nowak 2007). The first suggestion of an MR body scanner was in 1969 by Raymond Vahan Damadian. His study discovered that NMR can show differences between tumors and normal tissues through their magnetic relaxation times. However, it was not until 1977 that he scanned a whole human body for cancer diagnosis. By using the NMR idea, Dr Paul Lauterbur and Sir Peter Mansfield invented MR body imaging in 1973 (Lauterbur 1973). In 1975 Richard Ernst first demonstrated the use of frequency encoding, and the Fourier Transform, which has since been used in all MRI scanners (Ernst 1992, Pekar 2006). The first human head image was in 1978 by Hugh Clow and Ian R. Young (Geva 2006). Misconceptions on the term nuclear in NMR led researchers to change the name from NMR to MRI. That helped avoid the belief that MRI was harmful like nuclear radiation (Goldberg 2007). There was a dramatic increase of clinical applications and research using this technique from 1980. In addition, it has become the most popular diagnostic method as MRI is very safe and does

not require exposure to radiation as in other tools such as X-ray and CT (Detre and Floyd 2001).

The next section discusses some basic principles involved in creating an MRI signal. These are Magnetism, Resonance, Radio Frequency Excitation and Reception and Relaxation. Therefore, it can be said that the underlying physical property is the nuclear magnetic resonance phenomenon. The signal created from hydrogen nuclei is the key to MRI, because hydrogen nuclei have a magnetic moment due to the spin motion around their own axes which cancels in the absence of a magnetic field. Thus the net magnetic moment of the object is zero in zero field (Figure 1.1a). In a classical picture, spins can be thought to behave as tiny bar magnets which will interact when placed in an external magnetic field (Haacke, Brown et al. 1999). The protons will be aligned either parallel or anti parallel with the strong magnetic field B_o (Figure 1.1b).

Depending on Boltzmann statistic the number of spins in the lower energy level (N^+), slightly outnumbers the number in the upper level (N^-) at room temperature. Equation (1.1) describe the population of energy levels.

$$N^-/N^+ = e^{-\Delta E/kT} \qquad 1.1$$

where; ΔE is the energy difference between the spin states, k is Boltzmann's constant, 1.3805x10-23 J/Kelvin, and T is the temperature in Kelvin (Weast 1972).

In the external magnetic field the protons start precesing at the Larmor frequency, which is proportional to the applied magnetic field strength and given by:

$$\omega_o = \gamma B_o \qquad 1.2$$

where; ω_o is Precessional or Larmor frequency (MHz), and γ is a constant called the gyromagnetic ratio, which is 42.58 (MHz/T) for hydrogen.

B_o is Magnetic field strength in Tesla (T).

For this study the experiments were mainly conducted using a 1.5T scanner, therefore the precessional frequency was 63.8MHz. In addition, there were investigations at 3T with a precessional frequency of 127.6 MHz.

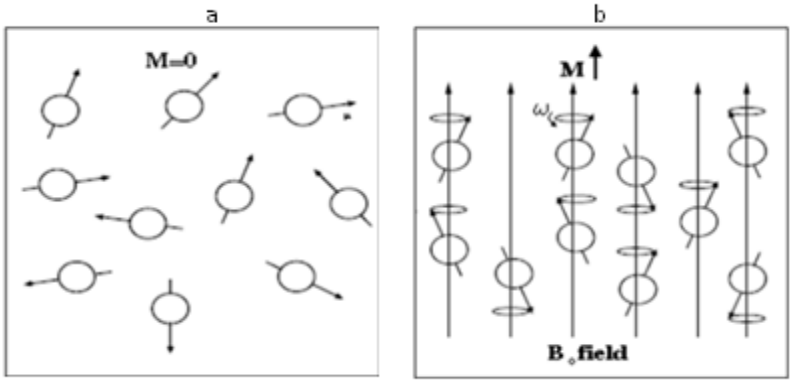

Figure 1. 1: A) Hydrogen nuclei in the absence of external magnetic field. B) Alignment of spin precessing in the external magnetic field

When a radiofrequency (RF) pulse at the Larmor frequency, to match the precession frequency of the protons, is applied with suitable energy, this RF energy will be absorbed by protons that have a lower energy state which will transform them to a higher energy state. This process is called Resonance. The transmitted RF at frequency f1 produces an additional magnetic field B_1 which is much weaker than the magnetic field B_o. This additional field causes the tipping of the net magnetization of the protons away from the z-axis and starts them precessing in the x-y plane (Mxy); this process is called excitation figure 1.2a.

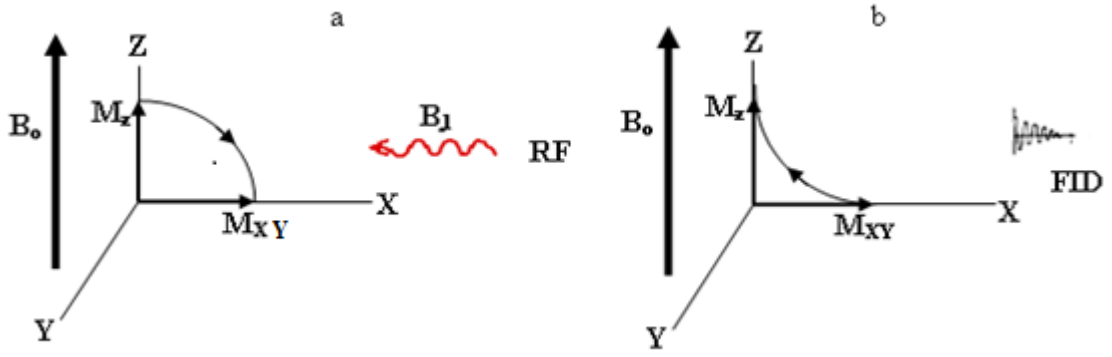

Figure 1. 2: A) the excitation process. B) the relaxation process

After termination of the radio frequency, the magnetization starts to return from the flipped state to its original position along the z-axis (Mz). During this process the protons emit radio-frequency waves that are detected via an RF coil figure 1.2b. There are two relaxation times, T1 and T2, which refer to the z-direction (spin–lattice relaxation or longitudinal relaxation) and x-y direction (spin-spin relaxation or transverse relaxation) respectively Figure 1.3. The T2 relaxation phase is when the MRI signal is produced when the magnetisation is perpendicular to the main magnetic field. More description of MRI acquisition parameters and various pulse sequences is covered in detail in Appendix A.

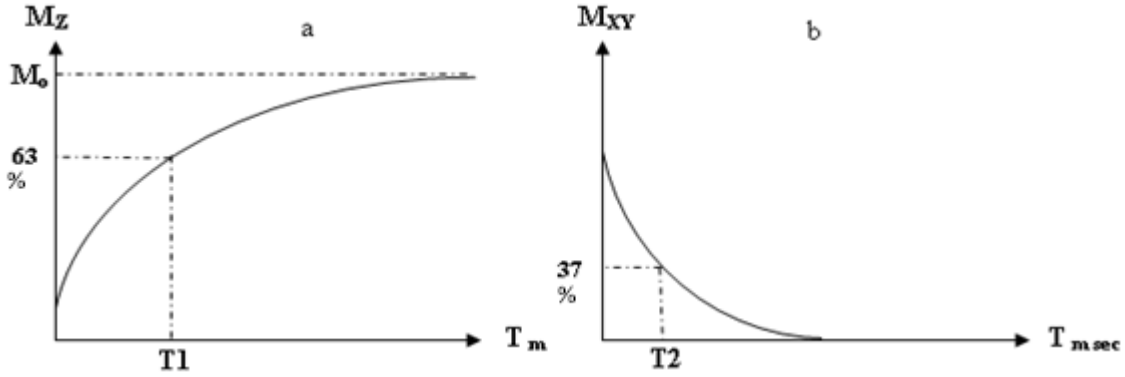

Figure 1. 3 Relaxation curve. A) Spin–lattice relaxation or longitudinal relaxation T1. B) spin-spin relaxation or transverse relaxation T2.

1.8 Functional Magnetic Resonance imaging (fMRI)

1n 1990, Ogawa added another advantage to the MRI technique. This made the method dependent on the oxygen level in the blood (BOLD), which can then map the brain's activities. However, the first successful and published study was in 1991 by John W. Belliveau and colleagues. Most studies these days use this technique for brain activity mapping (Ogawa, Lee et al. 1990). However, this method does not directly measure brain activity but is dependent on the neurovascular and hemodynamic responses connecting and encoding the brain functional information. This technique nowadays is most widely used by physicians, neurologists and physiologists, for diagnosis and research respectively. It can be used to study brain function in vivo to provide both biological and anatomical information. In addition, cognition and sensory stimulation can be assessed from brain functional imaging.

The change in oxyhemoglobin level in the blood from neural activity leads to the change of magnetic field inhomogeneity which is used in the BOLD technique. BOLD primarily measures the difference between the oxyhaemoglobin and deoxyhaemoglobin magnetic

properties. Deoxyhaemoglobin is paramagnetic and oxyhaemoglobin is diamagnetic (Rajagopalan, Krishnan et al. 1995). Changing deoxyhaemogobin levels lead to a difference between MR signals from the vessel and its surrounding tissue. The MR proton signal will be dephased by this difference in blood composition and the value of T2* will decrease. In other words, there is a lower T2* weighted signal when there is more deoxyhaemoglobin (Moridani 2009). This causes the signal to drop by approximately 0.5 – 3 % at 1.5T due to dephasing of the proton spins. When a neuron population is activated, the change in concentration of the deoxyhemoglobin in the blood vessels will be detected as a signal change. However, increased blood flow results in an overall increase in oxyhaemoglobin concentration and thus an increase in BOLD signal during activation. This mechanism can be mapped as a change in the intensity of the acquired MR images, which can be seen appropriately (Chow, Dagens et al. 2008).

Another technique can also be used for fMRI, which is less popular than BOLD, called Arterial Spin Labelling (ASL). This method has lower temporal resolution than BOLD and weaker responses as well (Buxton 2002). It depends on cerebral blood volume (CBV) and cerebral blood flow (CBF) where it is designed to trace blood flow effects related to brain activity. Dynamic contrast agent studies using exogenous contrast agents such as Gd-DTPA are also very effective in diagnosing disease states involving altered perfusion(Vre and Lemort 1995).

The most popular common method of fMRI is blood oxygenation level-dependent (BOLD) imaging. However, the temporal relationship between the measured fMRI signal and underlying neuronal activity remains unclear. Fast fMRI has been developed recently to study neuronal activity. However, conflicting results have been reported by different research groups creating intense debate on their significance. Following is a brief review of the principles of these two techniques.

1.9 The BOLD technique

Blood Oxygenation Level Dependent (BOLD) fMRI is based on physiological responses related to brain activation. After particular tasks the neurons start to communicate with each other in certain parts of the brain, and these areas then consume

extra energy and oxygen, hence creating higher rates of blood flow. This process leads to an increase in the concentration of oxygen in the blood (oxyhaemoglobin) in the active region, and a decrease in the deoxyhaemoglobin, which is different from the resting state. Hence, this method is sensitive to oxygen level changes in red blood cells.

This haemodynamic response happens during a series of changes related to the tasks during the scan. These tasks induce neural activity and increase synaptic activity in the localized area, activities associated with CBF, CBV, CMRO2 and CMRglu; these are cerebral blood flow, cerebral blood volume, cerebral metabolic rate of oxygen and cerebral metabolic rate of glucose respectively. These changes in the biophysical parameters induce changes in the MRI signal(Faro, Mohamed et al. 2011). Figure 1.4 shows the schematic of fMRI signal changes during BOLD effect.

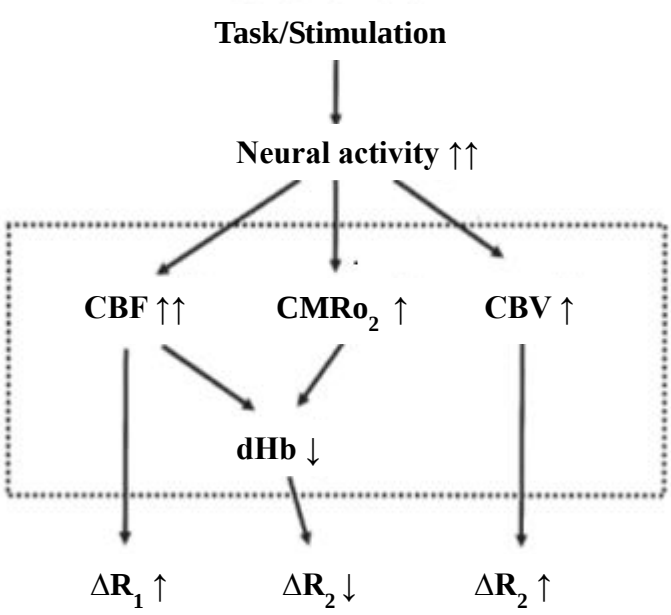

Figure 1. 4 The schematic of fMRI signal changes during BOLD effect(Faro, Mohamed et al. 2011).

High levels of local deoxyhemoglobin concentration in the brain lead to a rise in the field's inhomogeneity, hence reducing the fMRI signal. These events are related to the short duration of neuronal activity, but the MR signal changes over time much more slowly

reflecting the underlying blood oxygenation changes which is called the Haemodynamic Response Function (HRF). Figure 1.5 shows the standard shape of the evolution of the Haemodynamic Response Function and the associated change in MR signal at 1.5T.

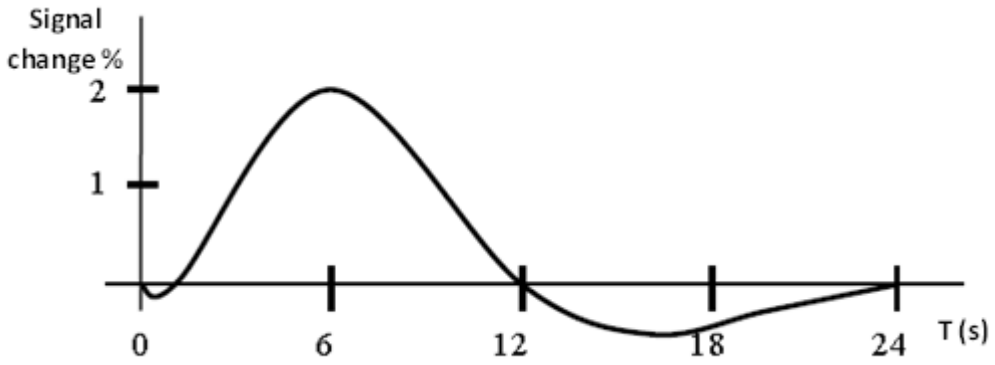

Figure 1. 5: The standard shape of Haemodynamic Response Function (HRF)

Three points can be seen from the figure; first, there is an "Initial dip" which shows the decrease of oxygen in the first 1 to 2 seconds, leading to the decrease in the BOLD signal. Second, is "the positive BOLD effect", which starts approximately after 2 seconds and which reaches its peak at 5 to 8 seconds. This increase is related to the increase in oxygen which is supplied by the extra blood due to neural activation. Finally, after termination of stimulation the signal starts to decay and returns to normal levels due to deoxyhemoglobin being higher than the oxyhemoglobin, and the changes in blood flow and blood volume. BOLD fMRI indirectly detects or measures neuronal activity via this assumed haemodynamic correlate (Logothetis and Pfeuffer 2004). The most commonly used imaging sequence used in BOLD fMRI is a gradient-echo EPI pulse sequence.

BOLD-fMRI thus has low temporal resolution due to the hemodynamic response, hence the underlying neuronal activity is not fully understood. Therefore, in this study attempts are made to detect the magnetic field of neuronal activity through the neuron's action potentials by using fast fMRI.

1.10 Direct Neuronal Detection

Direct neuronal detection potentially offers many advantages over the BOLD technique which indirectly measures brain activity from neuronal activation. It directly measures the neuron's electromagnetic fields due to ionic currents generated during action potentials or neuronal firing. This has, in principle, much higher temporal resolution and can also have better spatial resolution as it does not rely on an underlying network of vessels like BOLD.

For this investigation, electromagnetic detection through magnetic resonance was used to try and detect axonal magnetic fields. This study was an effort to discover whether current generation MRI scanners have the ability to detect these very tiny modulation signals. This method has been given many different names by researchers, including ncMRI, fast fMRI, NMF, msMRI and DND, which mean detecting neuronal currents by MRI, using short TR with fMRI, Direct MRI detection of the neuronal magnetic field, magnetic source imaging using MRI, and direct neuronal detection using MRI respectively. This study uses the terms advanced fMRI, fast fMRI or DND.

Theoretically, detecting neuronal magnetic fields by using MRI is straightforward. Very weak magnetic fields will be generated around the axon and dendrites due to transient currents produced from neuronal activity. It has been reported that the evoked cortical magnetic fields of a sensory stimulation by using MEG at the scalp (2-4 cm) is about 10^{-13} T (Cohen 1968, Andrä and Nowak 2007). Therefore this will be higher at the source itself ($\sim 10^{-9}$T) and it could be possible to detect this by MRI. These tiny fields lead to changes in the precession rate and loss of phase coherence of the protons spin which then produces relative differences in MR image intensity and regional T2*. Although these changes seem to be very small, it is thought that the transient currents may indeed cause measurable changes in MRI signal intensity which can be detected with higher spatial and temporal resolution than BOLD. Figure 1.6 shows the comparison of spatial and temporal resolution of different functional imaging methods. To find more about these tiny fields, it is useful to start by discussing the basic neuron's working mechanism and structure.

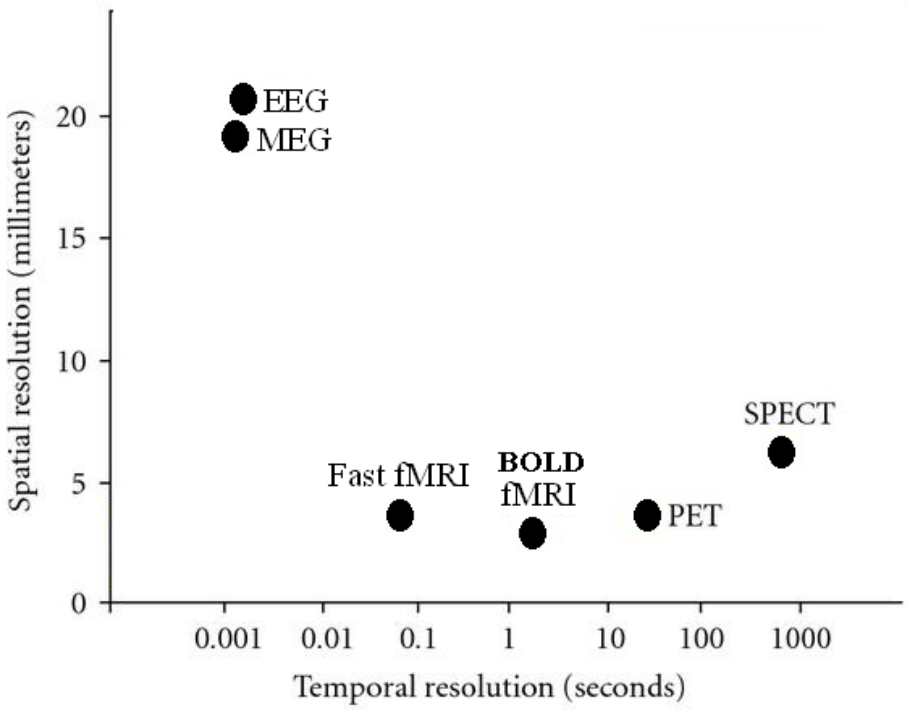

Figure 1. 6 Comparison of spatial and temporal resolution of different functional imaging methods

1.11 The Neuron

Neurons, or nerve cells, are the basic building units of the brain and nervous system that process and transmit information using electrochemical signals known variously as action potentials, nerve impulses or spikes. Neurons are specialized to transmit or receive information to/from all parts of the body and extend throughout the central nervous system (brain, spinal cord). They are responsible for controlling all movements and sensors in the body. There are three basic different types of neurons, each responsible for different tasks: Sensory neurons carry signals to the central nervous system during sensory stimulation; Motor neurons send signals from the central nervous system to the muscles of the body; and Interneurons conduct signals between other nerve cells in the central nervous system.

The neuron is divided into three main parts. First, the dendrites are connection points between neurons that are specialized structures for receiving impulses from other neurons; second, the cell body or soma contains the nucleus, in which many processes happen as it is a centre for receiving and sending nerve impulses. The third part is the axon or nerve fibre, which is covered by a sheath and specialized to carry the action potential generated by the cell body, figure 1.7.

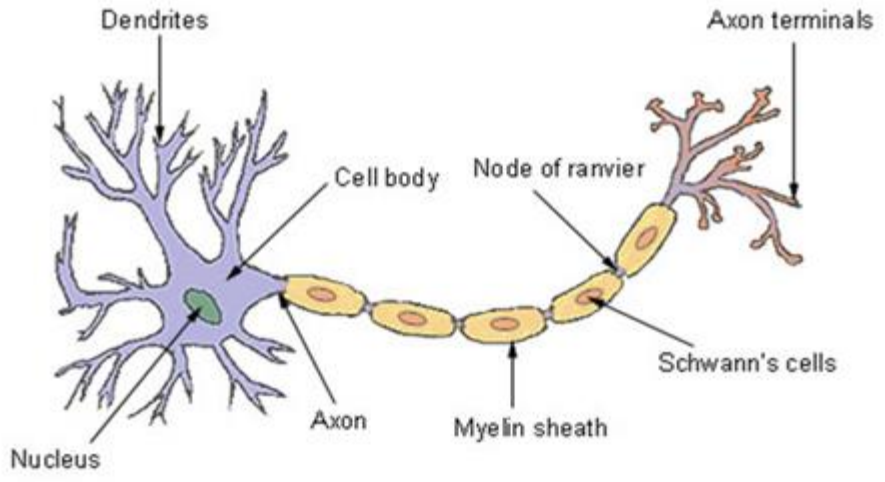

Figure 1. 7 Structure of a typical neuron
http://home.apu.edu/~jsimons/Bio101/action_potential.gif [access 20/02/2013]

1.12 The Action Potential

The axon is specialized to transmit the signals that are generated in the cell body via ionic exchanges. This means that the neurons have the ability to send electrical signals in the form of action potentials. In response to the appropriate stimulus, series of these electrical impulses occur near to the cell portion of the axon. This electrical signal moves across the neuronal membrane, in much the same way as the electrical signal does in an electronic device. However, this signal is created by ions not electrons. This ionic exchange happens because of the difference in the concentration of ions inside and outside the neuron that leads to a potential across the membrane. The electrical changes start from the resting membrane potential, when a neuron is not transmitting a signal; hence the inside

of the cell is negative and the outside positive and resting at a voltage of -70 mV across the membrane. This means the neurons are polarized at rest.

The action potential is generated by voltage gated ion channels and an ionic pump, which controls the equilibrium potential in the cell membrane due to the difference in ionic concentration causing an ionic gradient. The responsible ions are sodium (Na+), with higher concentrations outside than inside the cell membrane, and potassium (K+), which has a much higher concentration inside the cell than outside the cell; each plays a central role in cell-to-cell communication. The Na+ channels open during stimulus of the synapses in the neuron at a particular voltage called the "threshold potential", which causes the sodium positive charged ion to move from outside the membrane to inside in a high flow of ions (Bear, Connors et al. 2006). This movement leads to an increase in the positive charge on the inside of the membrane by a process called membrane depolarization. Then the overshoot steepens until it reaches the peak of the spike, where the depolarization in the area of the neuron is about 50 mV; thus the sodium channels close themselves by inactivating the gates and opening the potassium channels. These channels allow the potassium ions to move out of the cell; therefore the voltage becomes negative inside the cell, through a process called repolarization. These processes are shown in the figure 1.8. The repolarization becomes more negative and comes under the resting potential because the potassium channels remain open until the resting point is achieved; this is called hyperpolarization and the action potential may fall as low as -80 mV. Then the sodium and potassium pumps start working to re-establish membrane potential.

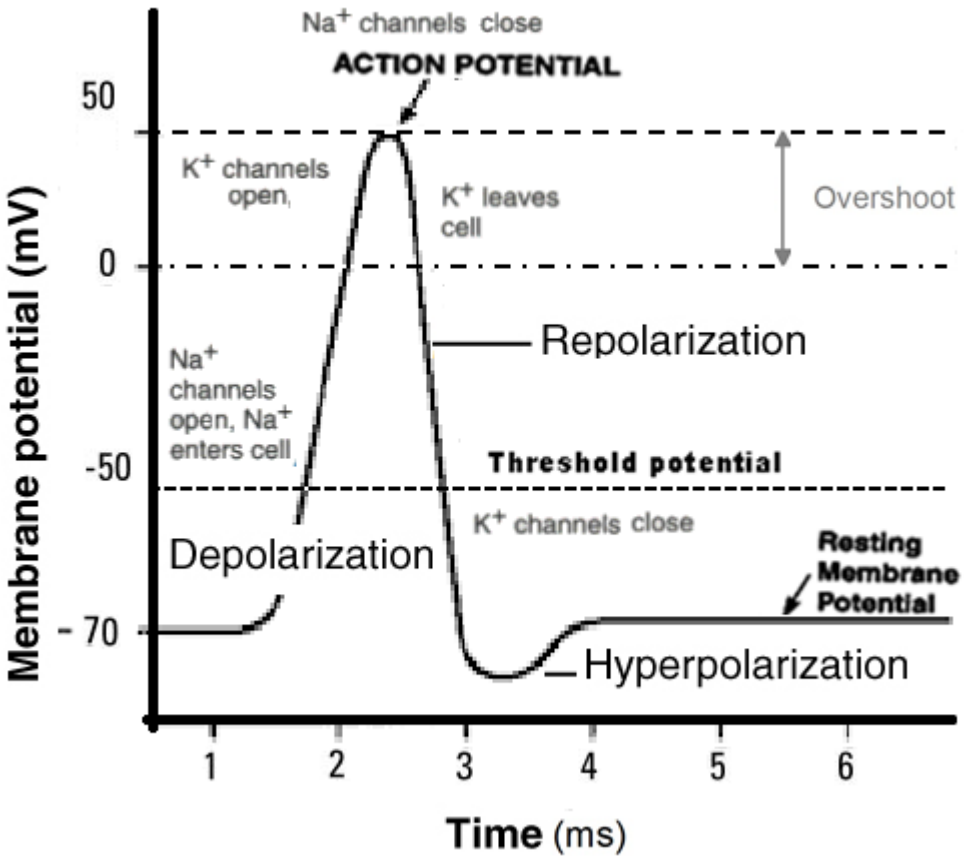

Figure 1. 8: Shows the action potential on an expanded time scale(http://sdsu-physics.org/physics180/ physics180B /Chapters/epotential_apps.htm [19022013]).

The figure above shows the action potential that occurs between 4 -5 ms, and the next spike is not generated until after the resting membrane potential for the previous action potential has been reached again. In addition, this action potential increases until the stimulation reaches the maximum voltage, which occurs between (1-2 ms) after the start of the action potential. The individual neurons transmit spikes electrically from the axon of the cell to be received by dendrites in the next cell, therefore this mean the impulses are transferred in

one direction. A group comprising hundreds or thousands of individual neurons makes up a fascicle, and the nerve contains more than one fascicle. The nerve serves as a cable that connects the brain to all body parts, but, unlike a cable in theory, because the connection is made by ions not electrons.

The transmission of a current through any conductor leads to generation of a magnetic field around the wire, according to Ampere's law and the Biot-Savart Law, which are both laws that can be used to determine the magnetic field. Hence, the nerve can be considered as a transmission cable driven by the action potential (Debanne, Campanac et al. 2011). Recently, many studies have used direct neuronal detection technique in MRI to detect the nerve response through these very weak fields at about 1nT(Chow 2005, Anwar 2011), However this phenomenon is still not well understood.

1.13 Ionic Current and Magnetic field associated with the axonal action potential

We discussed in the previous sections how the neurons generate action potentials via ionic exchanges between (Na+) and (K+). Thus, this ionic activity and different concentrations between intracellular and extracellular components produces electrical signals then the action potential produces the magnetic field that may have an effect on the imaging process. In other words, the produced local magnetic fields disturb the main magnetic field, which could be enough to appear as contrast on MR images. The action potential in the neurons generate electrical impulses along the membrane, which is treated as a cable carrying current (Rosch and Markov 2004).

This section discusses the magnetic field generation that surrounds the neurons by using Ampere's law.

To find the magnitude of magnetic field near a cable carrying current I at a distance r equation 1.3 is used. The direction of the magnetic field is perpendicular to the axon or the nerve, and this illustrated in chapter four (figure 4.1).

$$B = \frac{\mu_o I}{2\pi r} \quad \ldots\ldots\ldots\ldots \quad 1.3$$

where; B is the magnetic field

I is transmembrane current

μo is the permeability of free space is equal to $4\pi \times 10^{-7}$ T.m/A.

This law means that the magnetic field becomes weaker further away from the axon, therefore, due to the very tiny magnetic field from the source, the effect will only be seen very close to the membrane.

1.14 Previous Studies using fast fMRI

Previous studies have used MRI with different magnet field strengths, imaging parameters, imaging coils and experimental paradigm designs. Controversial results have been reported over the last decade. They are divided into two groups – those who report a positive detection of neuronal currents using MRI (Kamei, Iramina et al. 1999, Konn, Gowland et al. 2003, Xiong, Fox et al. 2003, Bianciardi, Di Russo et al. 2004, Liston, Salek-Haddadi et al. 2004, Chow, Cook et al. 2006, Chow, Dagens et al. 2008, Xue, Chen et al. 2009, Rodionov, Siniatchkin et al. 2010, Paley, Kaka et al. 2015) and others reporting failure of detection by MRI (Singh 1994, Chu, de Zwart et al. 2004, Mandelkow, Halder et al. 2007, Parkes, de Lange et al. 2007, Tang, Avison et al. 2008, Luo, Jiang et al. 2011, Huang 2013).

Many studies have attempted to theoretically calculate the magnetic fields that are generated from action potentials of nerves for comparison with measured waveforms (Swinney and Wikswo Jr 1980). The Wikswo study established that the current around the nerve or through the membrane would have very small effects but could be detectable without injuring the nerve membrane.

Following is a brief review of previous studies performed theoretically or experimentally on phantoms, in vitro, or in human volunteers.

1.14.1 Theoretical Studies

A numerical study by (Blagoev, Mihaila et al. 2005) used two models of 1 mm^3 of neural tissue. The first assumed a random distribution of neurons and synchronous firing while the second model was based on more realistic assumptions of the positions of neurons in the cortex. The study concluded that the sum of magnetic fields generated from axons were close to zero, therefore the phase change due to this effect would also be close to zero.

In 2005, (Blagoev, Mihaila et al. 2005) reviewed the challenges and reported a fundamental survey on neuronal magnetic field detection. The study demonstrated that the best chance of detecting neuronal magnetic fields was by minimizing or separating the BOLD effect. In addition, the probability of measurement depends critically on the predictability, geometry and current strength of the neuronal firing as well as the sensitivity of the MRI scanner. Another study by (Xue, Gao et al. 2006) presented a theoretical study to calculate the percentage signal change that is produced by neural firing. The study reported that the neuronal magnetic field can potentially change the magnitude signal of MRI depending on the dendrite number. In this study, they assumed one million dendrites were firing simultaneously for a duration of 10 ms. They calculated that the percentage signal change could be up to 2% corresponding to neuronal currents of 5 nA. However, they reported that there was no associated phase shift due to the symmetrical distribution of dendrites in a voxel. Otherwise a phase change could also be detectable. The next numerical study was published by (Park and Lee 2007). They used both axons and dendrites as models of the local magnetic field source. Their study reported that, by separating the BOLD effects, weak effects could be measured due to dendritic magnetic fields but nearly zero changes were expected from axons on the MRI signal. In the same year 2007, (Blagoev, Mihaila et al. 2007) used a model to assess the possibility of using MRI for neuronal current detection in the human brain using a realistic neuron model. It was found that no effects or magnetic fields should be detected close to the neuron, but that the modulation was well approximated by a dipole source from several centimetres. The simulation showed a percentage signal change of 1.6% and a phase shift of 1°.

In 2008, two papers were published by Cassara, A., et al. The first paper investigated the possible use of a resonant mechanism to achieve direct neuronal detection using ultra-low field MRI (Cassarà and Maraviglia 2008). They demonstrated that direct detection should be possible with the characteristics used for the theoretical study. The second study introduced a new simulation of a direct neuronal detection MR sequence (Cassara, Hagberg et al. 2008). They predicted the time course of the MR signal during neuronal activity and found that the percentage signal and phase change depended on the echo time, voxel-size and neuronal density.

Feasibility of direct detection was investigated by Xiong, Hong-Chuan, et al. (Xiong, Huang et al. 2009). They also used a numeric simulation model investigating whether dendrite branches participated in producing the local magnetic field. The study assumed the radius of the dendrite was between 0.25 μm to 0.5 μm with produced intracellular currents of 1 nA to 5 nA. The report showed that the dendrite branches may increase the ability of an MRI scanner to detect neuronal magnetic fields.

A theoretical study of imaging neuronal currents was published by Anwar, et al. (Anwar, Cook et al. 2010). The model presented an estimation of a maximum percentage MR signal change of 0.35%.

A study by Luo, Q. and J. H. Gao in 2010 investigated the optimum TE for direct neuronal detection at 1.5, 3, and 7T (Luo and Gao 2010). It was shown that a different optimum TE was needed for magnitude or phase images. In general the optimal TE in magnitude images was greater than the optimal TE in phase images and the sensitivity was higher in scanners that have lower magnetic field for human brain studies. In addition, a dual echo imaging sequence was suggested. A second theoretical study was published by the same group in 2011 (Luo, Jiang et al. 2011). This study aimed to establish a simulation model to improve the description of neuronal morphology and physiology. The findings of this study indicated that the amplitude of the local magnetic field was dependent especially on the density of synchronously firing neurons and imaging conditions, and the change is too weak about 0.000014, which could not be detected by MRI during physiologically-evoked experiments. However, the phase change could be up to 0.2° with spontaneous alpha wave activity.

In 2011, a study was published by Anwar, S. M., et al. (Anwar, Cook et al. 2011) which estimated the axons magnetic field using a computational hybrid model of the human optic nerve. The study reported a mean local magnetic field of 2.5 nT, hence the percentage signal change corresponding to this was 0.35%. This demonstrated that it could be possible to detect neuronal magnetic fields using MRI.

1.14.2 Phantom Studies

A number of phantom studies have reported both positive and negative claims regarding detection of weak magnetic fields similar to those expected from neuronal firing. Studies using either magnitude or phase MR images are reviewed here.

In 1994, Singh attempted to determine the limitation for detection of phase shifts in 1.5 T MRI using a cylindrical phantom filled with saline solution. He used a spin echo pulse sequence with a TR of 2000 ms. A current pulse ranging from 0.025 to 3.3 mA was sent through the phantom in synchronization with the 90 degree radio frequency pulse. His study demonstrated that the MRI phase sensitivity was measured to be 6.8^{o} while in vivo studies require a precision of 0.35^{o} in the phase shift (Singh 1994).

In 1999, a study on a simple phantom consisting of a copper wire was published by Bodurka, J., et al. (Bodurka, Jesmanowicz et al. 1999). They used EPI to measure magnetic resonance phase images with an externally injected current (10 -100 μA). They demonstrated feasibility to detect phase changes of 0.8±0.1 degrees and the detectable magnetic field was about 1.7 ± 0.3 nT. In addition, the study also calculated the magnetic flux density for the same experimental setting and found that the phase change depended on the location of the wire inside the voxel. The study used a 3T magnet with a fast gradient echo pulse sequence at TR= 200 ms. Another study in the same year was reported by Kamei et al. (Kamei, Iramina et al. 1999). They developed measurements with an electric current dipole made of copper wire in a phantom using a microscopic MRI technique principle. The study reported the magnetic resonance signal was affected by a current dipole of 450 nAm with a minimum detectable dipole moment of 90 nAm. The magnitude changes were due to the distance of the copper wire and the direction of the current.

In 2001, it was suggested that neuronal effects might be detected by measuring the spatial displacement due to ionic currents using the Lorentz effect (Song and Takahashi 2001).

The study was performed on a phantom with current pulses ranging from 0 to 500 μA using spin-echo with TR=1000 ms on a 7T scanner.

In 2002, A second effort at imaging neuronal currents in a phantom was published by Bodurka, et al. (Bodurka and Bandettini 2002). They used single-shot SE-EPI sequence to detect NMR phase changes on a phantom with TR=1000 ms using a 3T scanner. They demonstrated magnetic field changes of 2×10^{-10} T with a stimulation lasting for 40 ms.

In 2003, several groups investigated direct MR detection using different models. Konn, D., et al. (Konn, Gowland et al. 2003) investigated the feasibility of direct MR detection of neuronal activity in the brain using a conducting sphere model of radius 80 mm. They explored the effects of the magnetic field distributions for both phase and magnitude images. This work demonstrated the minimum detectable current to be about 4.5 nA with an associated magnetic field of $1.1 \pm 0.5 \times 10^{-10}$ T using EPI at 3T. Another group, worked on a new method of estimating alternating currents using ghost images that are produced during current fluctuation of the magnetic field (Yang, Cook et al. 2003). This method was known as (GRACE), and they demonstrated that this method could be used to directly map fields or directly detect local MR changes induced by neuronal firing events. Data were acquired on a 1.5 T MR system using oil phantoms with I=7 mA, an applied frequency of 1 Hz and acquisition TR of 100 ms. In 2004, same group expanded on this imaging technique to detect firing of the optic nerve with sequential averaging (Chow, Cook G et al. 2004).

Other groups also investigated the sensitivity or detection limitation of MRI on the neuronal electrical current. In 2004, A study by Hatada, Tomohisa, Masaki Sekino, and Shoogo compared the sensitivity detection limitation of both theoretical and practical measurements for detecting weak magnetic fields with a phantom which was fitted with four columnar copper wires and filled with gel (Hatada, Sekino et al. 2004). They injected different rectangular current pulses (100 μA to 20 mA) to the electrodes with TR =900 ms at 4.7T. Results from this study demonstrated a sensitivity limitation of approximately 10^{-8} T and 10^{-7} T for theoretical and practical estimates respectively. The authors demonstrated that the sensitivity limitation depended on the acquisition parameters and an optimal value for TE of 5 ms. Another group in 2005 investigated the sensitivity of MRI detection with magnitude signal changes using a glass sphere phantom (Pell, Abbott et al. 2005). The

phantom consisted of a carbon fibre wire immersed in silicone oil, and applied a current pulse frequency of 50 Hz with an amplitude of (100 - 1.7) μA. Their results determined a lower detectable limit of 1.7 μA corresponding to a magnetic field of 0.34 nT and they expected that this result was close to that generated by neuronal firing. They reported that the magnetic field changes should be detected using a gradient-echo EPI sequence and TR=1000 ms with a 3T MR scanner.

In 2008, an investigation was reported using very low field magnetic resonance by Kraus, et al. (Kraus Jr, Volegov et al. 2008). This study presented theoretical and experimental (current phantom) evidence using a modulating field of 100 μT. The study showed that the magnitude percentage signal change was larger than the phase shift in practice. They demonstrated that magnitude imaging might be the best technique capable of directly detecting neural activity in human subjects using an evoked response.

In 2010, Anwar, et al. presented another theoretical model to estimate the MR signal changes due to neuron current (Anwar, Cook et al. 2010). The model was theoretically strong enough to change the main field, and therefore could be used in phantom experiments or in vivo. This result was supported by an experimental phantom study using a 9.4T MRI system with TR=100 ms.

A new approach at imaging neuronal currents was published by Höfner, et al. in 2011 (Hofner, Albrecht et al. 2011). The method was based on the use of low-field nuclear magnetic resonance (LF-NMR) using an integrated current dipole to simulate neuronal activity. In addition, subject studies were conducted to study the feasibility of detecting somatosensory evoked neuronal currents. The authors claim a successful phantom study that showed the method could alter the 1H-NMR signal. They suggested to make the method feasible in a human subject they would to needed improve the SNR at low field by at least a factor of 38.

1.14.3 In Vitro Studies

Many in vitro studies have also been reported, identifying targets to assess the feasibility of detecting effects similar to those expected from neuronal firing in vivo.

A study by Joy et al. in 1989 was the first to use a neuronal magnetic field method (Joy, Scott et al. 1989). However, this study was performed on both phantoms and human subjects but will be discussed here. This study demonstrated MRI could be used to directly detect local magnetic fields that are induced by biological currents through measurement of MR phase shifts. In their study, they applied 43 mA pulses to a phantom perpendicularly to the field using TR = 800 ms imaged using phase images. Phase images, were also performed using 20 mA pulses with TR = 1200 ms using a saline solution. They then repeated these experiments on the forearm of a human volunteer with 2 mA pulses using TR = 1000 ms. Unfortunately they did not discuss the magnet field strength used for the study. However, they reported that MRI could be clearly detected from externally applied currents in vivo using phase images.

In 2004, a study by Park, et al. investigated neuronal activity detection using MRI with dissected snail ganglia (Park, Lee et al. 2004). The study claimed that the MR image intensity change was up to 5.49±1.94% due to the local magnetic fields produced by the neuronal currents when the ganglia was strongly activated by a nitric oxide donor, sodium-nitrosocystein. This study used a spin echo pulse sequence with TR= 500 and a 3T MRI scanner.

In 2009, Luo, Qingfei, et al. used bloodless turtle brain to remove BOLD effects using visually-evoked responses at 9.4T (Luo, Lu et al. 2009) this study presented a detection threshold for signal change of 0.1% and phase change of 0.1°. The study reported that these changes were below their detectable levels.

Work done by Poplawsky in 2012 was reported as the first evidence for direct detection in vitro from the stimulated median giant fibre of the earthworm using a free induction decay (FID) with a sampling interval of 0.32 ms in the absence of the BOLD effect (Poplawsky, Dingledine et al. 2012). They demonstrated high temporal resolution by measuring possible changes in the FID magnitude and phase difference of $(-1.2 \pm 0.3) \times 10^{-5}$ radians from the timing of the action potential using 9.4 T with TR=2000 ms and a flip angle of 90^{o}.

1.14.4 Human Studies

A large number of human studies have tested the hypothesis of direct neuronal detection using different MRI methods and experimental paradigm designs. Many of these

studies confirm that local magnetic field could be detectable under some conditions using MRI. Others reported the sensitivity and limitation of current generation MRI preventing detection of such ultra-low magnetic fields due to ionic currents. In addition, contamination by other effects, for example hemodynamic responses, are thought to dominate the responses. In this section, these human studies will be reviewed and some ideas proposed that could be developed and used in this study.

In 1994, a study by Singh, M. determined the limitation of MR phase shifts using phantom and human subjects (Singh 1994). The phantom had 50 ms current pulses applied with current ranging from 25 μA to 3.3 mA, while the human subject was stimulated with 1 kHz audio to activate the auditory cortex. The study reported that no stimulation related phase signals were detected above the noise level using a spin echo pulse sequence with TR =2000 ms and a 1.5 T scanner. Thus, the phantom results suggested a precision of 0.35 degree was required to detect evoked magnetic fields in a human subject, while the sensitivity of the scanner used was 6.8 degree.

A group developed an electric current dipole measurement method based on a microscopic MRI principle in a phantom (Kamei, Iramina et al. 1999). The technique was then used to determine human brain activity in the motor and sensory cortices. The study reported that evidence of a signal in the brain during middle finger and thumb tapping was successful due to induced neuronal current distribution at 1.5T with EPI using a long TR=4000 ms. However, the current in the motor area could not be detected.

Another group presented a novel MRI technique for mapping brain functional activity using neuronal current effects (Xiong, Fox et al. 2003). They demonstrated that a detection percentage signal change of 1% was achieved with a temporal resolution of 100 ms. This study used a visuo-motor paradigm at TE=50 ms with a gradient-echo echo-planar-image pulse sequence and a TR of 1000 ms at 1.9T.

A failed study was published by Chu R. and others, reportedly due to the limitation of MRI to separate slow effects (BOLD) processes from potential rapid neuronal currents in vivo (Chu, de Zwart et al. 2004). They used a method to measure both the BOLD response and rapid fMRI simultaneously and separately using a gradient-echo EPI sequence with a 3T scanner and a TR=1500 ms using a 25° excitation flip angle. They concluded that the sensitivity of MRI to the neuronal activity was too low and not practically detectable or

useful under their experimental conditions. In the same year 2004, a combined EEG and fMRI study was presented by Liston, et al. (Liston, Salek-Haddadi et al. 2004). They collected all fast and slow signals using EEG correlated fMRI during runs of a 3-Hz generalized spike–wave discharge in epilepsy patients using a gradient echo EPI sequence with a TR of 3000 ms. Significant BOLD response was detected. However, they also demonstrated significant activity at a time of the order of 30 ms associated with the direct 3 Hz modulation. They suggested further study was required to validate these signals. Another combined work by Bianciardi et al studied the detection of neuronal currents using BOLD measurements and use of visual evoked potential recording (Bianciardi, Di Russo et al. 2004). They claimed the feasibility of measuring neuronal currents and they preferred the use of SE rather than GE image acquisition. However, this method was contaminated by hemodynamic changes. The study used a checkerboard segment with stimuli flashing at 6.7 Hz for 20 symmetric ON/OFF cycles using a 1.5 T scanner with TR= 3200 and TR= 1300 ms for GE-EPI and SE respectively. A study by Konn et al. investigated alpha wave activity detection (Konn, Leach et al. 2004). Two conditions were used on human volunteers using visual stimulation with the eyes closed in darkness and open during stimulation. A 3T scanner was used with echo-planar images and the minimum accessible TR of 40 ms was used to cover alpha waves in a single slice. The study reported that no signal was recorded from neuronal activity, and that it was difficult to detect using current generation MRI scanners. However, they reported that it might be possible using higher static field (e.g. 7 Tesla) with EPI in the future.

Significant effort has been made by Chow et al. in 2006 (Chow, Cook et al. 2006). The group reported that neural activity could be detected by MRI using a fast gradient-echo EPI sequence. Two set of experiments (phantom and in vivo) measured percentage magnitude signal changes at a success rate of 56%. They found RMS fields in the range of (1.2–2.1) nT and (0.4–0.6) nT for the optic nerve and the visual cortex respectively. However, they did not find any change using the phase image data sets. The studies were performed at 1.5T with a short TR=158 ms. Another study by the same group was performed on the human optic nerve using strobe light stimulation (Chow, Cook et al. 2006). The group reported a success rate of 58% in measuring responses in magnitude images with a percentage signal change of (0.15 ± 0.05)% due to estimated magnetic field of (1.2 ± 0.4)

nT and 0.8% in phase image experiments using a light stimulation frequency range of (0.7–3.3) Hz with a 1.5T MR scanner using Gradient Echo-Echo Planar Imaging and TR= 158/172 ms for magnitude and phase images respectively. Therefore, this study demonstrated preliminary evidence of neuronal magnetic field detection using MRI.

In 2007, Parkes et al. investigated the ability to directly detect the neuromagnetic signals by using steady-state visual evoked potentials. The team showed no frequency component corresponding to the frequency of the steady-state visual evoked potentials and no activity that could be attributed from neuronal activity due to the sensitivity of the magnitude MRI signal using TR=1000 ms at 1.5T (Parkes, de Lange et al. 2007). Another study by Mandelkow, H., et al. combined EEG–MRI to localize the neuronal current source frequencies (Mandelkow, Halder et al. 2007). The study found no sign of alpha waves and the results were contaminated due to cardiac pulsation artefacts which could not be avoided with the analysis method used. Jasanoff reviewed developments of three kinds of bloodless techniques to measure brain function such as; diffusion-weighted imaging; direct neuronal detection, molecular imaging and signalling species (Jasanoff 2007). In addition, he reported their relative advantages and disadvantages and future prospects. A summary of his work was as follows regarding detection of neuronal magnetic fields; it is difficult to detect these tiny amplitude local magnetic field and BOLD fMRI remains the best for use by neurobiologists and psychiatrists, However, many research studies are increasingly pushing the possibility of direct fMRI detection through improved imaging methodology.

In 2008, Tang et al. used a hybrid ms/BOLD MRI acquisition sequence on a 3T magnet with long TR=1200 and 1500 ms based on direct detect magnetic field dephasing due to evoked response potentials. They were unable to detect any significant changes due to high BOLD signals (Tang, Avison et al. 2008). Another investigation by Chow et al reported observation of the direct neuronal detection by comparing BOLD responses with those of DND using block paradigms in the human visual system at 3T with GE-EPI and TR = 77 ms. They found different frequency responses corresponding to both slow BOLD responses and fast DND responses (Chow, Dagens et al. 2008). In the same year 2008, a study by Hagberg et al. reviewed the spatial and temporal resolution stability problems due to physiological noise processes for both BOLD and direct neuronal detection techniques (Hagberg, Bianciardi et al. 2008). This investigation was performed with a 3T scanner

using three different models on volunteers with TR=2000 ms. The study suggested that the detection of local magnetic field requires long scan times with long term stability. In addition, they suggested it was difficult to avoid or separate the BOLD effect and physiological noise sources signals from neuronal magnetic field signals.

Xue, Y. et al. in 2009 showed more evidence of neuronal current signal detection in the sensory cortex, and demonstrated an 80 ms latency after stimulation onset. Unilateral electric stimulations were used with a square pulse duration of 5 Hz applied to the median nerve at the right wrist by a Grass S8 stimulator. In addition, the results demonstrated amplitude changes of 0.2–0.35% using a GE- EPI pulse sequence with long TR = 2000 ms and flip angle = 80 degree using a 3T magnet (Xue, Chen et al. 2009).

In 2009, Paley et al. reported no clear evidence for a correlation with axonal firing in the optic nerve (Paley, Chow et al. 2009). This study used the ghost reconstructed alternating current estimation (GRACE) method during visual stimulus at 3T with a gradient echo sequence and TR = 200 ms. However, the phantom images clearly indicated the ghosting pattern using a weak current of 357 μA. The GRACE method has the advantage that it uses a high spatial resolution spin echo (non-EPI) sequence with low image artifacts but achieves a frequency response inversely proportional to the TR. As modern imagers can achieve TR times in the millisecond range, this extends the frequency response for MRI direct detection studies to several hundred Hertz.

In 2011, Luo et al. investigated neuronal current during absent or at least minimised BOLD effect using a long interstimulus interval visuomotor paradigm (Luo, Jiang et al. 2011). They presented significant BOLD effect activation and no magnitude percentage signal change related to the neuronal current using TR = 1000 ms and a flip angle = 70^0 using a 3T magnet.

A more recent study by Huang in 2013 presented a failure to detect any signal from the visual cortex using a 3T magnet with TR= 300 ms and a flip angle of $36^{o.}$ Signal changes were less than 0.07% under the experimental condition (Huang 2013). No significant neuronal current induced MR signal attenuation was observed in the visual cortex for any participating subject.

In conclusion, in rapid fMRI high temporal resolution is required to observe signals correlated to the action potential frequency. In additions methods which also generate high spatial resolution are advantageous. However, from the mixed results presented above it is clear that the sensitivity limitation remains the fundamental challenge facing researchers in this field.

1.15 The Goal and the Thesis Outline

This study focuses primarily on amassing evidence to experimentally confirm the hypothesis that it is possible to measure direct neuronal responses using fast fMRI with carefully designed experimental stimulation paradigms and analysis methodology. Possible fast fMRI responses have been investigated in the median nerve, thalamus and motor sensory cortex during wrist stimulation by transcutaneous electrical nerve stimulation (TENS). Stimulation of the visual system using a strobe light was also used to investigate possible rapid responses in the visual cortex and was compared with the BOLD response. In addition, fast fMRI was used to investigate both direct neuronal detection and BOLD response in the motor cortex during real and imaginary movements of the right and left hand. All the studies were performed in healthy volunteers with full ethical permission granted by the University ethics committee. Phantom experiments were also designed and performed to assess the sensitivity and reproducibility of the MRI systems used for the study.

An introduction and literature review has already been presented in this first chapter; the next chapters in the thesis are organised as follows:

Chapter two describes the overall methodology, the design of imaging experiments and the different pulse sequence parameters used, the stimulation paradigms and the techniques used to analyse the fast fMRI data sets.

Chapter three covers the development of a neuronal model phantom to simulate action potentials more closely. Data acquired from this neuronal model phantom is used to support the hypothesis that neuronal magnetic fields can be detected by MRI to map brain activity.

Chapter four presents neuronal activity detection attempts by recording a time series of dynamic MR images from the median nerve during TENS stimulation of the wrists of adult volunteer subjects and correlating the stimulation frequencies with the MRI responses.

Chapter five presents possible response results from functional activation of the adult human visual cortex using stimulation with a strobe light over a range of frequencies. A comparison with the BOLD effect was also made.

Chapter six presents results using median nerve transcutaneous electrical nerve stimulation (TENS) to activate the thalamus and motor sensory function using fast fMRI. In addition, fast fMRI was used to investigate direct neuronal detection in the motor cortex during real and imaginary movements of the right and left hand in healthy volunteers.

Finally, chapter seven highlights the conclusions of this thesis with regard to the initial hypothesis concerning the feasibility of direct neuronal detection with fast fMRI, summarizes the contributions and discusses important directions for future work.

CHAPTER 2: Methodology

2.1 Introduction

This chapter details the design of the experiments, analysis of results and presentation of data presented in this thesis. In summary, experiments included measurements of phantoms (conductive gel placed on a spherical phantom, an axon simulating phantom and a cylindrical NaCl solution phantom) using both 1.5 and 3T MR scanners, adult human median nerve stimulated with electrodes connected to a TENS machine using a 1.5 T scanner, adult human visual cortex stimulated with strobe light using a 1.5T scanner as well as adult human motor-sensory cortex activated by a TENS machine through the median nerve using a 1.5T scanner. In addition, real and imaginary finge tapping were studied at 3T. For each study the methods and stimulation paradigm is described. The results of all the experiments described in this chapter are presented in full in separate results chapters. The analysis program and design is described at the end of this chapter.

2.2 Phantom Study Designs

Any object or wire with a current generates a magnetic field and can perturb the scanner's magnetic field. For this study, the following phantoms were designed;

2.2.1 Axon phantom

This small phantom was manufactured using 3D printing (courtesy of John Haycock, Tissues and Biomaterials Engineering) and applied to detect ultra- weak magnetic field changes. The phantom consisted of a cylindrical shape with a diameter of 2.8 mm and a length of 10 mm made of PEG Polyethylene glycol. Inside the cylinder, seven uniformly spaced tubes of approximately 250 μm diameter and 10 mm length were filled with a NaCl conductive solution (1.25 gm/L concentration) representing the neuronal axons. The phantom was connected to the TENS machine through twisted pair wiring, which delivered small electrical pulses to the ends of the phantom. Figures (2.1-2.2) show typical phantom images that were obtained in order to assess the feasibility of neuronal current detection using different field strengths.

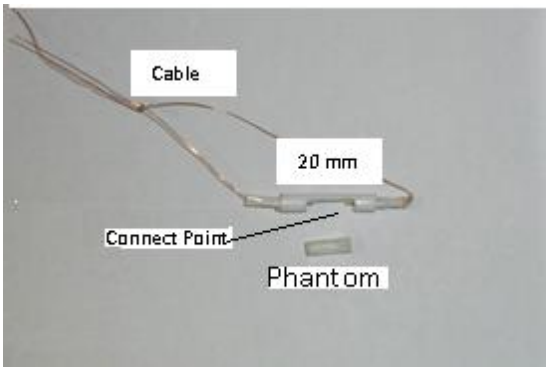

Figure 2. 1 illustrates the axon phantom connection

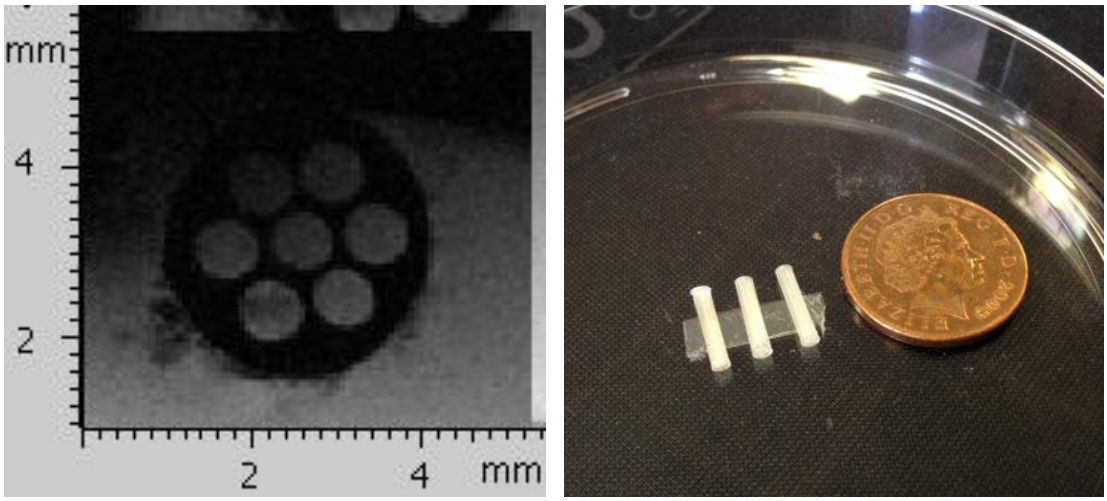

Figure 2. 2 Axon phantom, left image shows axial plane, size and the structure. Right image, as a size comparison, here are the axon phantoms laid out next to a one penny coin.

The phantom was tested at high field, 9.4T, and using a 3T scanner. 3D images were also performed on a 1.5T scanner.

Figure 2.3 the axon phantom placed inside a reference phantom used for RF loading with a high in-plane resolution of 0.7 mm acquired at 1.5T with the following parameters TR/TE = 38/20 ms using an 8 channel wrist coil.

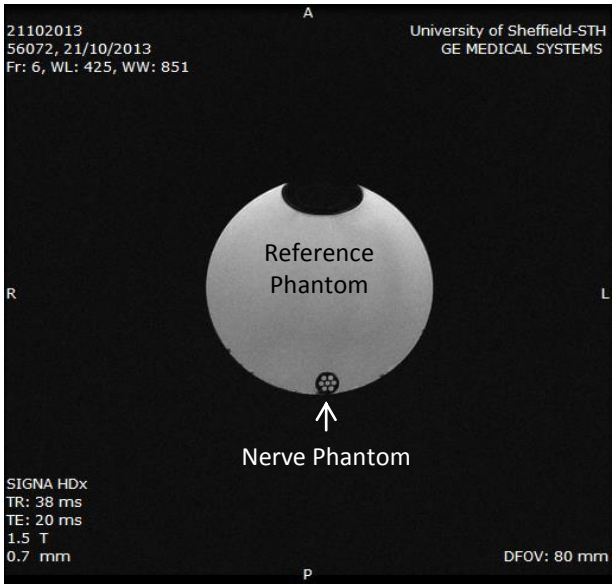

Figure 2. 3 An MRI of the axon phantom was acquired at 1.5T with TR =38 ms, TE 20 ms. with a larger phantom used for reference

2.2.2 Conductive Gel Phantom

A 27 cm diameter spherical phantom was used with a thin layer (about 1 mm) of conductive gel (Signa Gel; Parker Laboratories Inc., Fairfield, NJ, USA). Approximately 4 cm^2 on the top of the phantom was coated with the conductive gel. Two conductive rubber electrodes were placed 2.5 cm apart controlling the resistance to reduce the input current to a suitable value. These electrodes were supplied by the TENS machine, and the average

amount of current flowing through the gel during pulsation was approximately 50 µA. These experiments were acquired at 1.5T using and 8 channel head coil.

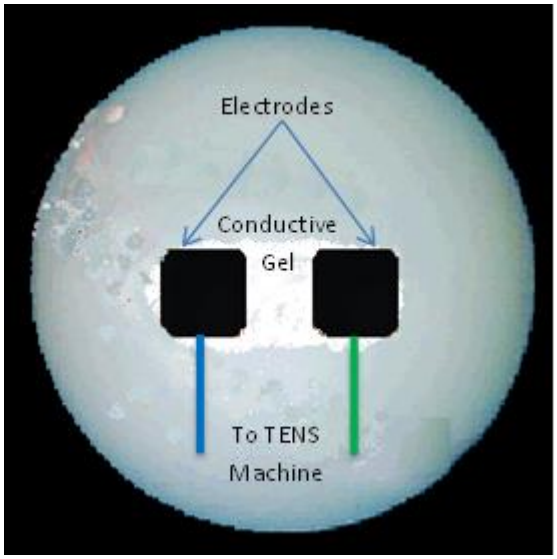

Figure 2. 4 shows the position of the electrodes and how the gel was coated on the spherical phantom

2.2.3 NaCl Solution phantom

Due to continued material failure issues associated with using the 3D PEG printed axon phantom in a conductive solution, it was decided to make a simpler version using a single tube from a more suitable plastic material. A small polyethylene tube with outer diameter of 3 mm and inner diameter of 1mm and length 70 mm was used to simulate an axon. Suitable current (depend on the NaCl solution concentration) was applied to the phantom using the TENS machine (figure 2.5) through extended twisted pair cables attached to the end of the phantom. The solution contained 1.25 grams/L of NaCl with 2 μs/cm, 1.25 MΩ resistance, measured by a digital ohmmeter (Fluke 125 ScopeMeter, 40 MHz, UK). This small phantom was accompanied by a larger water reference phantom (20 mm in diameter and 35 mm in length) to assist in loading the MRI scanner for correct RF matching.

Figure 2. 5 Shows the NaCl phantom connection

2.3 Subject studies and experimental design

2.3.1 Ethical Approval and Subject Preparation

Ethical approval for the study was given by the Research Ethics Administrator of the Medical School at the University of Sheffield on 10th January 2012. Healthy adult volunteers gave written informed consent in accordance with the School's Ethics Reviewers requirements prior to participation. After the volunteers had completed safety questions and demonstrations of competence, they underwent the TENS and MRI scanning.

Twelve healthy volunteers were chosen for the whole study (mean age 32.5±13 years) without any history of medical or neurological illness. Most of these were involved in two different studies. In addition, two volunteers participated once per week on average over the entire period of study. This study performed 145 experiments overall; 34 experiments on seven volunteers involved the median nerve response (where the single hand/wrist used was chosen randomly), six subjects were chosen to investigate stimulation of the visual cortex, 38 experiments in total, and the motor-sensory cortex and thalamus investigations were conducted on six volunteers in a total of 33 experiments. In addition, five subjects participated on the 3T scanner to investigate real and imaginary finger tapping in a total of 40 experiments.

Subjects lay supine on the patient table inside the magnet bore with their hand resting inside the wrist 8-channel array coil throughout the experiment during the stimulation of the median nerve. Subjects were also supine in the normal position during the presentation of the motor sensory cortex and thalamus TENS stimulations, For the visual stimulation experiments, the volunteers were looking up at a mirror angled at 45° to allow them to see the light strobe coming through RF shield window. During the experiment, the volunteer needed to lie comfortably and be relaxed inside the MRI system to avoid any movement. The MRI scanner is very sensitive to any subject movement. The volunteers were monitored visually during the experiments to confirm adherence to the experimental paradigm.

Figure 2.6 illustrates the position of the subjects and the TENS location. The median nerve was activated by placing electrodes on the palm within the coil, while the motor sensory cortex was activated using the TENS stimulation away from the imaging coil as seen in figure 2.8.

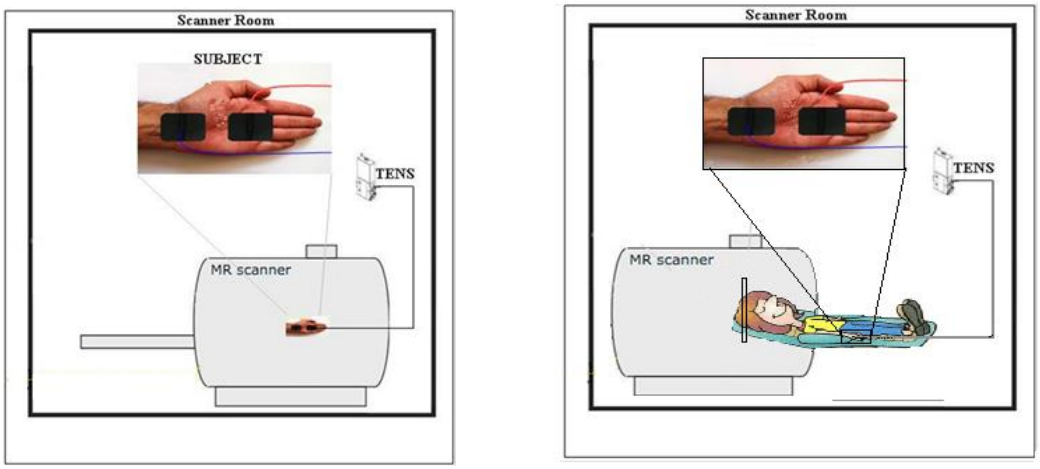

Figure 2. 6 illustrates the position of the subject, left is the position of the subject (median nerve), located in the wrist coil. Right figure is the ROI of the motor cortex which was activated using a battery operated TENS device.

2.3.2 Stimulus Presentation

Electrical stimulation of the hand, (chosen randomly) was delivered at the palm with two non-magnetic conductive electrodes (conductive rubber) using conductive gel to ensure good electrical contact with the skin. The TENS electrodes were positioned approximately 3 cm apart. The electrodes were connected to the TENS via a twisted pair of cables to avoid the possibility of induced eddy currents and any risk to the TENS device from radiofrequency field pulses. Minimal stimulus intensity was used for the subjects, so that the electrical pulses were just able to be felt and this was tested outside the scanner just before the fMRI scan

Electric stimulation was applied in the same way for all three fMRI experiments i.e. median nerve, motor cortex and thalamus activation. To provide the median nerve response data, a

standard close fitting eight channel wrist coil array was used to allow high image quality at very small FOVs, and a brain coil with 8 channels was used to investigate the motor sensory cortex, thalamus and visual cortex.

A Mini quartz-halogen strobe light (QTX 20 W Mini) was used to stimulate the visual cortex. The strobe was located outside the MRI room adjacent to the RF screen window in direct line with the centre of the magnet bore. The light was observed as an effective point source from within the magnet through the angled mirror. The strobe delivered a high light intensity with an adjustable flash rate which was calibrated using a photodiode and digital oscilloscope. All visual stimulation experiments were performed with a darkened control and MRI room with approximately fifteen minutes of subject dark adaptation during acquisition of scout and 3D data sets prior to the functional imaging studies.

Both the TENS and visual stimulation paradigms will now be presented in turn.

2.3.2.1 TENS Machine Stimulus Paradigm Presentation

The Transcutaneous Electrical Nerve Stimulator is a compact electronic device, which transmits electrical pulses through electrodes to the skin, thereby stimulating the underlying nerves. These electrodes are placed over the specific nerve of interest to stimulate it without the need for skin penetration. This system was used to investigate possible responses from the median nerve and activation of the somatosensory cortex and thalamus. In addition to its extensive clinical use for the treatment of pain, the TENS machine is increasingly being used for research purposes. The (TPN300) type of TENS machine unit was used in these experiments as a simple non-invasive technique for stimulating the median nerve during investigation of median nerve and somatosensory cortex responses. Two stimulation paradigms were applied in each fMRI session at different frequencies and each lasted only 44s. However, each subject also required a control scan without any stimulation. The two frequencies used for stimulation were in the range of (2.1 - 4.1 Hz) for both the median nerve function and motor sensory cortex investigation.

An appropriate choice of TENS parameters was selected for the experiments such as the stimulation site, mode, frequency, intensity and pulse width. Figure 2.7 shows two typical

frequency paradigms used in the experiments. A continued paradigm (all ON-blocks) captures 500 time frames of GE-EPI magnitude images.

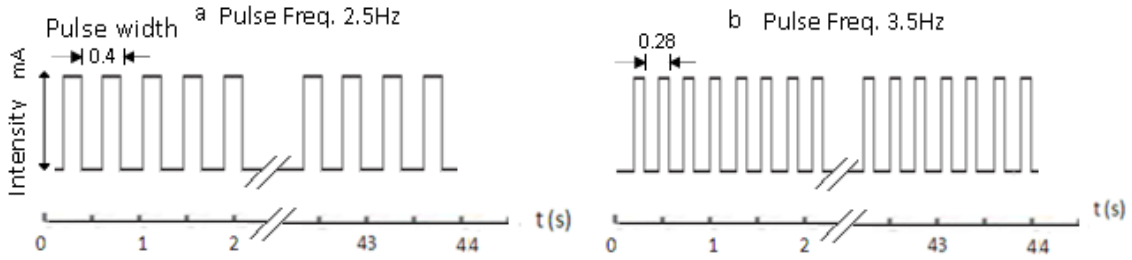

Figure 2. 7 TENS encoding stimulation [mode, frequency, intensity and pulse width]; Designed for, left) 2.5 Hz and right) 3.5 Hz

1-Stimulation site; for all experiments the palm of the hand was used to stimulate the median nerve.

2- Mode; this type of TENS has a three way mode switch: B, N and M, which represent Burst, Normal and Modulation respectively. The normal mode was used in all experiments.

3. Frequency; the machine offers a frequency range from 1-200 Hz. To stimulate the median nerve and provide a signal within the acquisition bandwidth available without aliasing, given the repeat time used, the frequency was in the region of 2.1 - 4.1 Hz. In these experiments 2.5 and 3.5 Hz frequencies were most commonly used, which equate to 0.4 seconds and 0.285 seconds between pulses. These frequencies were chosen to minimise interaction with the respiratory and cardiac cycles.

4. Intensity; the applied current for this type of machine is between 0 -100 mA (assuming a 500 ohms load). Most of the experiments used about 30 mA as an average stimulation current (3/8 setting on scale) to produce a reported but not painful effect from the volunteer. This can be calculated from the equation 2.1 (Mickiewicz and Coombes 1986).

$$I = I_{RH}/(1 - e^{\frac{t}{k}}) \qquad (2.1)$$

where; I is pulse Intensity

I_{RH} is Rheobase (membrane excitability)

t is the pulse width

k is chronaxie constant, which is the minimum time required for an electric current to double the strength of the rheobase to stimulate a muscle or a neuron.

This equation has been described by the typical curve that is shown in figure 2.8.

5. Pulse Width; the TPN300 has an adjustable range of 50 - 250 microseconds, which controls the period of time the pulse is switched on. Typically 250 microseconds was used.

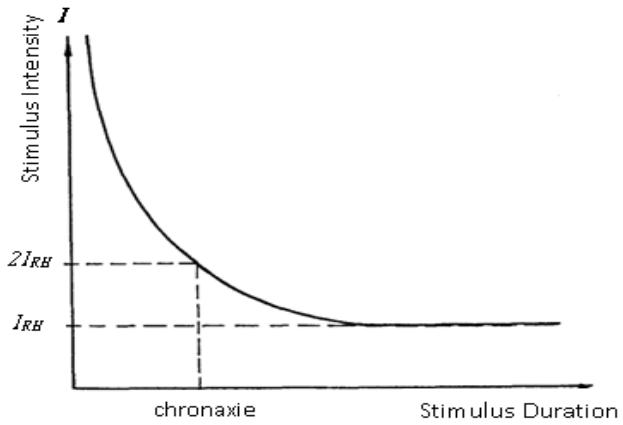

Figure 2. 8 Stimulation intensity versus stimulus duration

2.3.2.2 Strobe Light Stimulus Paradigm Presentation

To stimulate the visual system, the strobe was applied simultaneously with the MR acquisition over a range of frequencies (2.2 - 4.8 Hz).This range of stimulus frequencies activates the visual system strongly (Movshon, Thompson et al. 1978). The visual cortex receives visual signals from the eyes through the lateral geniculate nucleus (LGN). However, information is also transmitted from the eyes to the thalamus for initial processing by optic nerves. The strobe light was used to stimulate a burst of action potentials with different frequencies, which were chosen as far away from possible sources of the heart pulsation and respiration rate as shown in figure 2.9. It has been assumed that the rate of axon firing is the same as the strobe light frequency.

In figure 2.9, A is a normal breathing pattern, which is approximately one breath per 5 seconds, B the average heart rate at rest is about one pulse per 0.85 second, C Action potentials that occur during visual cortex stimulation and finally D the strobe stimulation rate.

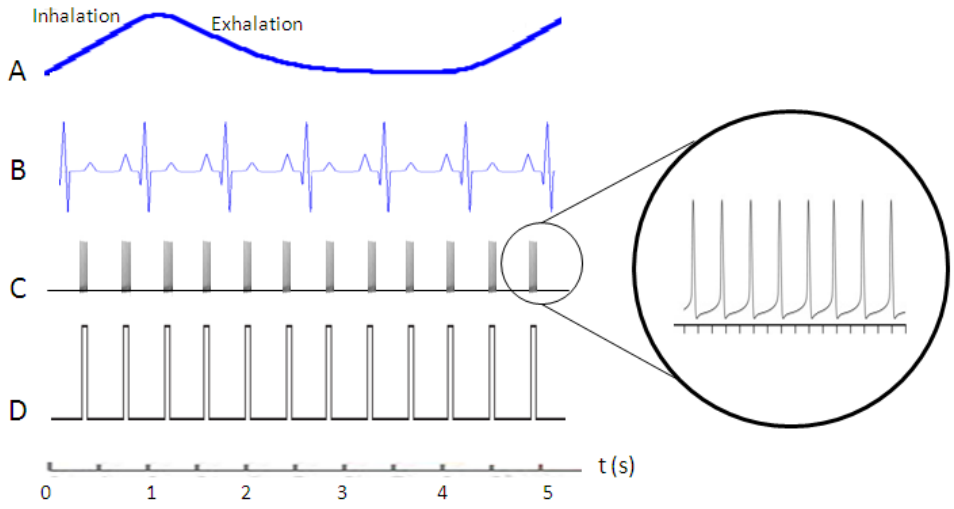

Figure 2. 9 illustration of pulsation and respiration rate during stimulation, A breathing rate, B heart beat rate, C action potential activation, and D strobe light stimulation

For the BOLD experiments, a four-block design (OFF-ON-OFF-ON) in which each block was synchronized to capture 15 time frames of GE-EPI magnitude images, giving a total of 60 frames in 120 s. The ON block used two different stimulation frequencies as shown in figure 2.10.

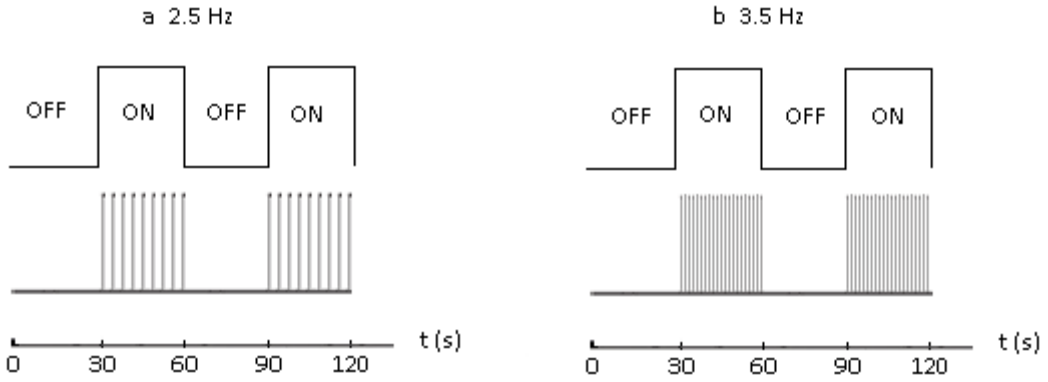

Figure 2. 10 typical two block design using strobe light, at 2.5 Hz, and b 3.5 Hz

2.3.2.3 Finger tapping paradigm

Five subjects were involved in this task, which included both real finger tapping and imaginary finger tapping. Each subject took part in four experiments which included rapid and BOLD fMRI responses during motor cortex activation using both hands (left and right) individually for each scan. The subjects were asked to tap their fingers at approximately 1.5 to 1.9 Hz repeatedly using three types of paradigms for both real and imaginary tapping. The paradigm design and duration of were as following;

First, a one block paradigm (continual finger tapping) during the entire scan for 32s during this time 500 frames were acquired as illustrated in figure 2.11.

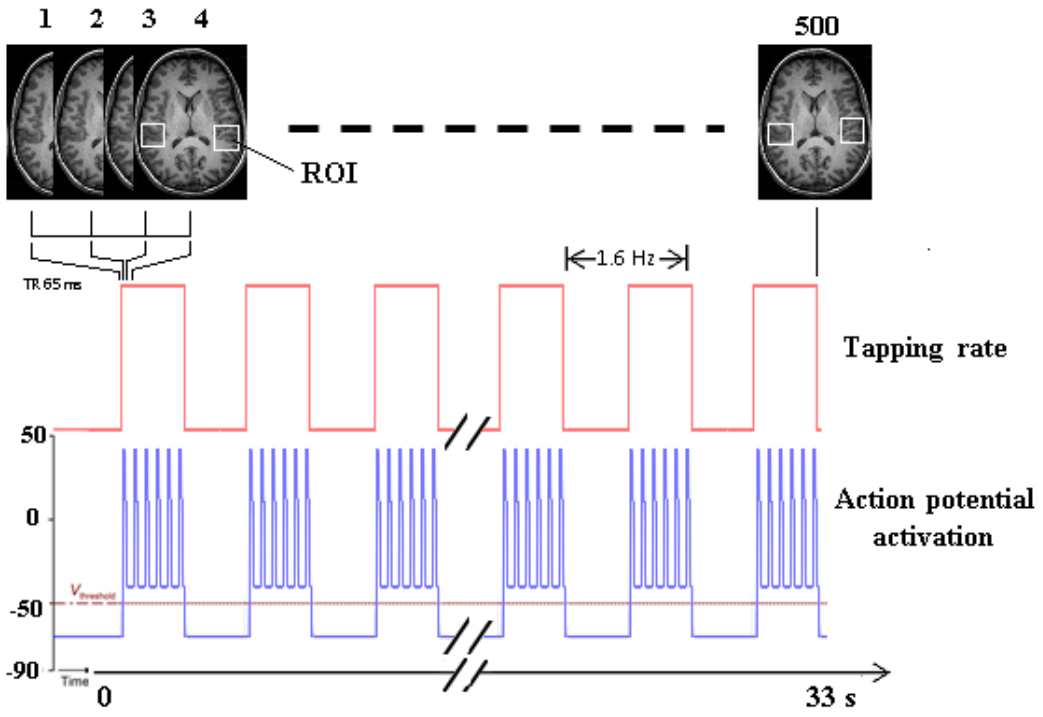

Figure 2. 11 one block finger tapping paradigm for 32 s acquired 500 scan during real and imaginary finger tapping

Second, a four block finger tapping motor sensory cortex stimulation paradigm (Rest- Tapping- Rest- Tapping) during fast fMRI acquisition of 500 scans during 32 s. Each block corresponded to 125 frames acquired in 8s with tapping frequencies between 1.5 and 1.9 Hz as shown in figure 2.12.

The third paradigm was a BOLD response stimulation. This paradigm also had four blocks but used a longer scan time of 120s to acquire 60 scans with 8 separate slices giving 480 frames overall. Each block was of 30s duration and each acquired 15 scans. Thus, the BOLD stimulation frequency used was (0.045 Hz).

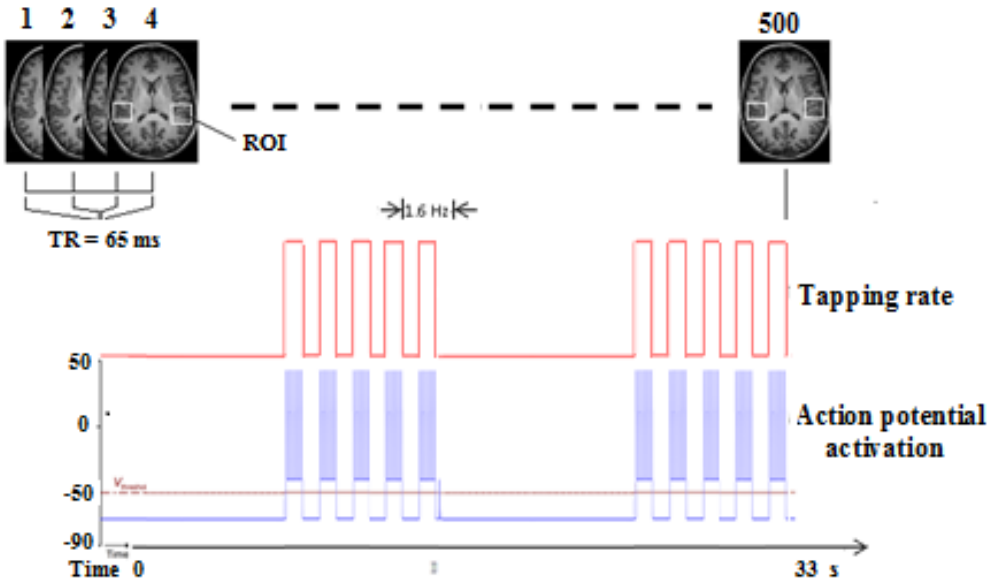

Figure 2. 12 Four block paradigm for the finger tapping motor sensory cortex stimulus (Rest-Tapping-Rest-Tapping) used during acquisition of 500 frames of GE-EPI.

2.3.2.4 Calibration of the frequency of the stimulation machines

To calibrate the strobe frequencies we used a digital oscilloscope (Tektronix TDS3032) to measure the pulse duration and spacing.

The TENS machine was connected directly to the oscilloscope while the Strobe flashing light was measured using a silicon photodiode connected to the oscilloscope as in figure 2.13.

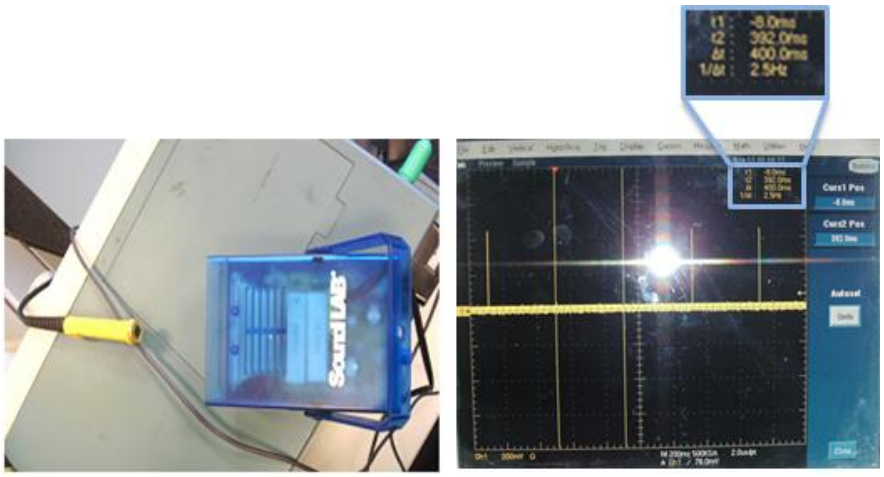

Figure 2. 13 Measuring the strobe light frequency

2.4 fMRI — Regions of Interest (ROI)

Regions of interest were chosen based on the anatomical scans acquired in each session. An ROI analysis was performed on several regions including activated and control areas. Figure 2.14 shows the anatomical structure and the position of the regions of interest used in this study.

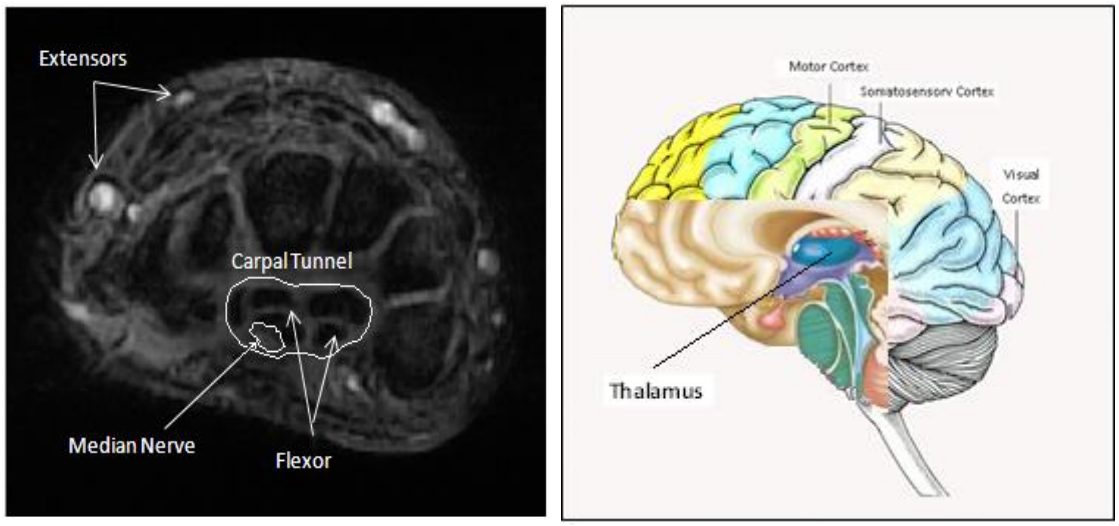

Figure 2. 14 shows the ROIs, left shows the median nerve in the carpal tunnel on an axial MRI image. Right shows the ROIs in the motor sensory cortex and visual cortex (Joseph 2009).

2.4.1 Median Nerve ROIs

The median nerve is responsible for both sensation and movement in the hand by controlling the forearm and hand muscles. Because the median nerve travels through the wrist, this location was used to investigate nerve function in this study. An axial plan was used to acquire the median nerve cross section, the vessels, and normal tissue. Figure 2.15, is a typical MR image showing an axial slice position on the sagittal plane scout image as used for planning the area of interest on the 1.5T scanner.

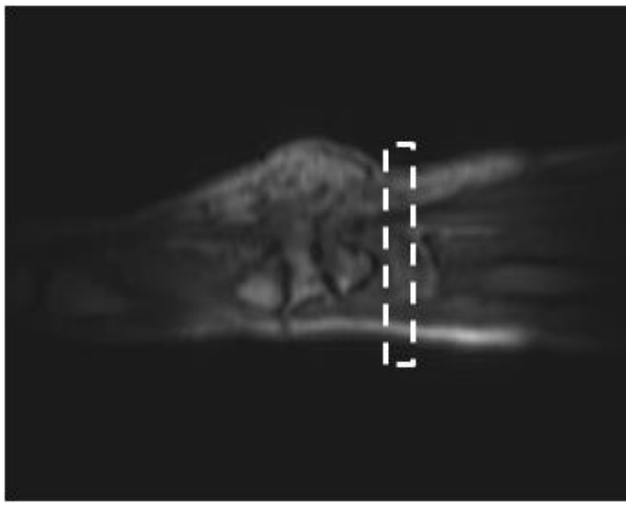

Figure 2. 15 A typical MR image shows an axial slice position in the sagittal plane scout image

2.4.2 Visual Cortex ROIs

Visual function is controlled by the visual cortex in the back section of the brain, which is known as the occipital lobe and which is responsible for processing all visual information as shown in figure (2.14 right). A single oblique axial slice containing the visual cortex was selected from a sagittal scout. Multiple slices were chosen for BOLD fMRI, which uses a longer repeat time than the fast fMRI studies. Figure 2.16 shows these oblique axial slices on a sagittal plane scout aligned with the visual cortex.

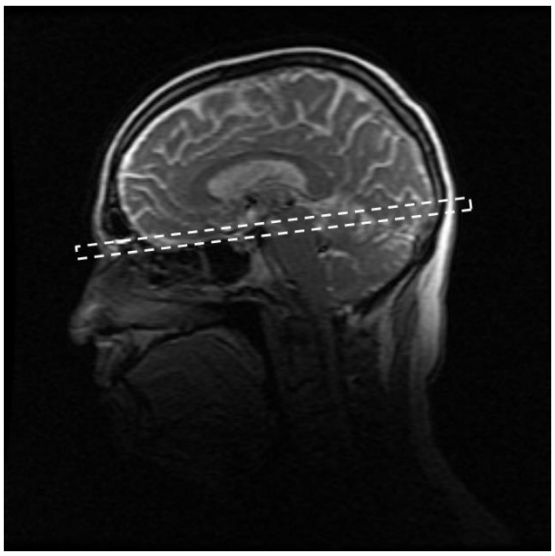

Figure 2. 16 A typical image in the sagittal plane image showing the oblique axial plane slice selected for the visual cortex

2.4.3 Motor Sensory Cortex and Thalamus ROIs

Motor sensory function is controlled by the middle section of the brain, which is known as the motor and somatosensory cortex; these are located in the frontal and parietal lobes as shown in figure 2.14 right. The Motor sensory cortex is responsible for the processing of the body's movements and senses. However, some of the tasks are associated with processes in both these areas, for controlling body movements. The thalamus is formed from gray matter and works as a relay for sensory signals to the cerebral cortex and as a regulator of sensory information. Thus in most motor sensory experiments, thalamus activation has been seen in functional images. In addition, it also receives auditory, visual and sensory signals as well as controlling sleep and awake states.

Oblique axial slices were defined to include the motor sensory cortex and also the thalamus. A second set of slices in the sagittal plane also covered both the motor sensory cortex and the thalamus as shown in Figure 2.17.

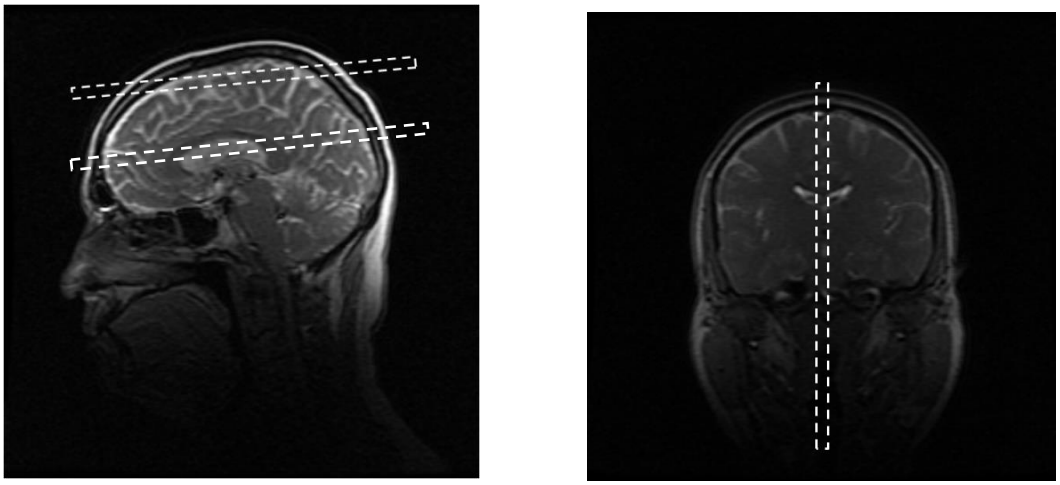

Figure 2. 17 Typical images that show the slices in, left) the sagittal plane image showing the oblique axial plane slice chosen for the motor sensory cortex at the top of the brain and the lower slice for thalamus investigation. Right) the coronal plane image shows the sagittal plane slice selected for the motor sensory cortex and the thalamus as well.

2.5 fMRI Data Acquisition

Experimental parameters to allow detection of the rapid fMRI responses, were based on the short repetition time method (Yang, Cook et al. 2003, Chow, Cook et al. 2007, Paley, Chow et al. 2009). The short TR sequence allows determination of frequency spectra from the fMRI time series which allow high frequency stimulations to be used without aliasing. For example, at 1.5T the minimum TR=88 ms, corresponding to a stimulation bandwidth of 5.68 Hz, while on the 3T scanner, a minimum TR= 63 ms was achieved corresponding to a bandwidth of approximately 8 Hz.

In summary, fast functional MRI and BOLD studies were performed on three different kinds of phantom and twelve normal volunteers on a 1.5T magnet (SignaHdx, GE Healthcare, Milwaukee, USA) and a 3 Tesla magnet (Ingenia, Philips, Best, The Netherlands) using a rapid gradient-echo EPI sequence. The data were collected

individually for both brain and wrist experiments to investigate motor sensory, thalamus and median nerve responses.

2.5.1 Data acquisition at 1.5T MRI

Functional MRI brain data acquisition was performed using a 1.5 Tesla (SignaHdx, GE Healthcare, Milwaukee, USA) with a standard 8 channel phased array radiofrequency head coil. Functional images were obtained using echo planar imaging (EPI), which was used to image the median nerve and entire brain for cognitive fMRI investigations with 500 dynamic scans and a single slice for rapid MRI. Fast fMRI was acquired with the following parameters: slice thickness =5 mm with a repetition time (TR) of 88 ms and an echo time (TE) of 25 ms, 64×64 Voxels, field of view (FOV) 240 mm, flip angle of 90^{o} with 3.75 mm in plane resolution. Each subject had a session of functional imaging that was repeated three times with two different simulation frequencies and control experiments without stimulation. In addition, anatomical images were acquired during each session. Three dimensional anatomical scans, with higher resolution (with good contrast between grey and white matter) were obtained for each subject to provide anatomical reference information for purposes of comparison and finding the regions on the functional images with a total scan time of 2.57 minutes and the following parameters: 3D FSE, 0.8 ms for each shot, flip angle = 90^{o}, FOV = 180 × 180 mm, TR = 5.4 ms, TE = 2 ms and slice thickness of 5 mm. However, for some experiments the parameters were adjusted dependent on the underlying region under investigation.

BOLD fMRI was also performed with the same stimulation frequencies using an 8 channel array head coil. A total scan duration of 120s provided a total of 480 frames using three types of tasks as explained in the previous section. An oblique axial plane was used to acquire both motor sensory and the visual cortices with the following parameters: TE = 25 ms, TR = 2000 ms, frames = 60, number of slices = 8 with no gap, matrix size of 64 x 64, flip angle = 90°, FOV 300 mm and slice thickness of 5 mm. Additional control experiments without any motor sensory or visual stimulation were performed on all volunteers. All experimental data was analysed using the same software method.

2.5.2 Data acquisition at 3T MRI

Rapid fMRI data sets were also acquired at 3 Tesla (Ingenia, Philips, Best, The Netherlands) using a Flex M coil which allows positioning close to the subject to increase SNR in phantom experiments. A highly sensitive 32 channel array head coil was used for all in vivo experiments. The fMRI measurement consisted of 500 echo planar images with a short TR = 65 ms (bandwidth of 8 Hz) and TE=35 ms giving a total scan duration of 32 s. The sequence used FOV=230 mm and matrix=128×128 or 96×96 giving in-plane resolution of 1.8 mm or 2.4 mm, slice thickness =5 mm, flip angle =70^{o}. The slice was selected in an oblique axial plane to include the motor cortex.

Longer scans were acquired with a total duration of 120 s to allow imaging 60 time points with 8 slices (overall 480 slices) for measurement of BOLD effects. This data was acquired with these parameters; TR = 2000 ms, TE = 35 ms, FOV= 230 mm and 8 slices were employed for observing finger tapping responses. The stimulation tasks for this scan were presented in section 2.3.2.3.

High-resolution T1-weighted reference images were obtained for localising ROIs with the following parameters, TE = 4.6 ms, TR=20 ms, voxel size = 1×1.29×1.5 mm and slice thickness = 1 mm.

2.6 Data analysis

Statistical analysis has significantly improved neuroscientists' understanding and interpretation of the nature of fMRI data and improved the ability to obtain relevant results. In this section, the analysis of the fMRI data acquired during the experiments is explained. This analysis connects the raw data from the scanner to the subject region activity. Hence, this allows further information to be gained about brain or nerve responses to relevant tasks. The Matlab analysis program with in-house written software used in this study was based on the General Linear Model (GLM) and also included Principal Component Analysis (PCA) mapping and Fourier analysis of Regions of Interest. The Matlab program analyses data from DICOM files directly without conversion. The major method of analysis of functional MRI images is by comparison of statistical patterns between time series of images in relation to the applied stimulus.

Improved detection of very weak signals from local axonal signals needs improved overall Signal to Noise Ratio (SNR). The Matlab program used to analyse functional magnetic resonance imaging data is based on the General linear model (GLM). GLM has been applied to advanced fMRI signal analysis by explaining the variation of the time course signals and providing the best data fit to the applied stimulation. Figure 2.18 shows the time series for all 500 shots acquired during 44 seconds, and each column represents a single voxel sampled at successive time points. The figure shows the stimulated paradigm as well using the TENS frequency and represents the output of data analysis from median nerve responses investigated using 1.5T with a wrist coil. The data were obtained using echo-planar imaging (EPI) in an axial orientation with TR= 88 and TE = 25 ms. Image size was 64 × 64 pixels (3.75× 3.75 mm).

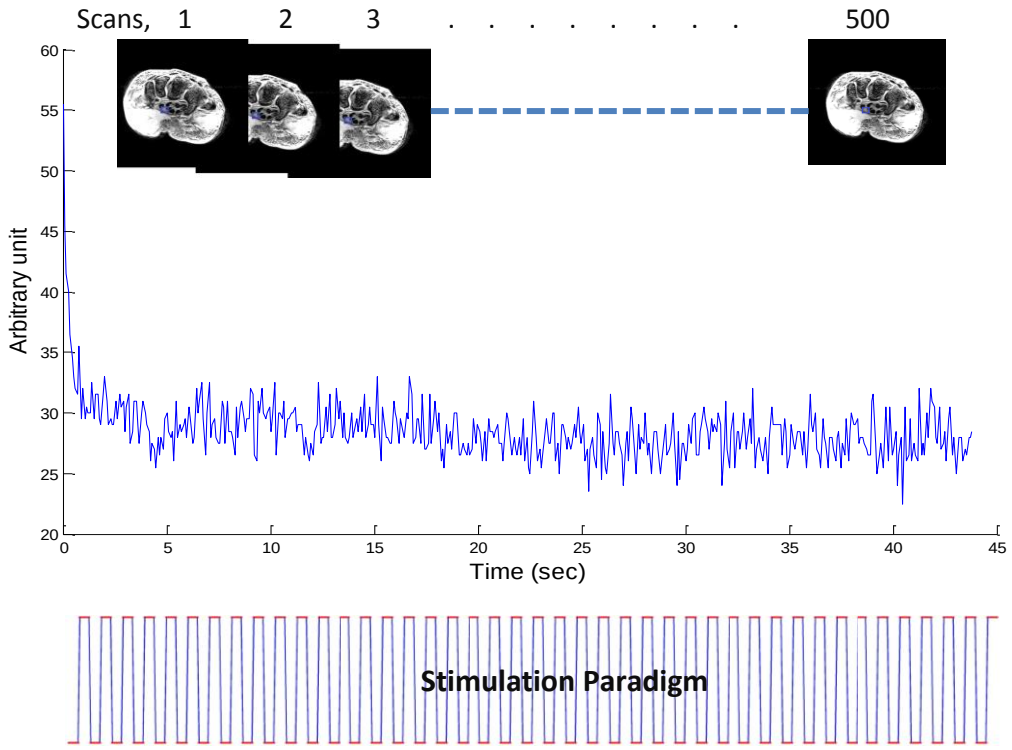

Figure 2. 18: Illustrates the ROI response for all 500 shots due to median nerve stimulation acquired at 1.5T with an 8 channel wrist coil used for median nerve experiments

The program next transfers this time series to a 1D Fourier transform to check the frequency correlation with the applied stimulus. Figure 2.19 is an example of frequency domain analysis of advanced fMRI data using the Matlab toolbox. The figure shows the spectrum without use of any frequency filtering. It clearly shows clear peaks at the respiratory, cardiac and axonal firing frequencies at 03, 1.1 and 2.8 Hz respectively.

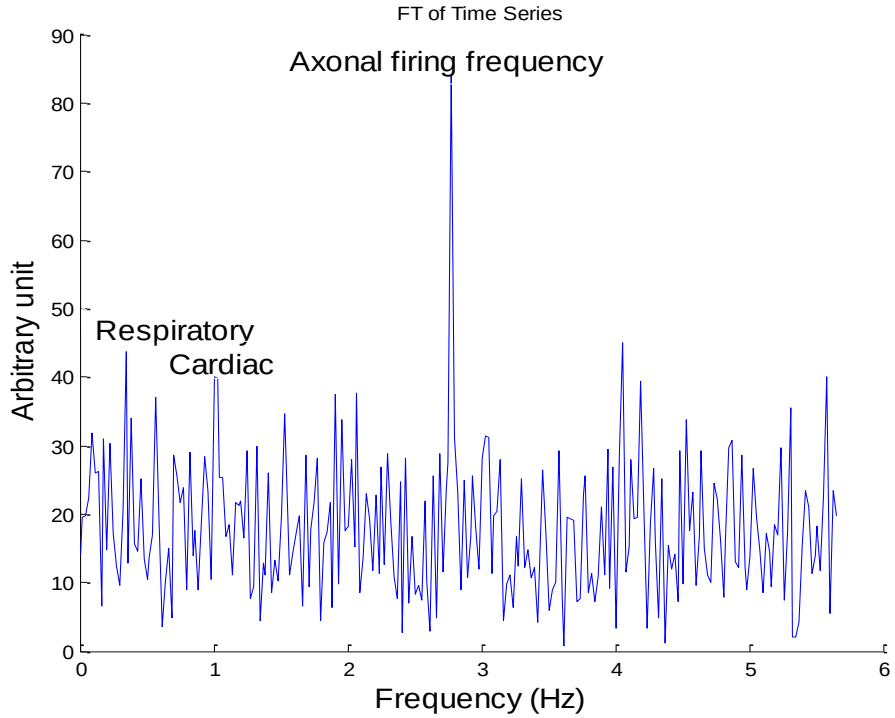

Figure 2. 19: Typical spectrum from the median nerve study, showing frequency response in the range 0 - 6 Hz with peaks at the respiratory, cardiac and median nerve response frequencies due to TENS stimulation acquired at 1.5T with TR= 88 ms.

The same Matlab program code was used for analysis of all experiments. In all the fast fMRI experiments carried out, 500 images or shots of one slice were acquired, resulting in 88 milliseconds per image being used as the time variable used in the analysis program. The BOLD experiments acquired 60 frames of 8 slices at 2000ms per time point thus having a much lower bandwidth in the analysis.

This toolbox has been developed to assist processing and analysis of fast fMRI datasets. In addition, the software offers tools for PCA and SPM analysis, which are principal component analysis and statistical parametric mapping respectively. PCA looks for the major components in the time series and grades them in order, such as PCA1, PCA2, until PCAn while SPM compares time series using a priori known frequencies of stimulation, such as 2.8 Hz. Typical BOLD frequencies are much lower at about 0.05-0.1 Hz.

PCA is a popular tool for the analysis of data from functional imaging experiments due to proficiency to account for unknown yet structured spatiotemporal processes, and has been used to examine different areas during brain function (Viviani, Grön et al. 2005, Suma and Murali 2007, Paley, Chow et al. 2009). It is a tool that detects important variations in high dimensional data in a set of orthogonal directions (Jolliffe 2002). The PCA technique decomposes the data in a new coordinate system and ranks them according to their contributions to the variability of the data from most to least important significant variations in the acquired fMRI data. SPM essentially performs a statistical t-test between on and off times within a time series.

There are several common objectives and steps to analyse fMRI data and many software programs have been developed for this purpose. First of all, before processing, there is movement and spin history correction to compensate for when the volunteers have moved inside the scanner. This problem was minimised in the current study by using very short acquisition times and careful monitoring of the acquired data for possible movement artifacts in cine mode. In addition, there is the possibility for spatial smoothing and temporal filtering of the data. These steps are for reducing or treating artifacts and improving signal to noise ratio. However, to investigate very fast, localised responses these steps are not used as they blur out the required information. Time series models were used to test whether the brain activity was related to the input function parameters. The aim was

to find precisely which part of the brain was active or responded to stimuli that were presented to the subjects.

The following figure, Figure 2.20 is a schematic diagram of the Matlab program which shows the basic steps of input, processing and output for fMRI data analysis. The first step in the diagram is preparation of the raw data (fast fMRI or BOLD fMRI) as a set of DICOM files. In this study, 500 image time points of a single slice were acquired for fast fMRI and 60 image time points with 8 slices for BOLD fMRI were used. After entering the first image number, the next step requires setting of the parameters used during scanning, such as the number of frames, width and height of the image (number of voxels), stimulated frequency, scan duration, slices (if multiple slices were acquired as with BOLD), start slice, Z score which defines the significance level of the test (typically Z=2.5) and the repetition time which allows the aliasing free frequency range measured to be defined in the programme (fmax = 1/2TR). The program starts by reading all the images that are acquired during the scan. The program also requires selection of the region of interest, which is done in coordination with the anatomical images. However, the active region can be selected in terms of the active voxel (high contrast) in the processed image or can be selected depending on the task-related region. Finally, the program produces a time series graph and Fourier transform of the time series on which the possible stimulus responses are shown.

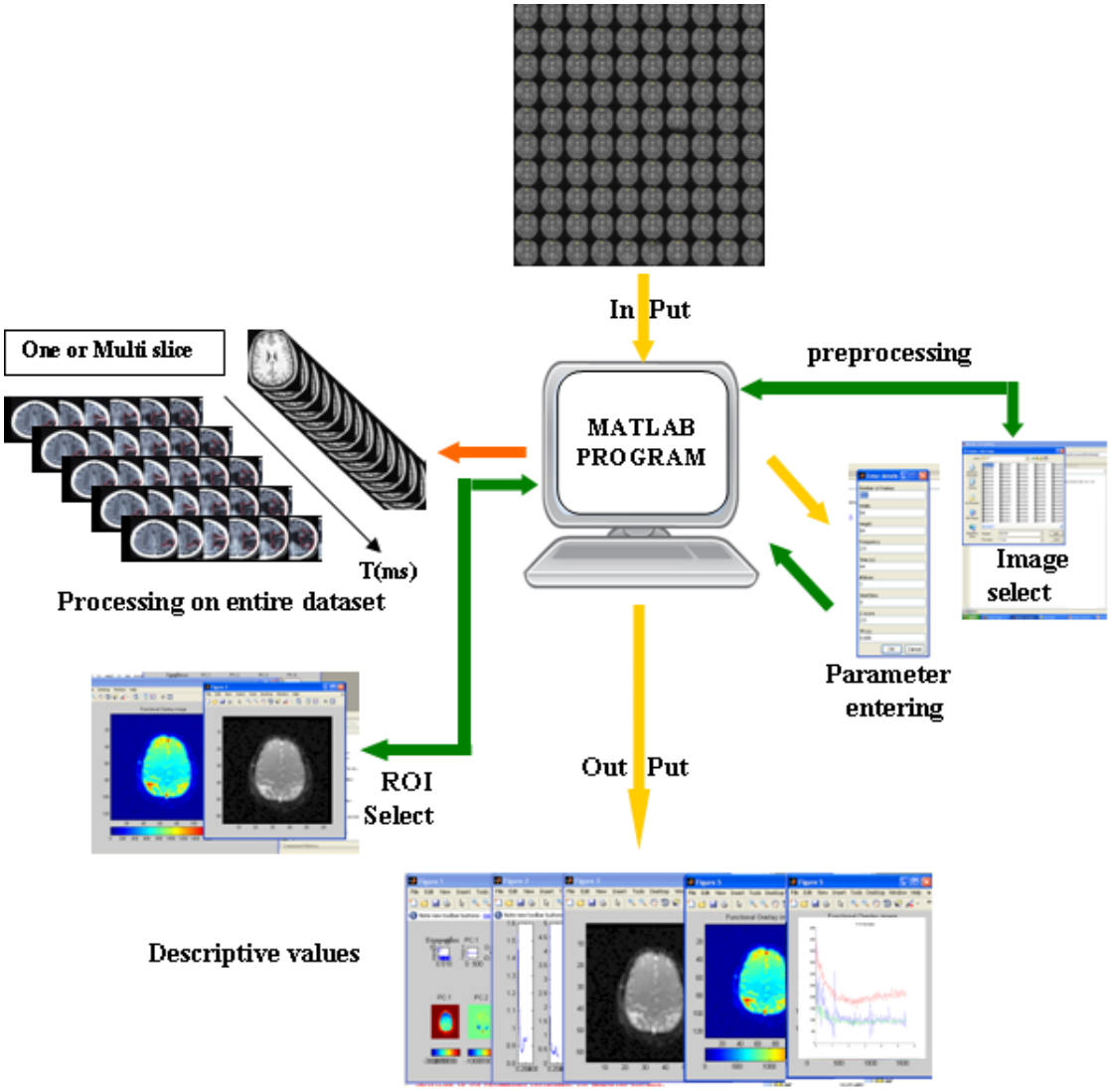

Figure 2. 20 Schematic of Matlab processing program

Chapter 3: Phantom experiments to estimate minimum magnetic field detection capability for rapid, electromagnetic functional MRI

3.1 Introduction

In this chapter, a Lorentzian model which relates the observed percentage MRI signal changes to a given magnetic field modulation is described. In addition, experiments which were performed on neuronal model phantoms designed to simulate the fields generated by firing neurons and axons are also presented. These experiments were performed at both 1.5T and 3T and provided information to help design the subsequent *in vivo* studies and to verify the sensitivity of the scanner to detect and pinpoint the firing of action potentials in axons and neurons. A TENS machine was used to produce weak, short transient currents in both a conductive gel and a conductive solution to simulate the firing of a set of axons. Factors affecting the sensitivity and detection limits of MRI for the detection of ultra-weak magnetic field changes are also discussed. Previous experimental studies have generally used sinusoidal or square wave frequency sources rather than short duration pulsed sources which better mimic axonal pulses.

3.2 Lorentzian Model to calculate the MRI signal percentage change for a given modulating magnetic field

The signal percentage change can be found theoretically using a Lorentzian model as described in formula 3.1 for the signal from a Gradient Echo sequence (Kennan, Zhong et al. 1994, Chow, Cook et al. 2006).

$$\% \left|\frac{\Delta S}{S_{eq}}\right| = 100 \times [1 - e^{-TE\gamma \Delta B_{cg}}] \qquad (3.1)$$

where: S_{eq} is the fully relaxed equilibrium signal, B_{cg} is the magnetic field around the conductive gel, and γ is the proton gyromagnetic ratio 42.577 MHz/T.

Therefore, to find the percentage signal change in all following studies, this equation was used.

3.3 Experimental Results in Phantoms at 1.5T

This section tests the implementation of a phantom which used a TENS machine to apply short electric pulses, simulating transient axonal pulses, to both; 1) a conductive gel and 2) a conductive solution in a micro test tube to simulate nerve function (further details about these phantoms were presented in the methodology chapter 2).

3.3.1 Neuronal/Axonal Simulating Phantom using Conductive Gel

A TENS device was used to simulate the short action potentials generated by axons in the conductive gel phantom described in Chapter 2. The gel (Signa Gel; Parker Laboratories Inc., Fairfield, NJ, USA) was smeared on the surface of a spherical phantom in a layer of 1 cm width and 2.5 cm length and approximately 1 mm thickness. An ohmmeter (Model 175, Fluke, Everett, WA, USA) was used to measure the resistance and Ohm's law used to calculate the applied current. The electric pulsation from the TENS machine generated a voltage V_p = 80 volt for a duration of 260 μs. Therefore, peak current flowing through the gel during pulsation was 44 ± 2 μA. The induced magnetic field around the area close to the gel, which was selected in the GE-EPI magnitude image at 5mm from the pulsation source was calculated using Ampere's law. The conductive gel field strength was calculated using the following equation (3.2).

$$B = \mu_o I/2\pi r \qquad (3.2)$$

where; μ_o is the permeability of free space ($4\pi\times10^{-7}$ H/m), and r is the radius (distance from the source).

Figure 3.2 shows the localization of a typical example of a fast fMRI experiment and the selected ROI (indicated by a blue box on a GE-EPI magnitude image of the spherical phantom), a 1×1 voxel with a voxel size of (3.75 × 3.75× 5) mm^3 used to analyse two

different stimulation frequencies (2.8 Hz and 3.7 Hz). In addition, control experiments were performed with the same acquisition parameters but no stimulation. Data from the ROI was processed in MATLAB with the code described in Chapter 2.

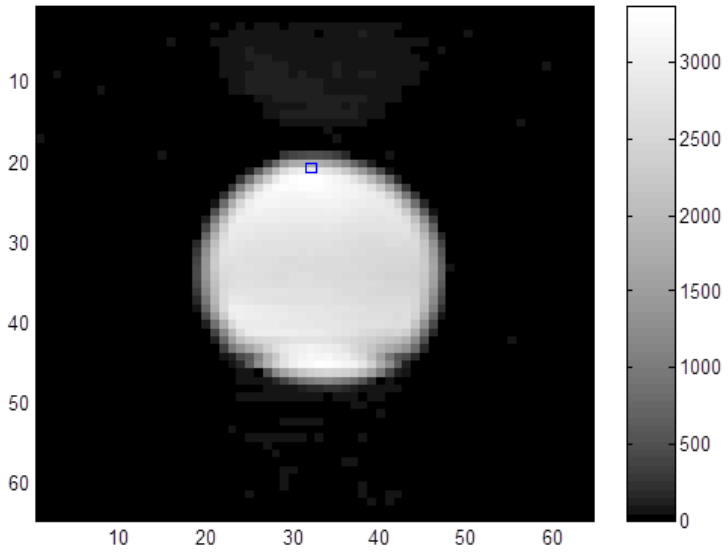

Figure 3. 1: GE-EPI magnitude image of the spherical phantom. Two different stimulation frequencies were applied to an electrically conducting gel used to simulate nerve function. The ROI (3.75× 3.75× 5 mm^3) selected for spectral analysis was located directly below the conducting gel.

It is obvious from figure 3.2 there is no significant peak in the 1D Fourier transform of the time series of 500 images in the control experiments.

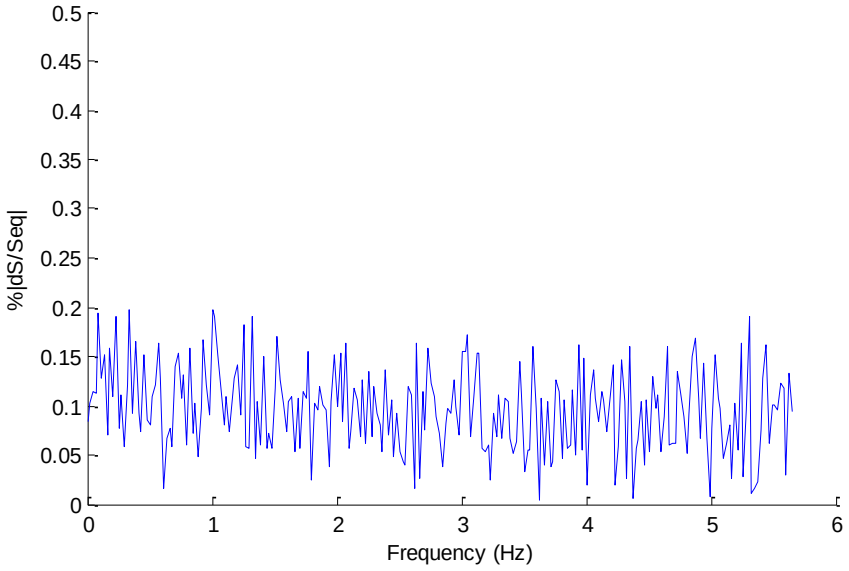

Figure 3. 2: Fourier transform of the MR time series showing the Frequency spectrum for the selected ROI in the phantom used conductive gel without stimulation during TR= 88 ms- typical experimental

Figure 3.3 shows two different frequencies from an acquisition using conductive gel at 2.8 and 3.7 Hz, using a Z score = 2.5. This figure shows significant response to the electric pulsation when compared to the control experiment.

The 1D Fourier transform of the time series from the selected voxel, showing a possible response at 2.8 Hz with a SNR of 4:1 (figure 3.3 top). Figure 3.3 bottom shows a different TENS frequency of 3.7 Hz. The SNR of the response peak was 3:1. The full equilibrium signal value of conductive gel at 1.5T was corrected by using an assumed T1 relaxation time of 280 ms, which is close to fat (de Bazelaire, Duhamel et al. 2004, Rakow-Penner, Daniel et al. 2006). Then, the mean percentage signal change for the TENS pulsation frequencies 2.8 and 3.7 Hz was 0.19 ± 0.01 % using the calculated magnetic field generated from the conductive gel. This change corresponded to a mean magnetic field of 1.8 ± 0.1 nT according to equation 3.1, and was generated by a current through the conductive gel of about 45 µA. The mean SNR at this frequency was also 4:1.

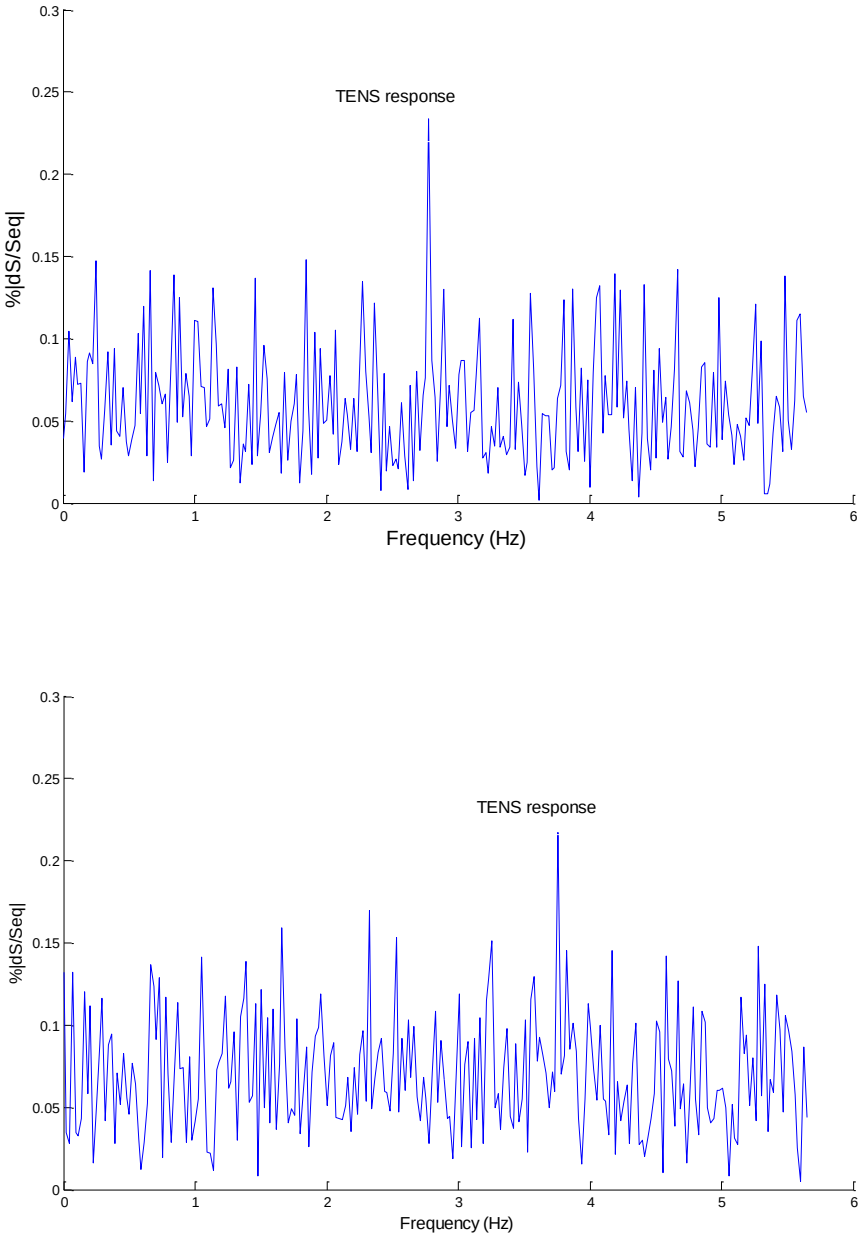

Figure 3. 3: shows the spectral responses from the ROI in the phantom shown in Figure 3.2 during TENS pulsation. (top) shows the response at TENS device pulsation frequency of 2.8 Hz and (bottom) current supply pulsation at 3.7 Hz.

Fig. 3.4 shows the General Linear Model (GLM) functional analysis of Experiment 1 using the electrically conducting gel. Activation was thresholded at a Z-score of 2.5. These responses show the detection at 1.5T MRI of the weak magnetic field of around 1.7 nT generated by the transient currents flowing through the gel. The signal to noise ratio (SNR) was >=4:1. There was a significant difference from the control experiment.

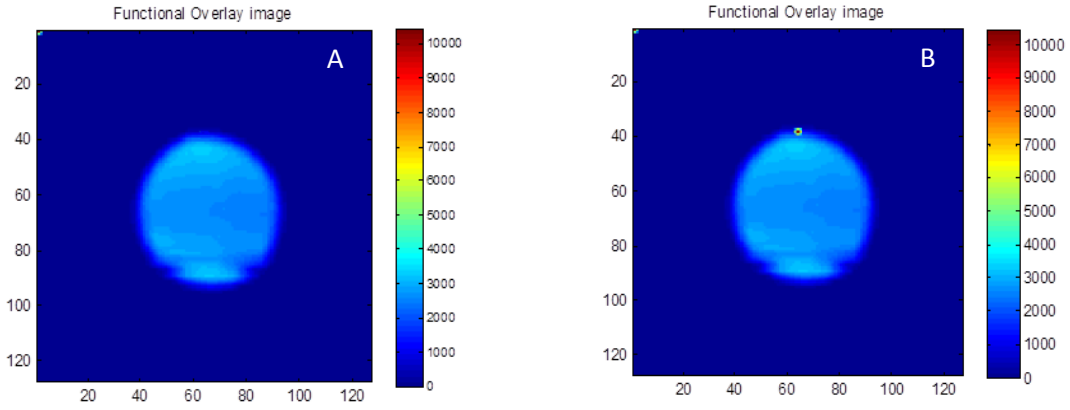

Figure 3. 4: Functional overlay images for current applied to the conductive gel on the surface of the spherical phantom at a frequency of 2.8 and 3.7 Hz. Images were acquired at 1.5 T MR with fast fMRI using a short TR = 88 ms and TE=25 ms. The Z-score applied to the analyses was 2.5. Pixels highlighted in red show locations where the Z-score is greater than the applied threshold.

3.3.2 Neuronal/Axonal Simulating Phantom using NaCl Conductive Solution at 1.5T

These experiments were carried out at 1.5T using the small tube phantom. This was placed next to a larger cylindrical water phantom (20 mm in diameter and 35 mm in length) to assist the scanner perform sequence calibration. Again the modulating magnetic field was generated by applying electric pulsation from a TENS machine applied through twisted pair copper wire inserted into the ends of the tube and sealed. More details on the phantom parameters were presented in the previous chapter, section 2.2.

Based on the measured resistance, this experiment used 8 µA current generated by the 80V pulse from the TENS machine. The predicted signal percentage change for this magnetic field, using the Lorentzian model, was expected to be detectable.

Figure 3.5 shows the GE- EPI magnitude image in grey scale and an ROI (1×1 voxel, blue box) selected in the solution phantom with a voxel size of (3.75×3.75×5) mm^3 and applied electrical pulsation frequencies of 2.8 and 3.2 Hz.

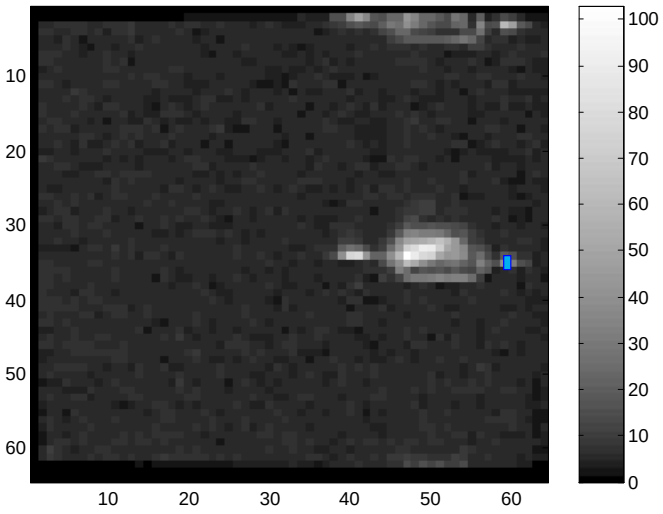

Figure 3. 5: show the GE-EPI magnitude image and the Region of Interest selected, 1×1 voxel with a voxel size (3.75×3.75×5mm^3), in each frame of the EPI sequence using short TR=88 ms at 1.5T

The NaCl solution experimental results for two different frequencies are given in figure 3.6. For the first frequency the TENS pulsation was clearly observed at 2.8 Hz (figure 3.6 top). This peak corresponds to the selected 1×1 voxel ROI (figure 3.5) on the right side of the tube acquired using the 8 channel wrist coil.

The second set of results was from TENS pulsation at 3.2 Hz. The same ROI was analysed on the GE-EPI magnitude image. The measured percentage signal change using the full equilibrium signal value of NaCl at 1.5T corrected using a T1 relaxation time of 1550 ms (Demangeat, Gries et al. 1997) was 0.04 ± 0.01%, with mean SNR = 3:1.

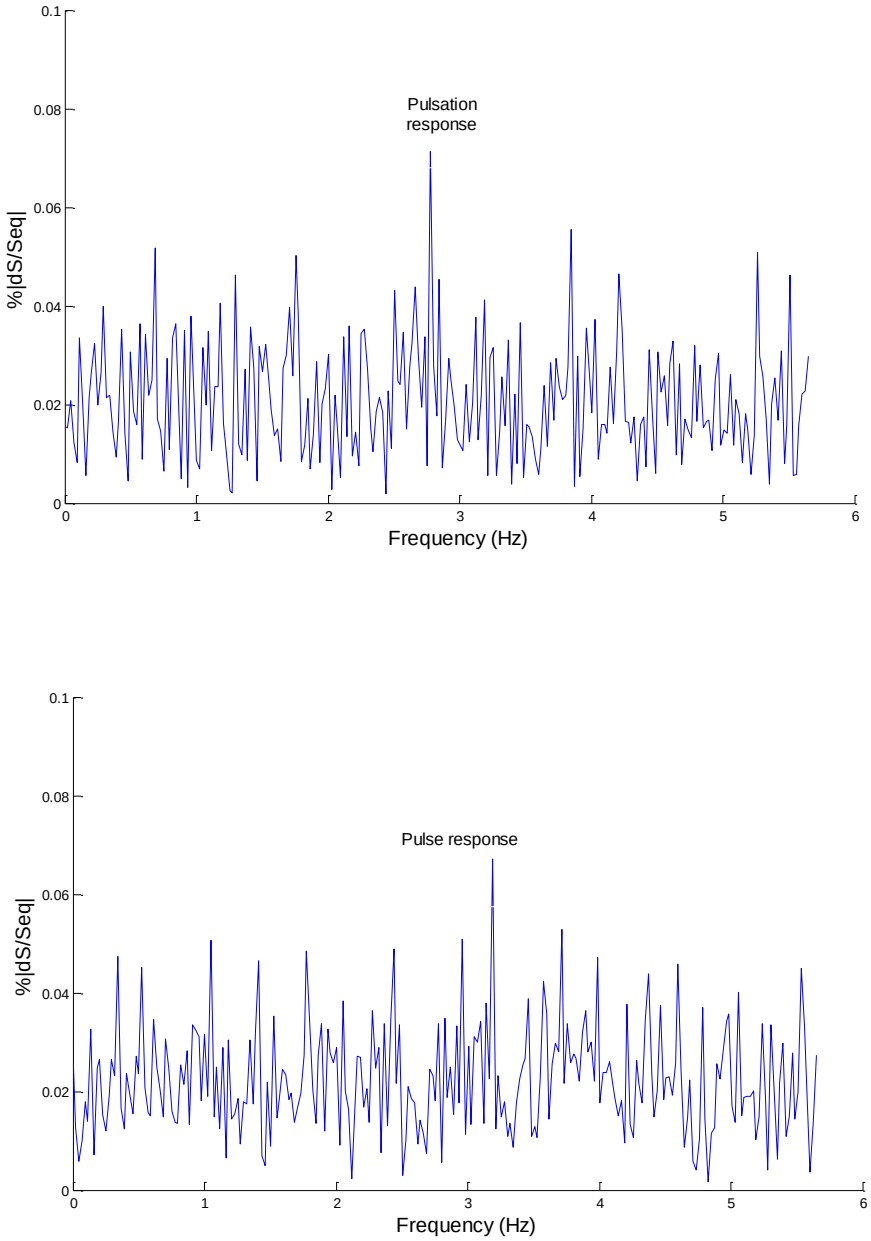

Figure 3. 6: show the 1D Fourier transformation of the time series. Top) shows the electric pulsation rate at 2.8 Hz and bottom) shows the response at 3.2 Hz, which was the TENS pulse frequency. Acquisition parameters were TR = 88 ms, TE = 25 ms, acquisition matrix = 64x64, using 8 channel wrist coil.

3.3.3 Neuronal/Axonal Simulating Phantom using NaCl Conductive Solution at 3T

The NaCl conductive solution phantom was also imaged on a 3T scanner. However, for this experiment a spherical water phantom was used to provide additional signal to allow calibration of the imaging sequence. A 32 channel array head coil was used for image acquisition. Figure 3.8 shows the ROI selected in the spherical phantom (blue box). Acquisition parameters for the EPI sequence were TR =63 ms, TE=25 ms image matrix =96x96, SLT = 5 mm. The selected ROI was about 5 mm in distance from the NaCl solution phantom. Therefore, the magnetic field at this distance according to Ampere's law can be calculated and used to predict signal percentage changes using the Lorentzian model.

The ROI selected on the GE-EPI magnitude image was (2.5×2.5×5) mm^3 and showed clear spectral responses to the TENS electric pulsation at the applied TENS frequencies of 3.8 Hz and 5.2 Hz.

Figure 3.8 shows the observed percentage signal changes. With TR = 63 ms, there is an 8 Hz effective response bandwidth. This was slightly wider than was achieved in the experiments at 1.5 T. The mean SNR values were 4:1 for both responses at 3.8 Hz (a) and 5.2 Hz (b) and the mean percentage signal change was 0.03 ± 0.02% corresponding to mean generated magnetic field 0.29 ± 0.01 nT.

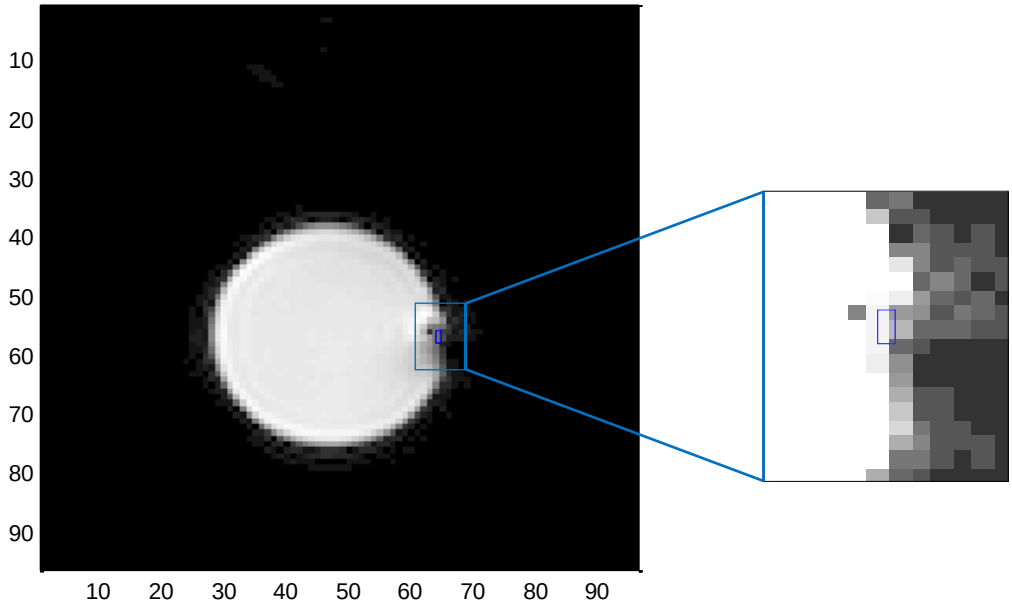

Figure 3. 7: GE-EPI magnitude image showing the Region of Interest selected on the spherical phantom with voxel size of (2.5×2.5×5 mm) in each frame of the EPI sequence. Electric pulsation rates of 3.8Hz and 5.2Hz were applied with acquisition parameters TR=63ms, TE=25 ms, image matrix = 96x96, SLT=5 mm using a 32 channel head coil

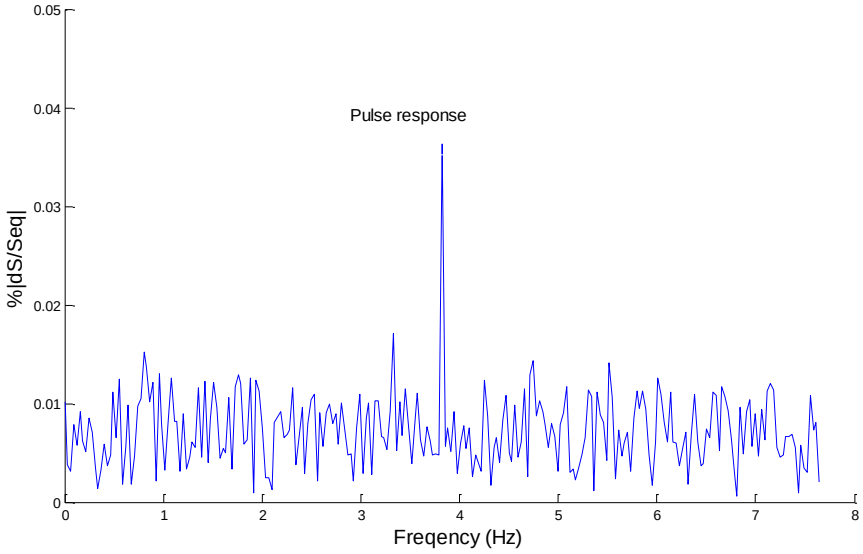

(a)

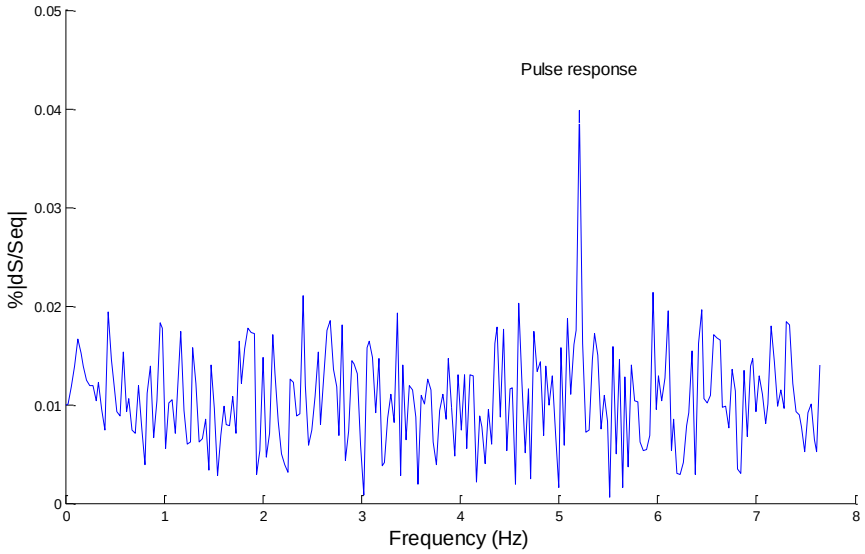

(b)

Figure 3. 8: Typical experimental results showing two different frequencies 3.8 and 5.2 Hz using fast fMRI TR = 63 ms with a TENS paradigm applied to the solution a) Measured frequency spectrum shows response at the applied pulse frequency of 3.8 Hz. b) shows a response at 5.2 Hz. These experiments were acquired at 3T

Experimental results for the phantom study performed at 1.5T and 3T are summarised in tables 3.1. 7 out of 19 experiments were successful on all phantoms with a 37% detection rate. The mean percentage signal changes were 0.19 ± 0.01 % for the conductive gel and 0.3 ± 0.04% for the NaCl solution.

Table 3. 1: recorded percentage signal change, generated magnetic field and SNR using different frequencies, phantoms and scanners

Experiments	Frequency (Hz)	%|ΔS/Seq|	ΔB (nT)	SNR
Conductive Gel	2.8	0.2	1.8	4:1
	3.7	0.18	1.7	3:1
Solution tube at 1.5T	2.8	0.04	0.37	3:1
	3.2	0.03	0.35	3:1
Solution tube at 3T	3.7	0.03	0.3	4:1
	5.2	0.03	0.38	4:1

3.4 Discussion of Fast fMRI Sensitivity for Direct Neuronal/Axonal Detection

In this chapter, statistical maps of neuronal/axonal simulating phantoms have provided both qualitative and quantitative assessment of the sensitivity of fMRI using EPI T2* contrast with rapid TR acquisition methodology. In this experiment using conductive gel, the external magnetic field used was 1.8 ±0.1 nT and the signal percentage change was 0.19 ± 0.01 %. This field is higher than expected for axonal magnetic fields.

The challenge for in vivo detection is thus, if the field generated by the firing axons is less than the minimum value measured here with the NaCl tube phantom, the SNR will fall below a detectable level of 3:1 leading to false negative results.

In this chapter, experiments were performed at both 1.5T and 3T, responses were clearly measured at the applied TENS frequency with sufficient SNR of 3:1 and 4:1 for both scanners respectively.

Current applied to a conductive gel from a TENS machine was used to mimic transient currents from neuronal and axonal activity with a relatively randomly oriented electrical current distribution. A field generated by the conductive gel was detectable with a 0.19 ± 0.01% signal change on the predicted equilibrium signal. In addition, a current pulsation of a micro test tube of NaCl solution could mimic a nerve; the generated magnetic fields in these experiments was 0.35 ± 0.03 nT due to chosen conductivity of the solution. These fields changed the magnetic field by 0.03 ± 0.005% of the predicted equilibrium signal.

Bodurka and Jesmanowicz calculated the magnetic field due to insulated thin copper wire that was supported by a plastic frame (3-inch long and 2-inch wide)(Bodurka, Jesmanowicz et al. 1999). The magnetic field strength 1.7 ± 0.3 nT was applied using a low frequency of 0.25 Hz and measured at higher TR=200 ms with a 3T magnet. Truong and others presented a study using phantom gel that consisted of carbon wires with long TR=1000 ms at 4T (Truong, Wilbur et al. 2006). They used the Lorentz effect imaging technique and a range of currents (0-500 μA) and the signal was observed on one side of the wire. They indicated that the magnitude images were not significantly affected by induced current or by eddy currents.

Our result in the micro tube shows the SNR at 3T is slightly higher than 1.5T, 4:1 compared to 3:1 respectively. However, this result refers to the use of different coils, a 32 channel head coil in the 3T and an 8 channel wrist coil in the 1.5T experiments. The use of coils with higher channel count are more sensitive and detect with higher SNR (Salomon, Darulova et al. 2014). However, the wrist array coil volume is considerably smaller overall than the 32 channel head coil, even though coil element sizes may not differ by too much

The results in this study clearly demonstrate the feasibility of imaging with currents on the order of microamperes and fields of the order of a nanoTesla with a temporal resolution on the order of milliseconds in gel and solution phantoms. Therefore, the results obtained in this work with fast fMRI constitute a promising step towards future work that will result in direct imaging in vivo detection of electric neuronal activity.

Chapter 4: Rapid functional MRI measurements of the wrist using TENS stimulation of the median nerve

4.1 Introduction

As positive results were found in the previous chapter from phantoms, it was then proposed to investigate the possibility of demonstration of neuronal current effects on MRI in vivo. In this chapter, the investigation was performed by recording a time series of dynamic MR images from the median nerve during stimulation of the wrists of adult volunteer subjects and correlating the stimulation frequencies with the MRI responses.

The median nerve was chosen for these experiments as it is positioned in the same direction as the z axis (main magnetic field), the ionic currents in the median nerve flow across the membrane and along the median nerve producing components of a transient magnetic field both perpendicular and parallel to the main magnetic field B_o field as illustrated in fig 4.1. Due to the magnetic field from the median nerve, the signal of the MR can potentially be modulated in phase and amplitude. These modulation components change dependent on the voxel position and its size. The normal median nerve, at the ROI used in this study, has an average cross-sectional measurement of 7-11 mm^2 (Middleton, Kneeland et al. 1987, Monagle, Dai et al. 1999, Uchiyama, Itsubo et al. 2005, Kunze 2010) and when correlated with subject age and body mass index, contains nerve bundles varying from 13-38 in number. Each bundle consists of 2×10^6 nerve fibres (the axons vary in diameter between 0.7 and 10 μm) that are oriented in parallel. When the median nerve is stimulated synchronously, all axons fire with the stimulated frequency and generate ionic currents. Therefore, we assume that the median nerve acts like a current source, and the magnetic field generated from the axons bundle at the wrist can affect the main magnetic field.

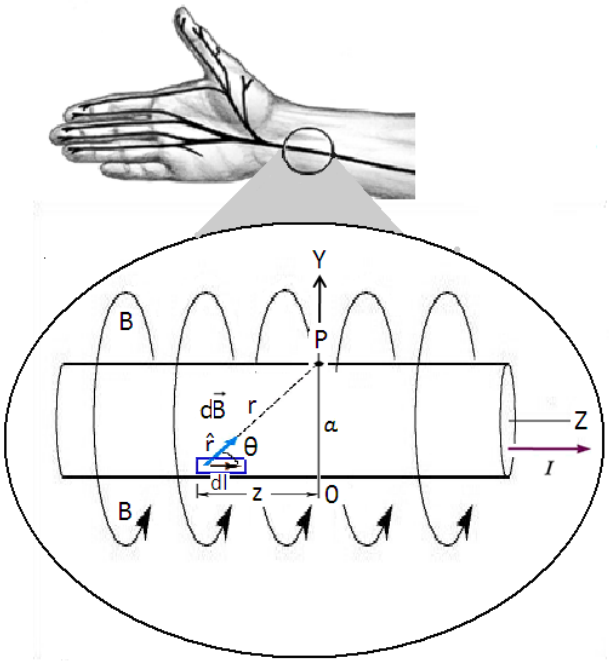

Figure 4. 1: Diagram of the median nerve, depicting the magnetic field of the transient current at the wrist that shows the magnetic field lines which carry an ionic current to form circles around the median nerve. Assuming a wire model for the field B, the direction of the magnetic field (Y-axis) is perpendicular to the median nerve (Z-axis) in the direction of the ionic current.

The aim of this study was thus to investigate whether fMRI responses can be measured during median nerve activity. The median nerve was stimulated at the threshold of action potential generation using transcutaneous electrical nerve stimulation (TENS).

In this chapter, experimental results are presented. First, a set of control experiments were performed without stimulation during all imaging sessions with the subject in a rest state. Then, data was acquired with two different stimulation frequencies on each subject, with frequencies ranging from 2.1 to 4.1 Hz. Each data set was carefully analysed for artifacts and for stimulus correlated modulation peaks which had a signal to noise ratio threshold of > 3:1. Finally, the difficulties and challenges of carrying out these experiments is discussed.

4.2 Control Experiments

4.2.1 Acquisition methodology

Seven healthy volunteers were studied using the TENS stimulation paradigm given in figure 2.7 in chapter 2 section 2.3.2.1. These experiments were performed on the 1.5T MRI system with an eight-channel wrist coil as described in Chapter 2.

4.2.2 Experimental results

There were a total of 17 control experiments performed during the wrist study. Each subject was first imaged without application of TENS stimulation as a control experiment, to carefully locate the median nerve. Figure 4.2a shows the anatomy of the wrist at the location used for imaging. Figure 4.2b shows the MRI reference image used to locate ROIs in the structures of interest.

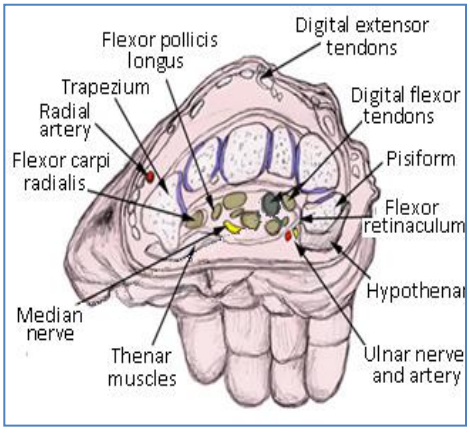

a

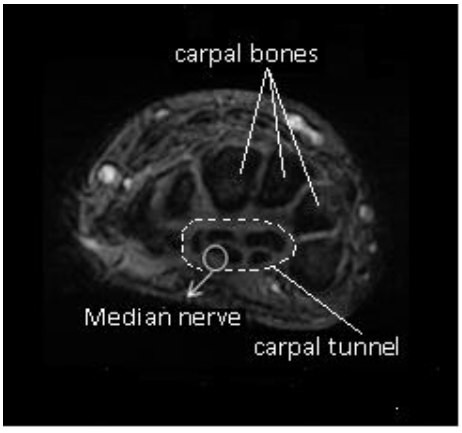

b

Figure 4. 2: a) Anatomical illustration - cross section of the wrist showing the median nerve position (Ethan et al. 2013). b) 3D wrist MRI anatomic image, T1-weighted axial view showing carpal tunnel including the median nerve.

The blue box 1×2 voxel in Figure 4.3a (voxel size 3.75 × 3.75× 5 mm^3) shows the corresponding location of the median nerve in the EPI functional image. The resulting response for the selected region of interest in the median nerve is shown in Figure 4.3b. It can be seen there is no response during control experiments. This represents the 1D Fourier transform of the time series of 500 fMRI acquisitions from the selected ROI. The horizontal scale represents a total frequency range of 6 Hz. This experiment showed peaks correlated with the subject's heartbeat and respiration rate only at 1.1 and 0.3 Hz respectively. No response was recorded from the location of median nerve as recorded in the stimulated experiments as shown in next section.

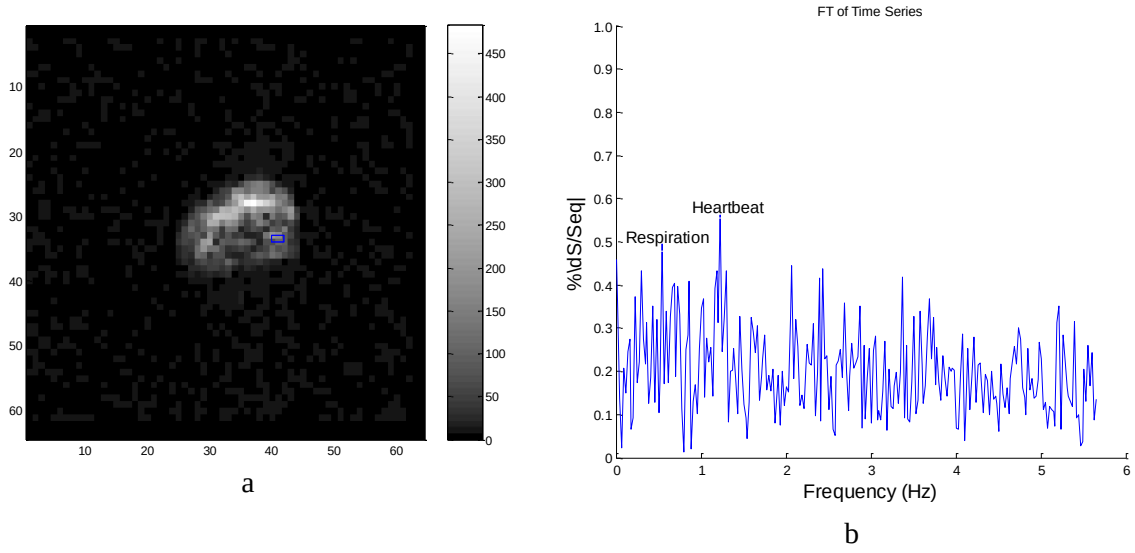

Figure 4. 3: a) GE-EPI magnitude image of the median nerve in a human volunteer wrist. b) Fourier transform of MR time series showing the frequency spectrum for the selected ROI in the median nerve without stimulation – result for a typical control experiment.

4.3 TENS Stimulation Experiments

4.3.1 Acquisition methodology

A time series of 500 images was acquired during stimulation of the median nerve using the TENS machine using the methodology described in chapter 2.

4.3.2 Analysis of different regions within the selected slice

Despite physiological noise deriving from sources such as cardiac pulsation, respiration and possible BOLD changes, significant responses during median nerve stimulation could be detected in most of the experiments. Fast fMRI responses detected during median nerve stimulation sessions were compared statistically with the control experiments. The response amplitudes and frequencies were quantified and analysed in the median nerve, vessels, and other regions of the wrist for each stimulated frequency during nerve activation. Two different frequencies were chosen for median nerve TENS stimulation in the range 2.1 to 4.1 Hz, for every subject in every imaging session. Figure 4.4 shows results from two different subjects acquired using a wrist coil, the first stimulated at 2.8 Hz and the second subject at 3.6 Hz. Two different ROIs were chosen (blue and red boxes), as shown in figures 4.4a and 4.4c, corresponding to the median nerve and other tissue within the wrist. Typical ROI sizes were 1x1 or 1x2 voxels. The blue traces show frequency spectra from the 1D Fourier transform of the MR time series from the ROI located in the median nerve. Spectral response peaks were observed at 2.8 Hz and 3.6 Hz, which were the actual TENS stimulation frequencies applied during imaging. In addition, weaker peaks were observed from these ROIs due to the heartbeat (approximately from 0.9 to 1.1 Hz) and respiration (between 0.2 to 0.3 Hz) from these subjects as well as a possible BOLD effect at very low frequency. The spectra shown in figures 4.4b and 4.4d from other tissue outside the median nerve region (red traces) exhibited no significant changes at 2.8 and 3.6 Hz; however, small physiological responses were seen, as mentioned before. These are typical of the positive results acquired from all the experiments although yielding a relatively low SNR = 3:1

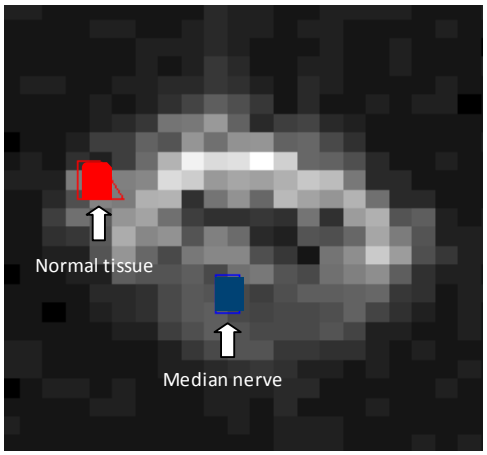

a

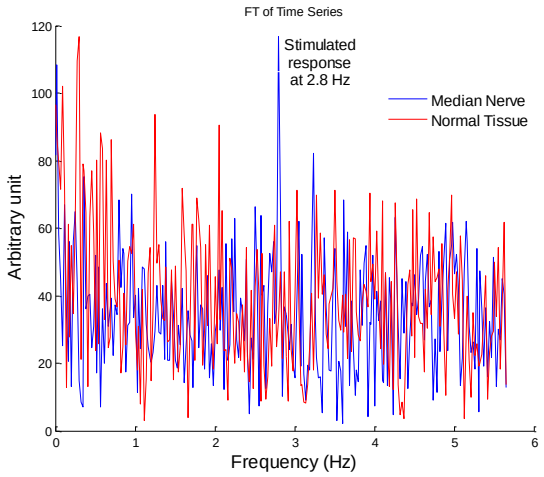

b

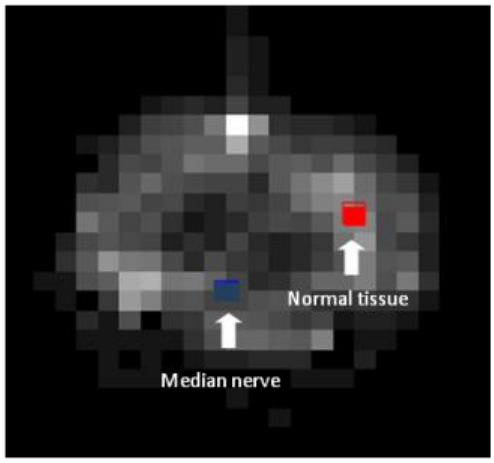

c

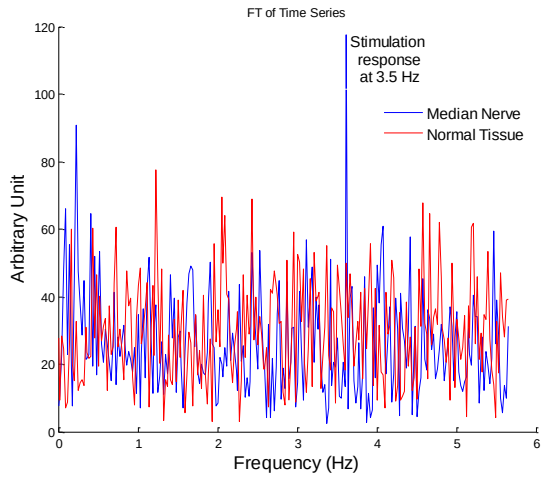

D

Figure 4. 4: Two different regions were selected in the median nerve (blue box) and another for muscle tissue that was chosen randomly (red box) during median nerve stimulation using a TENS machine at 1.5T. Mean GE-EPI shows two selected boxes coloured in blue and red as the ROIs for median nerve and normal tissue respectively. a) GE-EPI wrist cross section slice at stimulation frequency at 2.8 Hz, b) Measured frequency spectrum shows significant response at 2.8 Hz in the ROI In the median nerve (blue trace) and no significant response in normal tissue (red trace), c) Mean GE-EPI magnitude image at 3.5 Hz stimulated frequency shows selected ROI, blue box, in the median nerve and red box in the normal tissue, and d) Measured frequency spectrum shows response at the applied frequency as a blue trace with no peaks at the applied frequency in normal tissue. However, there were also peaks at about 0.3 Hz and 1 Hz corresponding to the respiration and heartbeat respectively in both experiments.

The peaks at the stimulated frequencies from these ROI were significantly different from the non-stimulated control experiments, according to a SPSS t- test ($p<0.05$), for all the positive experiments. Similar results were observed at the correct frequency with SNR > 3:1 in 29 out of 34 experiments from the median nerve with TENS stimulation at these relatively high stimulation frequencies (between 2.1 to 4.1 Hz).

4.4 Estimation of the magnetic field from the median nerve and expected signal percentage changes for the MRI magnitude signal

The external magnetic field from the median nerve due to a propagating action potential can be calculated from equation (4.1) (Chow et al. 2005), assuming that the magnetic field of the transient current through the median nerve has an effect over a range of 5 to 10 μm. This assumption is required to see the signal changes in MRI using TR = 88 ms and TE = 25 ms. From figure 4.6, at stimulation frequencies 2.7 Hz and 3.8 Hz, the signal percentage change due to this local field can be calculated by correcting for T1 relaxation to equilibrium.

$$\%|\Delta S/S_{eq}|=100\times[1-e^{-TR/T1}] \qquad 4.1$$

where: ΔS is the external magnetic field signal during stimulation (the signal from the ROI in the centre of the response peak as shown in these two typical experiments in figure 4.5).

S_{eq} is the signal relaxed to a state of equilibrium.

The fully relaxed signals were calculated for all subjects, an example for two typical experiments is shown in figure 4.5, which were stimulated with two different frequencies. A measured T1 relaxation time for the median nerve of 915ms was used, which is assumed to be similar to that of the sciatic nerve measured at 1.5 T, because the T1 of the median nerve has not previously been reported (Shen, Wang et al. 2008).

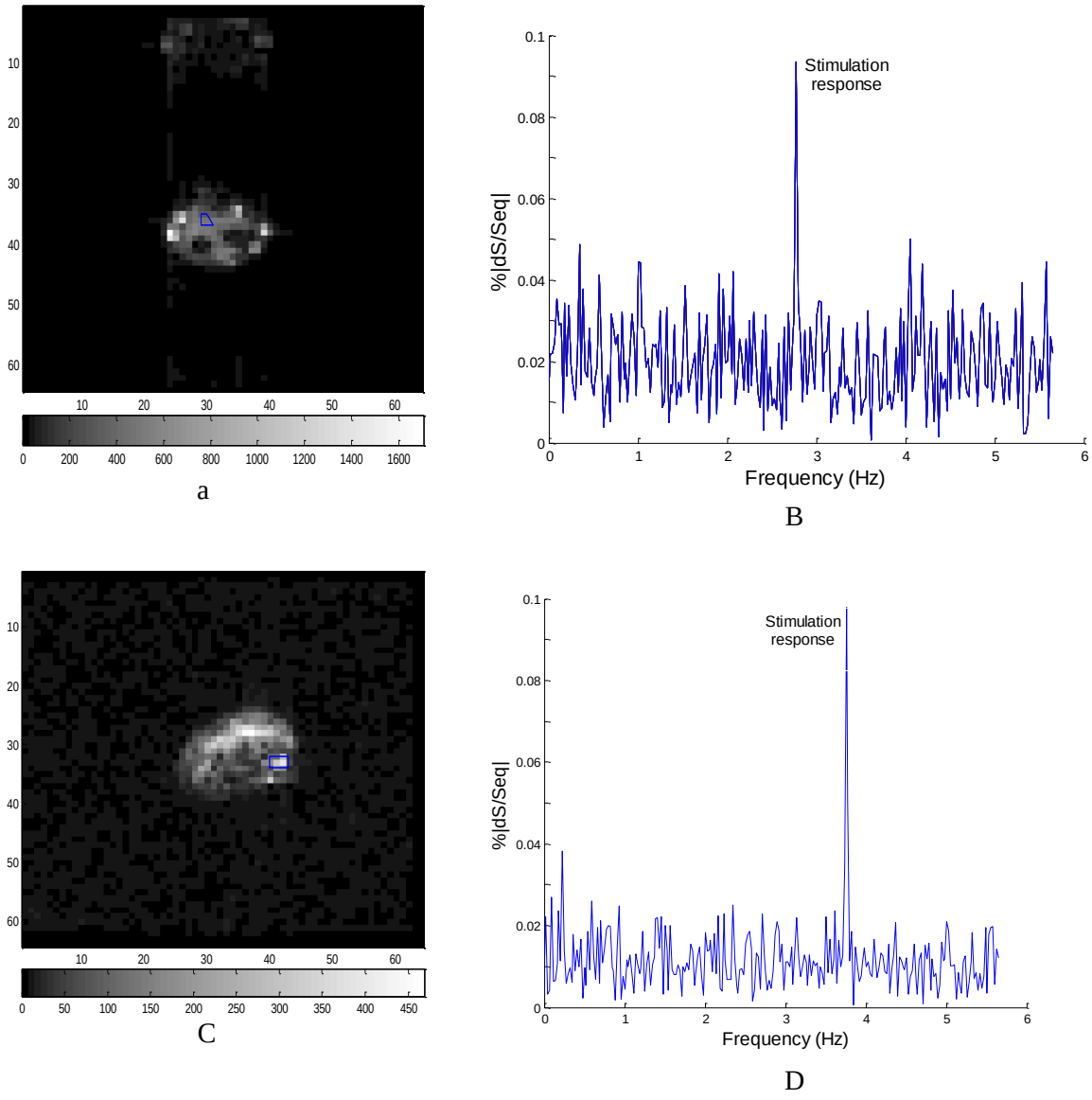

Figure 4. 5: Shows the percentage change of 0.09% for two different subjects for typical experiments on the median nerve stimulated at two different frequencies, using an eight channel wrist coil. a) mean GE-EPI magnitude image using 2.7 Hz to stimulate the median nerve with a 2×3- voxel ROI. B) 1D Fourier transform of MR time series showing spectral peak at the applied frequency. c) GE-EPI magnitude image with a stimulation frequency of 3.8 Hz. d) 1D Fourier transform of MR time series with a stimulation frequency of 3.8 Hz.

The percentage signal change $\%|\Delta S/S_{eq}|$ due to the stimulation of the nerve with these two different frequencies was estimated at 0.09%. These measurement percentage changes were calculated from the spectral peak responses with SNR 5:1 and 7:1 for 2.7 Hz and 3.8 Hz respectively.

Statistical mapping analysis at 1.5T used a Z-score of 2.5 to suppress physiological artifacts. Figure 4.6 shows results from the median nerve for a non-stimulated and stimulated median nerve with 3.6 Hz. No significant pixels were seen in the control experiments (figure 4.6a) but highly significant pixels were seen with the TENS pulse frequency at 3.6 Hz, highlighted in red in Figure 4.6b.

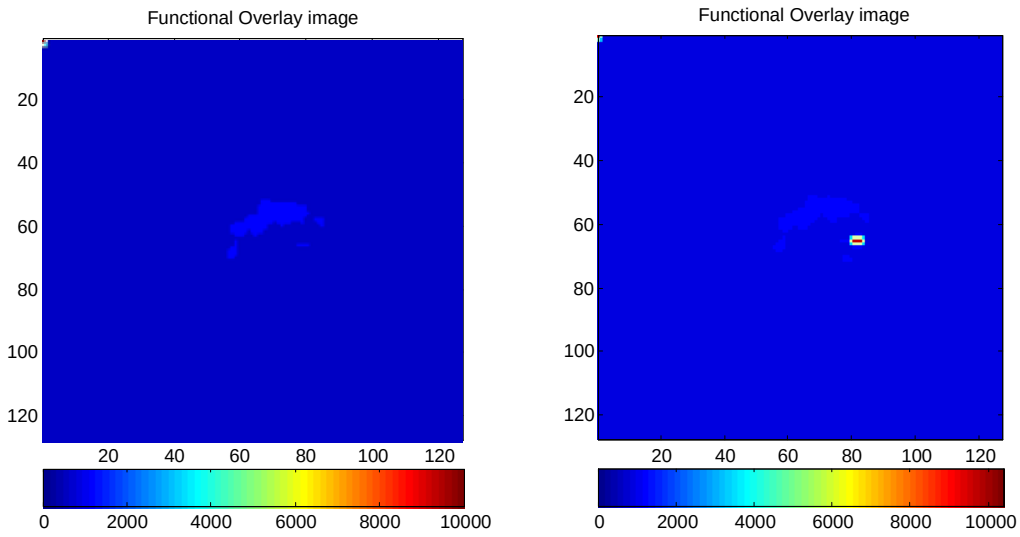

a

Figure 4. 6: Shows statistical maps from the wrist during median nerve experiments in the axial plane with TENS stimulation showing significant pixels highlighted in red using a Z score = 2.5 and TR = 88 ms. a) Overlay image shows no significant response in the ROI of the median nerve without stimulation b) Overlay image showing a highly significant response (highlighted in red) with a stimulation frequency of 3.6 Hz.

A large amount of physiological noise is also associated with these experiments possibly due to movement of flexors, pulsation of arteries and veins and other tissue signal changes. Hence the measured SNR was relatively poor at around 3:1.

In the previous two experiments, as shown in figure 4.6, the fluctuations in the Fourier transformation of the time series was used to investigate the SNR, using the standard deviation of the noise and the central intensity of the peak response as the signal. The maximum SNR in these voxels due to the generated local magnetic field is given according to the signal to noise ratio formula 4.2.

$$SNR = \frac{(\text{Signal})_{responses\ peak}}{(Noise)_{standard\ deviation\ \pm 0.5\ from\ the\ peak}} \qquad (4.2)$$

The noise from the selected voxels was measured over a spectral range of ± 0.5 Hz. The measured SNR, as shown in figure 4.6, for 2.7 Hz was 5:1 and for 3.8 Hz was 7:1. Table 4.1 shows values for the different stimulation frequencies and corresponding signal to noise ratios.

These differences in the SNR at the two stimulated frequencies in the selected voxels primarily depends on the number of dephasing protons in the nerve itself and their distance from the veins and arteries giving rise to physiological noise.
The measurements of these signal changes with the associated SNR are recorded in tables in Appendix B, which show the results from range of experiments repeated with used stimulation frequencies.

Table 4.1: SNR and the amplitude of the response peak with noise corresponding to different stimulated frequencies.

Stimulated frequency (Hz)	Signal amplitude (Arbitrary unit)	SNR
2.2	162.9	3:1
2.6	750.1	3:1
2.7	89.2	5:1
2.8	116.6	3:1
3.4	71.46	3:1
3.6	142.4	4:1
3.7	81.22	4:1
3.8	137.3	7:1

4.6 Generated Electromagnetic Field in the Median Nerve

The previous figures showed the MR responses due to the local magnetic field generated by the median nerve at different frequencies. Therefore, the fast fMRI technique did appear to detect a weak electromagnetic nerve response to electrical stimulation in these experiments and hence has great potential to calculate the magnetic field and the nerve current directly. The biocurrents are often several microamperes larger in the central neurons (Ferrari and Zakon 1993) and the magnetic fields depend critically on the distance from the source. This study investigated the magnetic field and ionic current due to action potentials from the median nerve in the selected voxels. The Lorentzian distribution model was used to

measure the change in magnetic field generated in these voxels (Song and Takahashi 2001, Chow 2005, Anwar 2011). Thus, it was assumed the signal change due to magnetic field modulation of a voxel of the median nerve ($3.75 \times 3.75 \times 5$ mm^3) could be calculated from equations 3.1.

In this case ΔB is the strength of the magnetic field (T) created in the selected voxels by action potentials in the median nerve.

Figure 4.8 shows the percentage change due to the nerve magnetic field generated from ionic currents, using the Lorentzian model described in equations 4.3 as a function of echo time. The mean ΔB for all the positive median nerve experiments, was 0.7 ± 0.1 nT measured at TE=25 ms. However, it is difficult to estimate appropriately the errors on this value due to the background physiological and electronic noise. In addition, the main current source of this magnetic field around the voxels is generated from hundreds of thousands of nerve fibres inside the stimulated nerve. The ionic current that generated this magnetic field can be calculated by using Ampere's law. The equivalent current was found to be $I = 0.65 \pm 0.1$ μA, which was calculated using a nerve radius r = 1.875 mm. Table 4.2 records the percentage signal change, axonal magnetic field and SNR with different frequencies.

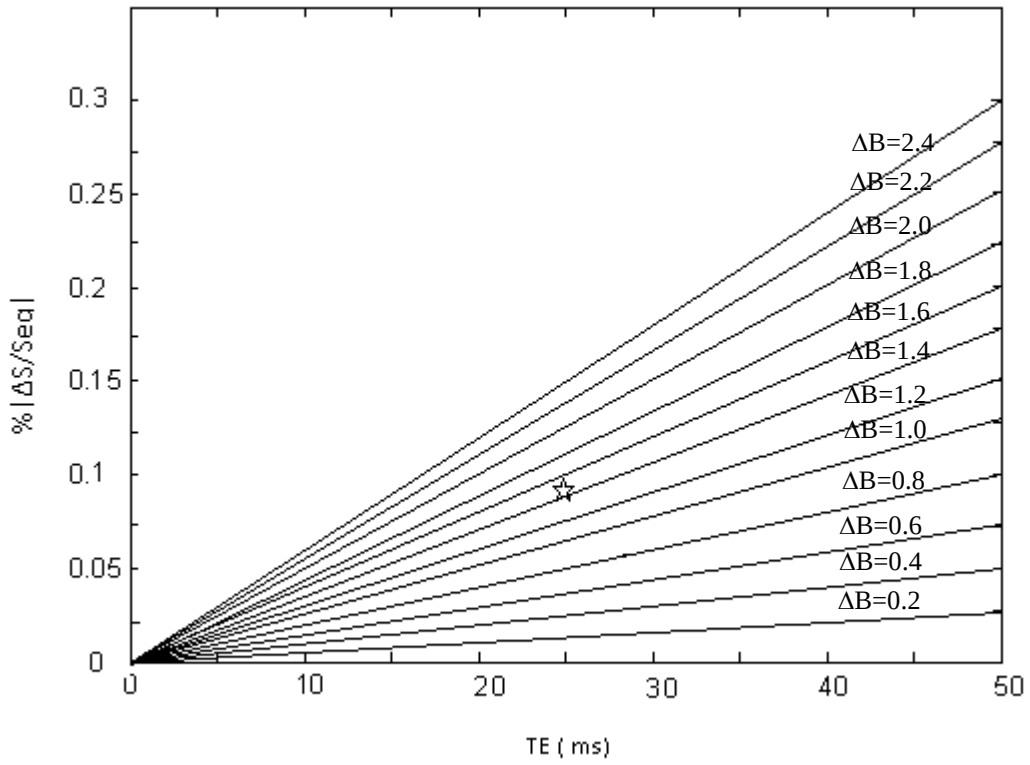

Figure 4. 7: Percentage signal change %|ΔS/Seq| plotted due to local median nerve magnetic field changes in (nT) using the theoretical Lorentzian model as a function of echo time (Chow et al. 2005).

Table 4. 2: Recorded percentage signal changes, axonal magnetic fields and SNR values using median nerve stimulation at different frequencies

Stimulation frequency (Hz)	$\%\lvert\Delta S/S_{eq}\rvert$	ΔB_{ax} (nT)	SNR
2.2	0.07	0.71	3:1
2.4	0.05	0.52	3:1
2.5	0.05	0.54	3:1
2.7	0.08	0.75	5:1
2.8	0.08	0.78	3:1
2.9	0.076	0.71	3:1
3.4	0.05	0.52	3:1
3.5	0.08	0.82	3:1
3.6	0.07	0.71	4:1
3.7	0.09	0.84	4:1
3.8	0.08	0.76	7:1

4.7 Non-detection experiments

In many of the experiments there was non-detection of the local magnetic field in the ROI. Therefore, this section presents some of these experiments where the neuronal magnetic field established was not large enough in magnitude to be detected by fast fMRI, due to voxel selection, contamination of the signal with haemodynamic responses, very small SNR and various forms of noise, such as (system noise, thermal noise, signal drift, subject dependent noise and physiological noise). Figures 4.9 provide examples of non-detected trials.

The localization was done by selecting three activated regions on the wrist, as shown in figure 4.9A, during electric median nerve stimulation at a frequency of 2.5 Hz.

The experimental results show three different types of frequency response from the Fourier transform of the time series of 500 fMRI acquisitions. The vessels, normal tissue and the median nerve were represented on the graph by different coloured traces.

They show that no response was recorded in the median nerve (blue trace), and the vessels show cardiac pulsations and harmonics (green trace), and no significant response was seen from normal tissue (red trace). Figure 4.9B relates to the second subject at 3.5 Hz. These experimental analyses were repeated five times and similar results were observed each time. It is obvious from the graph (4.9B) that no significant response resulted from median nerve stimulation at 3.5 Hz.

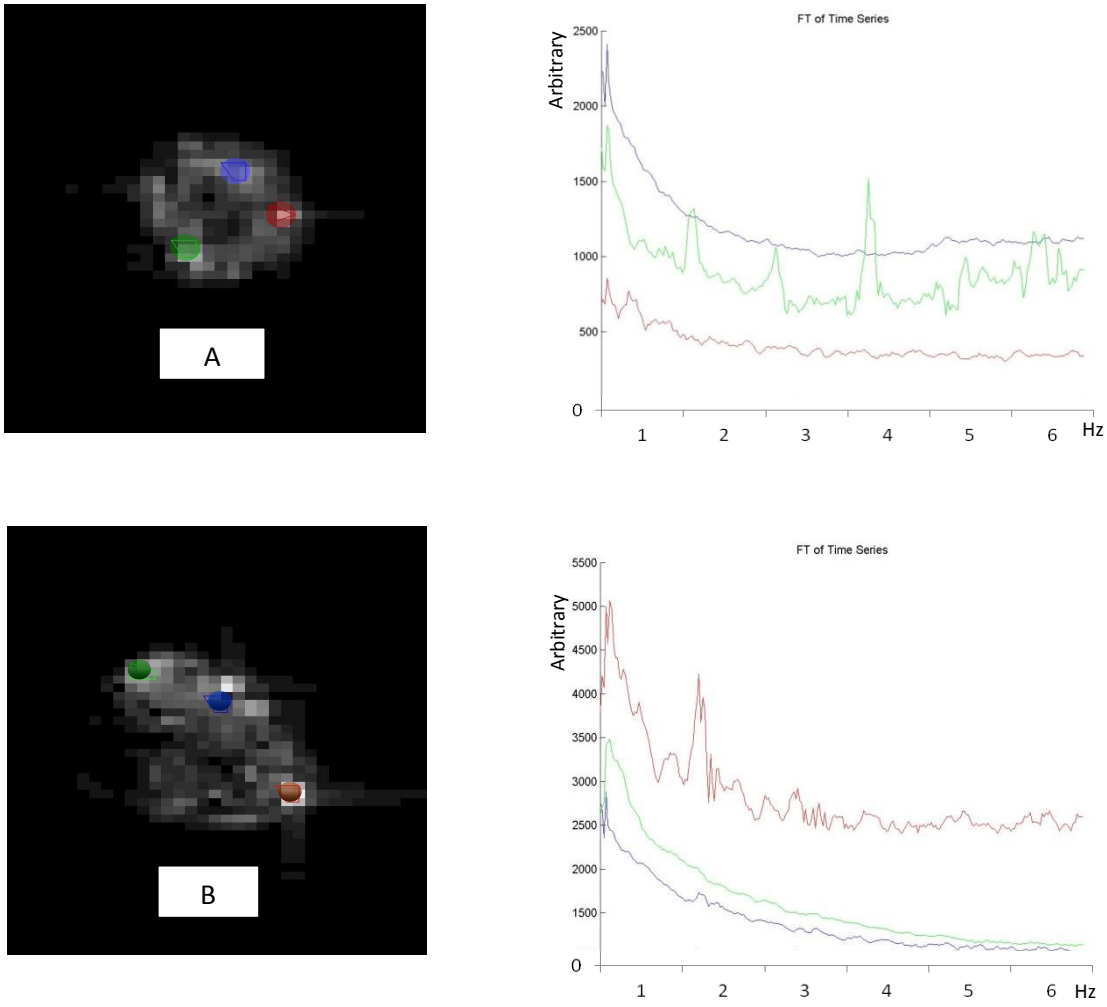

Figure 4. 8: Shows non detected experiments during median nerve stimulation at 2.5 and 3.5 Hz. A) Underlying three activated areas in the human wrist during external median nerve stimulation by 2.5Hz, and Fourier transform of MR time series at 2.5 Hz B) Underlying median nerve area during median nerve stimulation at 3.5 Hz.

4.8 Summary table of all experiments performed during the median nerve study

Table 4.3 summarises all the experiments performed with fast fMRI investigation using GE EPI magnitude images of TENS stimulation of the median nerve. Different frequencies were used over a range of 2.1 to 4.1 Hz. Seven male volunteers with no history of neurological disorders (aged 21–56 years) participated in this study and the hands used were chosen randomly. All subjects were subjected to three experiments: one control experiment without stimulation and two others using two different frequencies. Positive results similar to those shown in the previous section were observed in 29 out of 34 experiments. In these experiments, with TENS stimulation, significant differences were detected between stimulated median nerve and non-stimulated median nerve. These results showed a success rate of 85% in the median nerve, with variation of SNR from 3:1 to 7:1. The mean estimated local magnetic field was 0.7±0.1 nT.

Table 4. 3: Summary of experiments performed during the study, using stimulation of the median nerve in volunteer wrists of 2.5 to 3.5 Hz

Stimulated freq.(Hz)	No. of experiments	Detected	Failed to detect
2.2	1	1	-
2.4	2	1	1
2.5	3	3	-
2.7	4	3	1
2.8	5	5	-
2.9	1	1	-
3.4	2	2	-
3.5	3	2	1
3.6	3	2	1
3.7	6	6	-
3.8	4	3	1

4.9 Discussion

These in-vivo experimental results provide this investigation with convincing evidence for detection of weak magnetic fields generated by the median nerve during wrist stimulation by TENS. The responses were observed at high stimulation frequencies of 2.1 to 4.1 Hz. It is proposed that these results relate directly to axonal electrical activity and cannot be related to hemodynamic response because of the high frequencies used for stimulation. However, pulsation frequencies can be seen at approximately 0.3 Hz and 1 Hz corresponding to the respiration and cardiac rates respectively.

These results were typical of observations in 29 out of 34 experiments performed on the seven volunteers. The fast fMRI technique greatly increases spatial and temporal accuracy in detecting neuronal function.

Using the median nerve magnetic field as a source of MRI field modulation means that the ionic current flows both parallel and perpendicular to the main magnetic field and this is constant throughout the thickness of the slices, which renders the techniques practical for in vivo use, especially in the giant nerves.

In previous studies by Gambarota (2009) and Kunze (2010) the median nerve was imaged with MRI to study the properties and local deformation but not the possible electromagnetic response within the scanner (Gambarota 2009, Kunze 2010), whilst Anwar (2011), who focused on direct detection with 1.5T, provided some interesting results showing the possibility of detecting the local magnetic field directly with basic experiments (Anwar 2011). The results provided the percentage signal change, local magnetic field generated by the median nerve, $T2^*$ effects, SNR, phase shift and the current on the selected voxels. However, a study by Chow et al. (2005) focused on the optic nerve, using direct neuron detection and the percentage magnetic change was found to be about 0.17%, RMS axonal field of 1.23 nT with SNR = 6:1, which is slightly higher than in our study (Chow 2005). The first ionic current of the human median nerve bundle was recorded by Wikswo et al. (1990) using toroidal pickup coils (Wikswo, Henry et al. 1989). This study found the current to be 0.35 μA, then Ampere's Law was used to find the median nerve magnetic field, which was 0.035 nT and there was a phase shift of about 0.0004° in the median nerve bundle within a 2 mm radius. These results are lower than those observed in the current

study. Meanwhile, a study by Wijesinghe et al. (2009) used MRI to detect the peripheral nerve and skeletal muscle action currents (Wijesinghe and Roth 2009). They investigated the phase shifts due to four different measured action currents, including the human median nerve. This study was based on the Wikswo study and its values, and they found that the phase shift was less than one hundredth of a degree when induced in MRI; however, there is debate over the results for various reasons. One reason is that they calculated the magnetic field just outside the nerve, and another is that the magnetic field was changeable due to stimulation of different axons or bundles.

Our study results support the hypothesis of fast fMRI. However, these results show that current generation MRI is barely detecting these very small magnetic fields due to action potentials. Results can possibly be improved by reducing associated noise by optimizing parameters such as TE, TR, FOV, real time shimming and using improved RF coils. Increasing the sensitivity of the MRI system should produce higher SNR than the results presented here which show a mean SNR of about 4:1 is typical at 1.5T with fast fMRI. Higher SNR should give more access to measurement of neuronal function with high spatial and temporal resolution in a fraction of the time of conventional BOLD studies, which is important in a clinical setting.

Chapter 5: Visual stimulation – a comparison of direct detection fast fMRI with the BOLD technique

5.1 Introduction

The objective of this chapter was to attempt to detect magnetic fields induced by neuronal firing with 1.5T MRI during functional activation of the adult human visual cortex using stimulation with a strobe light over a range of frequencies. A number of different echo times were used to try and optimise the signal to noise ratio of the direct responses. In addition, a comparison of the direct neuronal detection method with the BOLD technique was performed for the visual cortex. Positive fast fMRI responses were found in a large fraction of volunteers, using a short repeat time EPI sequence which correlated with the BOLD responses, although the fast responses were much more highly localised with many fewer activated voxels.

5.2 Finding the optimal TE for the highest detection SNR for visual activation at 1.5T

In this section, measurements are presented to help determine an optimal TE for detecting the possible responses originating from neuronal magnetic fields during a rapid visual system stimulation paradigm as presented in section 3.2.2 in chapter 2. Two volunteers were studied with a total of 10 experiments using four different TE values (25, 35, 45, 55 ms). All experiments were conducted at 1.5T using an 8 channel head array coil, with an echo planar gradient echo sequence using a short TR = 88 ms, SLT = 5 mm, in-plane resolution = 3.75 mm. The same slice of brain was used for each experiment selected from a scout image to lie in a plane through the optic nerve and the visual cortex. A stimulation frequency of 2.5Hz was chosen so that the response could easily be separated from other fluctuations, such as respiration, heartbeat and other possible brain activity associated with specific tasks at different frequencies in the chosen ROI.

The optimal TE corresponded to the value with the highest signal-to-noise ratio (SNR) for the detected response. Figure 5.2 shows the Fourier transform of the MR time series (GE-EPI magnitude image) from an ROI selected in the visual cortex for TE = 25, 35, 45 and 55 ms at 1.5 T. In these figures, no spatial filtering was used in the analysis. All responses appeared to be highly localised in the visual cortex. Figure 5.1 shows results at different TE for the same selected voxels. In figure 5.2 A, the response at TE = 25 ms had a relatively

high SNR of 4:1. Figure 5.2B corresponds to TE = 35 ms and shows the heartbeat peak (at approximately 1 Hz) which is much higher than the stimulation frequency peak response, which had a poor SNR of 2:1. Experiments at TE=45 ms and TE =55 ms again only had weak responses, as seen from figures 5.2C and 5.2D, with SNRs of 1:1 and 2:1 respectively. These results are typical of experiments repeated on two subjects in five scan sessions with different frequencies in the range of 2.2 - 4.8Hz (see Table 5.2 for details).

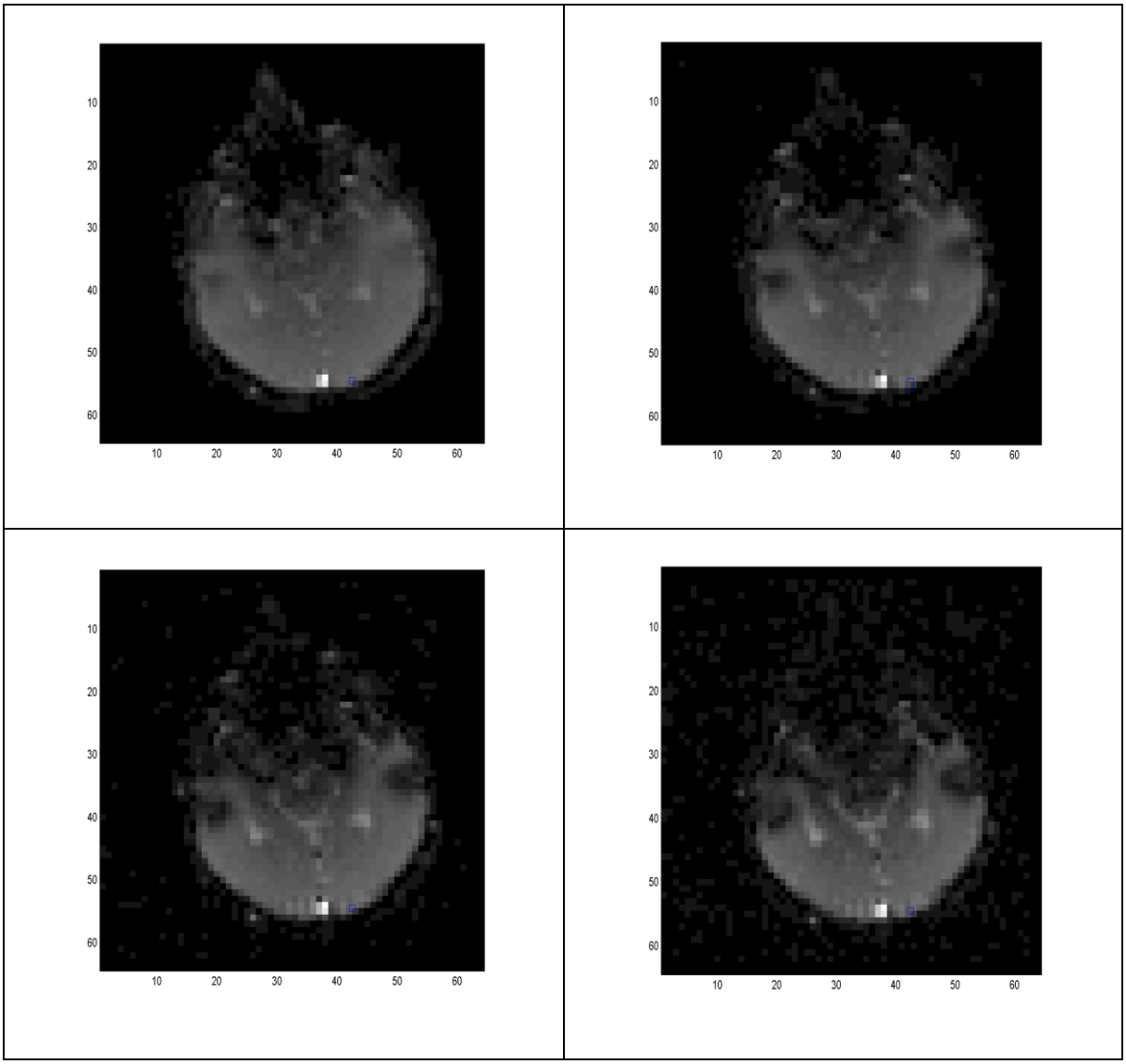

figure 5. 1 Typical experiments of visual stimulation using different TE (25, 35, 45, and 55)ms. The image show selected voxels(blue boxes) within same ROI and voxels.

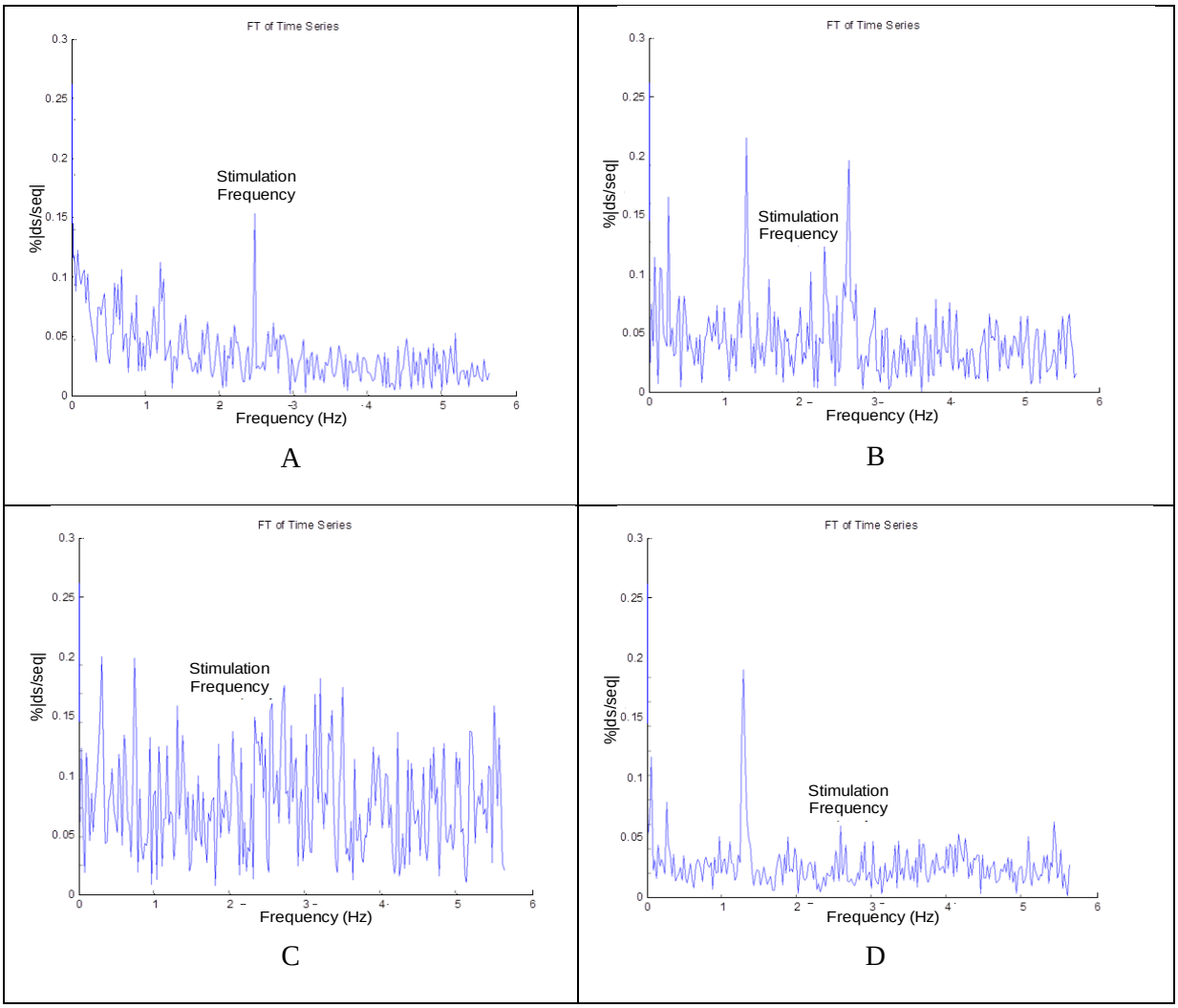

Figure 5. 2 shows responses at different TE for the same selected ROIs. In figure 5.2A, the response at TE = 25 ms shows a SNR of 4:1. Figure 5.2B corresponds to TE = 35 ms and shows the heartbeat peak (at approximately 1 Hz) is much higher than the stimulation frequency peak response. Figures 5.2C and 5.2D show experiments at TE = 45 ms and TE =55 ms again showing very weak responses with SNRs of 1:1 and 2:1 respectively.

Table 5.1 shows the average SNRs of responses at 2.5Hz stimulation frequency for different TEs acquired from the visual cortex at 1.5T. Use of TE =25 ms achieved the best detection sensitivity for direct measurements of the stimulation response of the visual system.

Table 5. 1: Four different values of TE with resulting response SNRs for the visual experiments acquired at 1.5T

TE (ms)	SNR
25	4:1
35	2:1
45	1:1
55	2:1

Figure 5.3 shows overlay images using different TE values acquired during visual stimulation, The Z score used was 2.5. The axial slice of the brain shows correlated pixels at the ROI and unknown active pixels due to strobe light stimulation using TE = 25 ms (figure 5.3a). There was no significant response in the visual cortex using TE = 35 ms, but again there were unknown active frequencies generated during the experiment (figure 5.3b). Figure 5.3c show significant responses (highlighted in red) in most areas but not in the ROI in the visual cortex of the brain using TE = 45 ms, and figure 5.3d shows active pixels in the ROI with low SNR as presented in the previous section. In addition there were significant responses from stimulation by strobe light generated in other areas of the brain using TE = 55 ms.

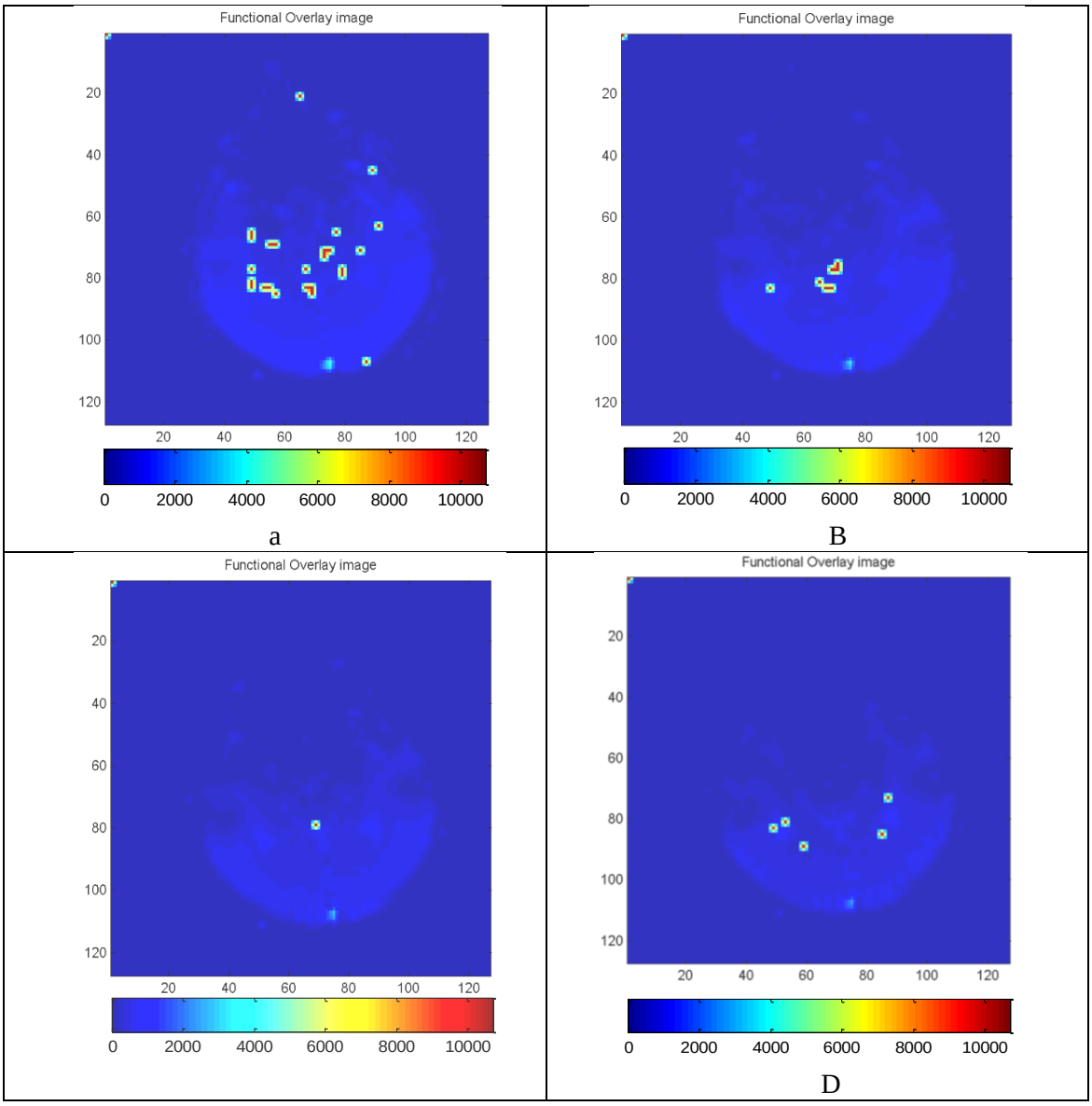

Figure 5. 3: Shows statistical maps from four different echo time in the axial plane with visual stimulation at 2.8Hz.Significant pixels are highlighted in red using a Z score of 2.5 and TR = 88 ms. a) Active pixels were seen using TE = 25 ms b) significant responses (highlighted in red) are seen in the other regions but no active response was seen in the visual cortex with TE = 35 ms, (c) no response was seen using TE = 45ms and d) a response was seen but with low SNR using TE = 55 ms.

5.3 Visual Cortical Activation

Thirty eight experiments using fast fMRI and thirty seven experiments using the BOLD technique were performed over eleven scan sessions on six different volunteers, with different stimulation frequencies between 2.2 Hz – 4.4 Hz, using the optimised TE = 25 ms. Other scan parameters were as described in the methodology, Chapter 2. The paradigm design was also presented in the methodology chapter (section 2.3.2.2). The following sections illustrate typical results acquired using both fast and BOLD fMRI techniques.

5.3.1 Fast fMRI Control experiments

All data sets were assessed for intra scan subject movement using a cine display and data sets were discarded if any head movement was observed. As scan duration was very short, movement was not usually a problem. Control experiments were carried out to verify that without stimulation, there were no effects of neuronal activity on the MRI magnitude time series spectral responses. Figure 5.4 shows a typical example of a fast fMRI experiment with no visual stimulation under dark-adapted control conditions with the same acquisition duration as used for the subsequent stimulation experiments. The ROI in Figure 5.4 left was selected in the visual cortex (highlighted in squares) with voxel size = $3.75 \times 3.75 \times 5$ mm^3. A 1D Fourier transform of the time series of 500 images was calculated for the ROI. In these control experiments, no spectral components were observed at the specific frequencies of the applied strobe light. However, spectral peaks were observed at the respiration and heartbeat frequencies (figure 5.4right). The ROI was moved systematically across each subject's entire visual cortex to search for responses. Each colour on the 1D Fourier transform graph in Figure 5.4b corresponds to the same coloured ROI on the GE-EPI magnitude image in Figure 5.3left.

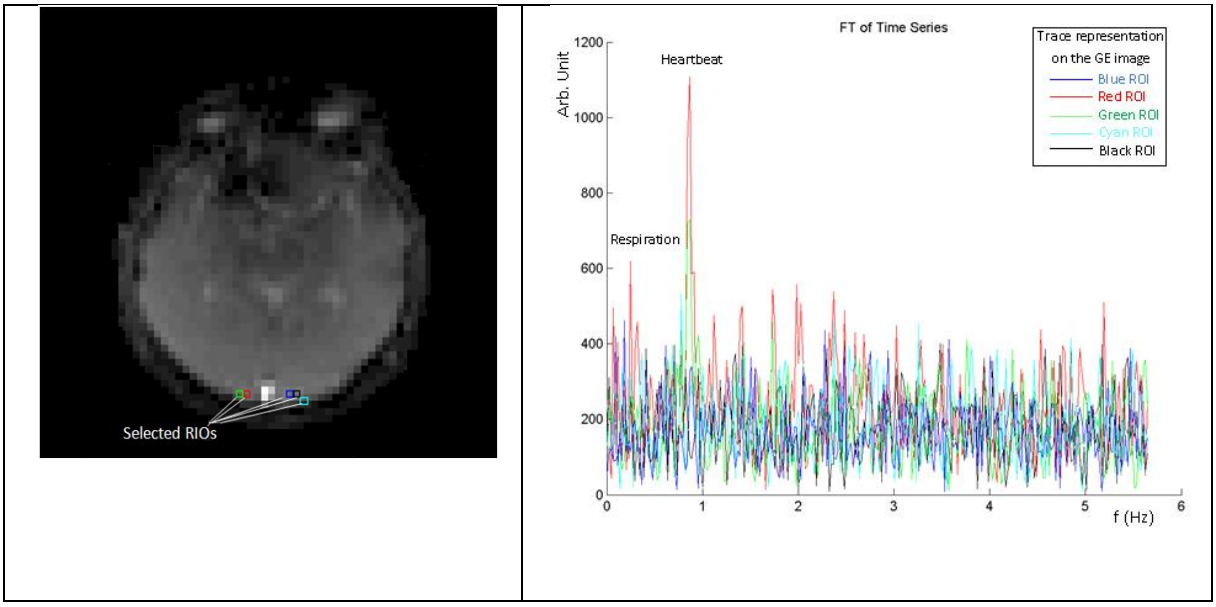

Figure 5. 4: left GE-EPI magnitude image – no stimulation. Selected ROIs are located in the visual cortex. right-Fourier transform of the MR time series showing the Frequency spectrum for the different ROIs in the visual cortex without stimulation - typical experimental result.

5.3.2 Fast fMRI experiments with Strobe Stimulation

Figure 5.5 shows two different experiments from an acquisition with visual stimulation at 2.8 and 3.6 Hz, using a Z score = 2.5. This image shows significant response to the stimulation when compared to the non-stimulated experiments (control experiments). The location was selected in the visual cortex as shown in figure 5.5a (grey scale image), which is the corresponding GE-EPI magnitude image. The ROI in the left side of the visual cortex

was a 1×2 voxel region acquired with a voxel size of 3.75×3.75×5 mm^3. The image acquisition parameters were the same as used for the control experiments as described in the Methodology chapter 2.

The 1D Fourier transform of the time series from the selected ROI is shown in figure 5.5b, showing a possible response at 2.8Hz with a SNR of 4:1. This observed response was from the same slice used in the control experiments.

Figure 5.5c shows a different experiment obtained with 3.6 Hz frequency stimulation using a strobe light at 1.5T. The highlighted region in the right side of the visual cortex was active using the same Z score = 2.5. The ROI was selected on the mean GE EPI magnitude image (figure 5.5c). A 1×3 voxel ROI (voxel size 3.75×3.75×5 mm^3) in the visual cortex was used to obtain the Fourier transform of the MR time series from the selected area.

In figure 5.5d the 1D Fourier transform of the time series of a 1×3 ROI selected in the visual cortex shows a response at approximately 3.6 Hz with strobe stimulation corresponding to the selected voxels. In this example, the strobe response was detected in the visual cortex at 3.6 Hz. The SNR of the response at the strobe frequency was 3:1. There was no detected peak at the stimulation frequency in the Fourier transform of the time series of an ROI in the visual cortex during control experiments. Two peaks were also detected from respiration at 0.3 Hz with a SNR = 3:1 and from heartbeat at approximately 1 Hz with a SNR = 3:1. All the fast fMRI experimental results using strobe light stimulation results for the visual cortex are summarised in table 5.2. Different subjects and frequency responses are presented in Appendix B. The following sections cover in more detail the various predicted calculations and measurements related to these frequencies (2.8 and 3.6 Hz).

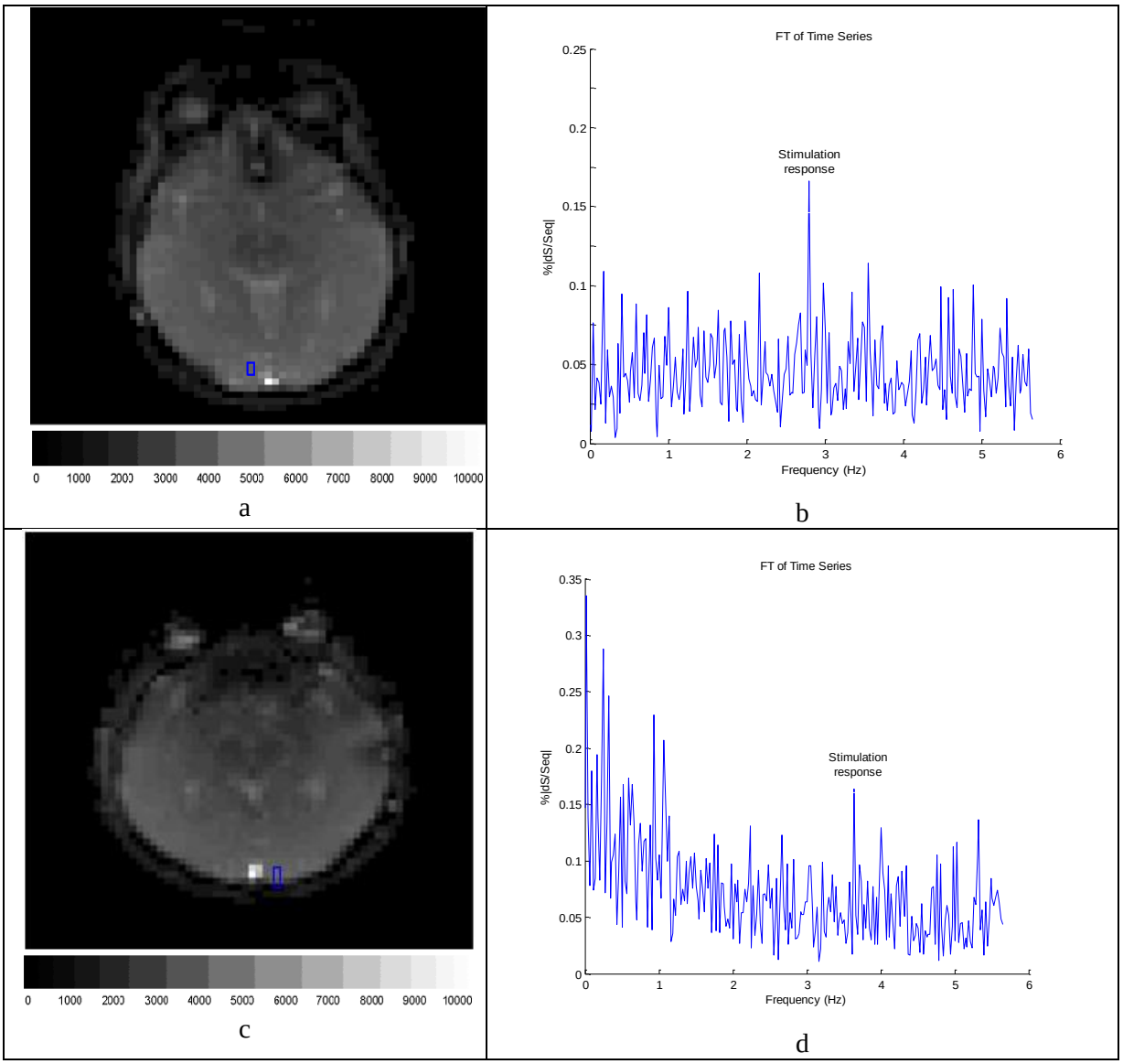

Figure 5. 5: Two typical examples of a visual stimulation paradigm using an 8channel head coil at 1.5T with two different frequencies of 2.8 and 3.6 Hz. (a) Mean GE-EPI magnitude showing the Region of Interest selected in the visual cortex at 2.8 Hz. (b) FT of the time series showing significant response in the ROI (c) Mean GE-EPI magnitude image shows selected voxel for 3.6 Hz stimulation (d) Fourier transform of MR time series showing the frequency spectrum for the ROI in the visual cortex with visual stimulation at 3.6 Hz

In these experiments, the measured percentage signal change for the stimulated frequencies 2.8 and 3.6 Hz were 0.07% and 0.09% by using the full equilibrium signal value of white matter in the visual cortex at 1.5T corrected using a T1 relaxation time of 660 ms (Ethofer, Mader et al. 2003, Wright, Mougin et al. 2008). These changes corresponded to axonal magnetic fields of 0.65 to 0.87 nT according to equation 3.1, and they were generated due to ionic currents ranging from 12 to 16 μA. The SNR values were 4:1 and 3:1 for 2.8 and 3.6 Hz respectively.

5.3.3 Summary of the Fast fMRI experiments on the Visual Cortex

Table 5.3 shows a summary of the data acquired at all the different frequencies and from different subjects. The selected ROIs contained 1×1 to 3×3 voxels with a voxel size of 3.75×3.75×5 mm^3. The table provides details of the full equilibrium signal, percentage signal change, axonal magnetic field, the generated current and the SNR. The mean measured percentage signal change for the stimulated frequencies range of (2.2 to 4.8 Hz) was 0.08 ± 0.01% with a mean SNR of 3:1. The corresponding axonal fields were ΔB_{ms} of 0.8 ± 0.1 nT generated due to an estimated mean ionic current of 14.7± 1.4 μA. In addition, table 5.4 shows strobe responses were detected with a success rate of 87% in experiments based on magnitude images using TE = 25 ms. Positive results were found in 33 out of 38 experiments. Furthermore, table 5.5 and 5.6 presents the GE-EPI magnitude image percentage signal change in the frequency spectra that resulted from the applied frequency ranges (2.2 – 2.8 Hz) and (3.1 -4.4 Hz) respectively.

Table 5. 2: The full equilibrium signal, percentage signal change, measured axonal magnetic field, generated current and SNR for the visual cortex experiments at different frequencies acquired at 1.5T

Frequency(Hz)	S_{eq} (A.u)	$\%\lvert\Delta S/S_{eq}\rvert$	ΔB_v (nT)	I (μA)	SNR
2.2	2391.6	0.09	0.84	15.8	4:1
2.3	2390.22	0.09	0.85	16.09	4:1
2.4	2375.8	0.09	0.86	16.3	4:1
2.5	1673	0.08	0.79	14.98	3:1
2.6	2242.7	0.07	0.73	13.74	3:1
2.8	1783.6	0.07	0.73	13.78	3:1
3.1	1834.9	0.08	0.79	14.8	3:1
3.3	2081.73	0.07	0.69	12.98	3:1
3.4	1798.8	0.08	0.83	15.59	4:1
3.5	2576	0.09	0.85	16.07	3:1
3.6	2620.19	0.06	0.65	12.3	3:1
4.4	1474.4	0.08	0.79	14.89	3:1

Table 5. 3: Visual cortex stimulation with strobe light detection acquired at 1.5T using head coil with TE=25ms

Frequency (Hz)		Detected	Not detected
2.2		2	-
2.3		3	1
2.4		2	-
2.5		2	-
2.6		4	-
2.8		2	1
3.1		2	-
3.3		3	1
3.4		5	1
3.5		3	1
3.6		4	-
4.4		2	-
Total	38	33	5

5.4 Analysis of visual cortex calculated signal percentage changes using fast fMRI

The mean measured percentage signals over all volunteers were presented in a previous section using equation 3.1 and the associated curve shown in figure 5.7. These measurements are the estimated local field at each selected ROI and assume the axonal population elongates along the x direction, and is perpendicular to the z direction as shown in figure 5.6. The range of field component values depends on the number of axons contributing in the selected ROI. Therefore, an increase in the number of axons increases the field strength due to simultaneous firing. The visual cortex contains around twelve distinct functional areas containing between 4–6 billion neurons. The mean neuronal density is approximately 57,000 in each mm^3 for the adult human brain (Colonnier and O'Kusky 1981, Leuba and Garey 1989, Wandell, Dumoulin et al. 2007). On this basis, the ROIs in these experiments contained approximately 10^7 neurons.

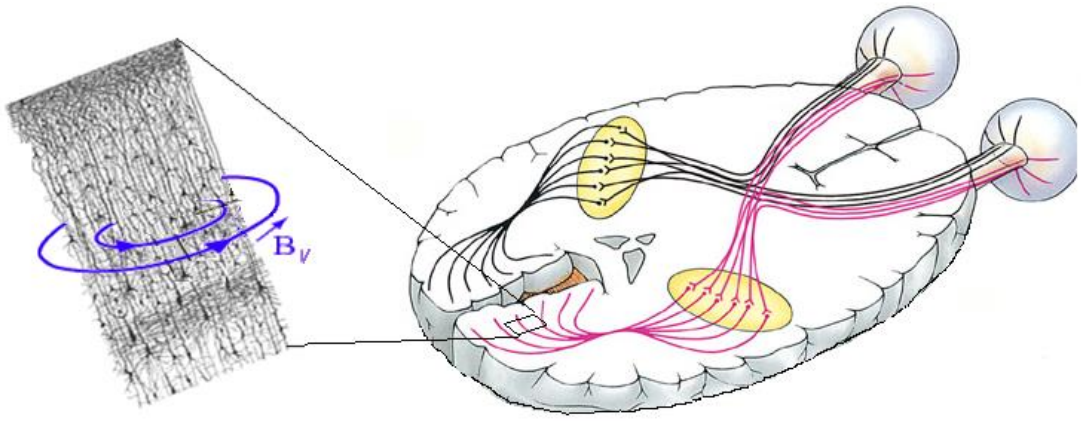

Figure 5. 6: Axial slice illustrating the voxel position, the elongated neuron population and the local magnetic field (axonal field) due to visual stimulation.

Figure 5.7 shows the visual cortex data acquired at a range of stimulated frequencies from (2.2 - 4.4 Hz) plotted on the Lorentzian model curve shown in figure 5.8 using Equation 3.1 and the expected axonal magnetic field range (0.65 – 0.869 nT).

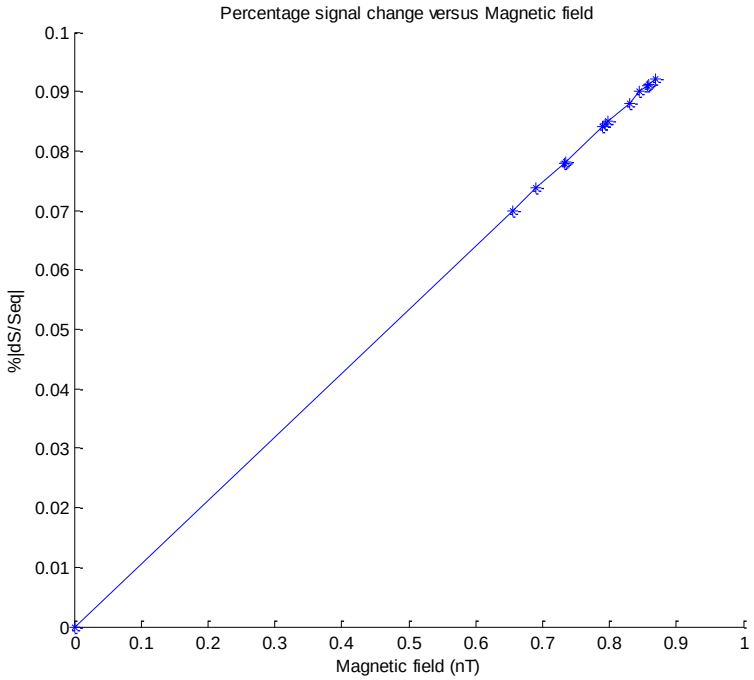

Figure 5. 7: Measured percentage signal change vs calculated external axonal field at TE=25 ms for stimulated frequency range of (2.2 -4.4 Hz)

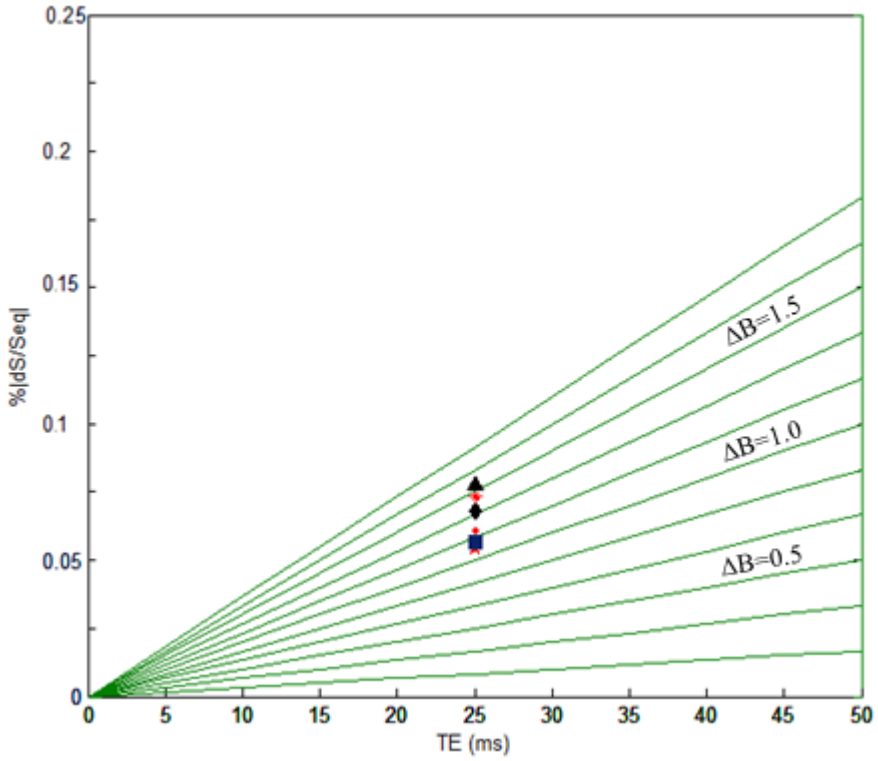

Figure 5. 8: Simulation of percentage signal change for the Lorentzian model by varying TE from 0ms – 50ms and plotting this study's percentage signal change corresponding to the externally applied axonal magnetic field results for echo time TE = 25ms.

It was assumed that all neurons fired simultaneously to generate the magnetic field during strobe stimulation, and that the total current was derived from the sum of all neurons in the selected ROI. Therefore, using these assumptions, each neuron generates an approximate magnetic field of 0.078 ± 0.007 pT and current of about 0.1± 0.01 pA.

5.5 BOLD fMRI experiments in the visual cortex with Strobe Stimulation

In Chapter one, BOLD fMRI was described in detail. The primary goal of this section is to compare the results of BOLD fMRI and fast fMRI using the same software for detecting stimulated responses. A repeated trial paradigm was used with stimulus frequencies in the range of 2.2 to 4.4 Hz and inter-trial times of 30 s. In addition, at the beginning of the experiment each volunteer was subjected to a control experiment with all OFF-blocks (no stimulation) in order to make comparisons with the response peaks in the stimulation experiments. The stimulation paradigms were presented in the methodology chapter (section 2.3.2.2). The results from the two methods will be compared in the next section. BOLD and fast fMRI experiments were performed sequentially on the same subjects for all stimulation frequencies. However, there were differences in the acquisition time and the type of tasks performed, which were also presented in the methodology chapter.

5.5.1 BOLD control experiments in the visual cortex

The control experiments were performed with all OFF-blocks (no stimulation). As expected no significant specific activity was found with no stimulation or in the control condition with all OFF-blocks; however, there were some artefacts in the motor-sensory cortex and from the eyeballs. The selected ROI was chosen from the GE-EPI magnitude image (figure 5.9a). The ROI in the right hemisphere of the brain at the visual cortex was a 1×2 voxel, and this region was acquired with a voxel size of 3.75×3.75×5 mm^3. Similar results were found in 27 out of 37 experiments on the four volunteers.

Figure 5.9b shows the response from the selected ROI (red box on the GE-EPI image) for the four block paradigm without stimulation, with no filters used. There was no significant response at the specific frequency that was applied during the stimulation experiment. However, artefacts peaks are evident. The peak amplitude at 0.016 Hz was not significantly different.

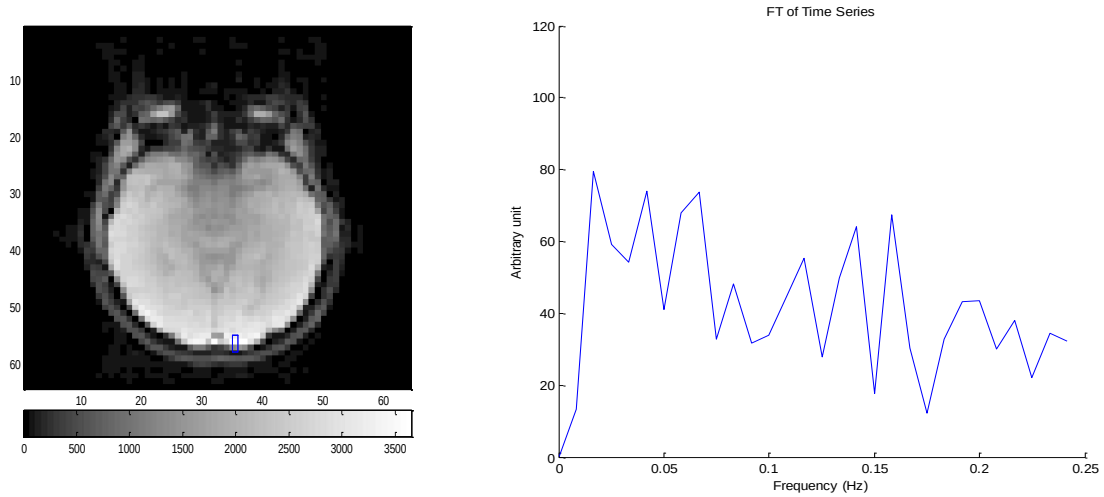

a b

Figure 5. 9: Typical experiment of control experiments without any visual stimulation (all OFF blocks) using BOLD technique TR= 2000 s and four block paradigms, a) GE-EPI magnitude image shows the selected ROI (blue box) using BOLD technique TR= 2000 s and four block paradigms, and b) Fourier transform of MR time series showing the Frequency spectrum for the ROI in the visual cortex

5.5.2 BOLD experiments in the visual cortex

The responses for an experiment with a four- block BOLD stimulation paradigm (OFF-ON- OFF-ON) on a typical subject with two different strobe light frequencies is shown in figure 5.10. Alongside a significant response in the visual cortex, the functional overlay image for the BOLD effect shows responses in the motor, somatosensory cortices and thalamus as well using a Z score > 3 for BOLD analysis as shown in figure 5.11. No spatial filtering was used in the analysis and the responses appear to be highly localised. These results are typical of those observed in the BOLD fMRI experiments for all subjects (presented as table in Appendix B).

The spectral response for the ROI selected in figure 5.10a (1×3 voxel) is plotted in figure 5.10b. The spectrum shows a significant peak in the Fourier transformation of the MR time series at 0.016 Hz that evidenced significant signal changes in response to the stimulation frequency (30 s OFF and 30 s ON). However, the strobe stimulation frequency was 2.8 Hz. The SNR was 4:1 with a percentage signal change of 1.2%. The frequency spectra showed no peaks at the respiration and heartbeat rates, as found in the fast fMRI experiments, due to the low range of frequencies measured in the BOLD experiments (0 – 0.25 Hz). There is a chance they may be aliasing and contributing to smaller peaks observed at other frequencies.

Figure 5.10c shows another experiment with 3.6 Hz stimulation frequency and a selected 1×1 voxel. The 1D Fourier Transformation of the time series in figure 5.10d shows the same frequency response 0.016 Hz with a percentage signal change of 1.9%. All the experiments were acquired at a TR of 2000 ms using the 8 channel head coil.

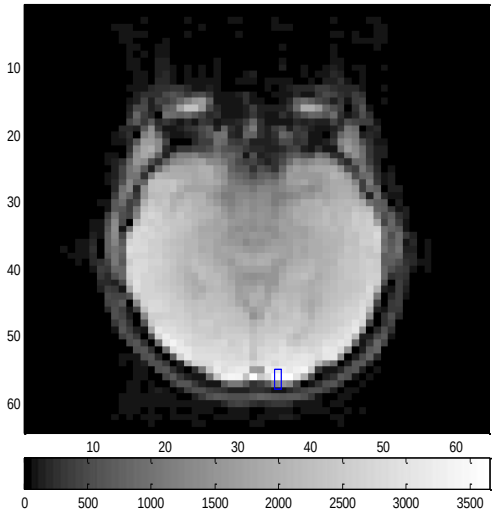

a

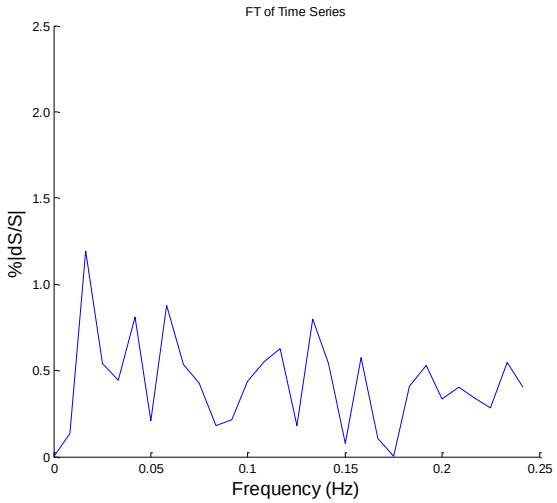

b

d

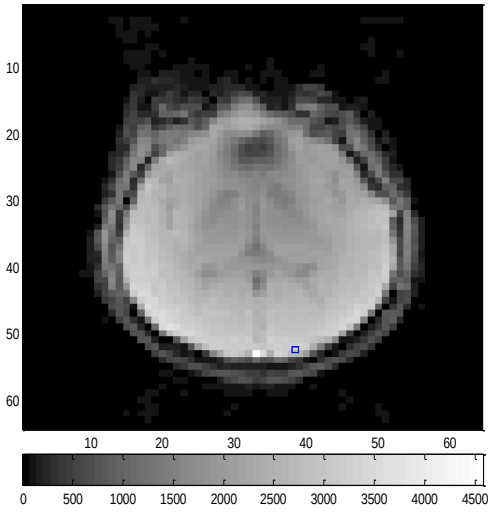

c

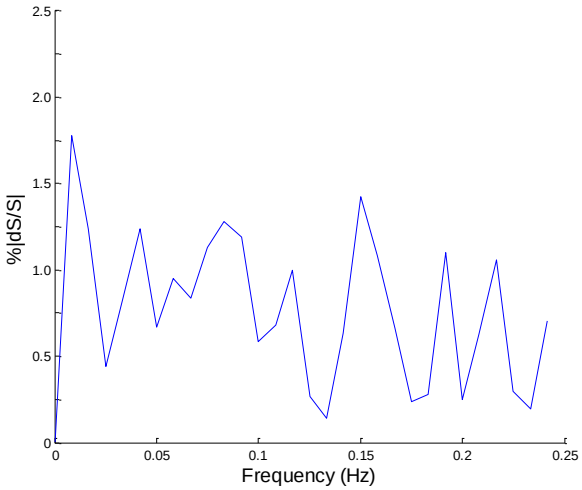

Figure 5. 10: Typical BOLD experiments with two different visual stimulation strobe light frequencies at 2.8 and 3.6 Hz and Z score = 3, (a and c) GE-EPI magnitude image showing the region of interest selected in the visual cortex (1×3 voxels and 1×1 voxel) with stimulation frequency at 2.8 Hz and 3.6 Hz respectively. (b and d) Fourier transform of MR time series showing the Frequency spectrum for the ROI in the visual cortex during visual stimulation at 2.8 and 3.6Hz respectively

Overlay images for both typical experiments are shown in figure 5.11 with a Z score of 3.0. The significant voxels are shown in red. These images were used as a reference to select ROIs in the GE-EPI magnitude image. It can be seen there was significant BOLD activation in both subjects using two different frequencies, 2.8 and 3.6 Hz in images 5.11a and 5.11b respectively.

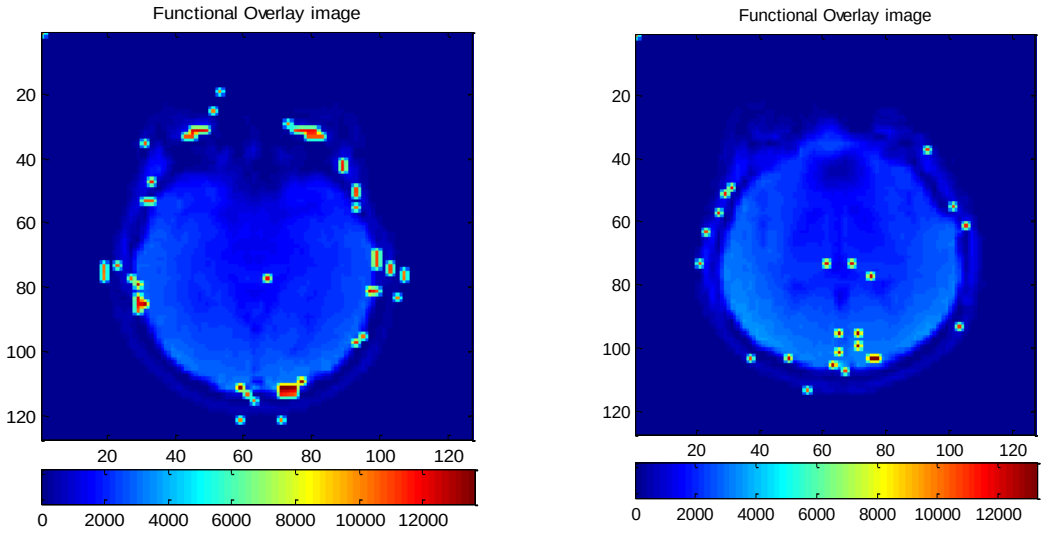

Figure 5. 11: Shows statistical maps from two different subjects in the axial plane with a strobe light stimulation, it shows significant pixels highlighted in red using a Z score of 3.0 and TR = 2000 ms. a) Overlay image shows significant response (highlighted in red) in the visual cortex. In addition, there are significant pixels in the motor sensory cortices, thalamus and other unknown areas due to a visual stimulation frequency of 2.8 Hz and (b) Overlay image showing response with a strobe light frequency of 3.6 Hz; it is clear there is significant response in the visual cortex and some other regions due to the BOLD response.

Results from experiments with stimulation frequencies between 2.2 - 4.4 Hz showed significant differences from the non-stimulated control experiments, according to a SPSS t-test ($p<0.05$). Figure 5.12 shows the time series analysis and the stimulation paradigm for a typical experiment. The response delay was approximately 12.5 s. The percentage signal

change of the BOLD response was measured in the visual cortex for specific frequencies as used for fast fMRI. A 1.9% signal change was found in the visual cortex due to the BOLD effect in typical experiments at 3.6 Hz.

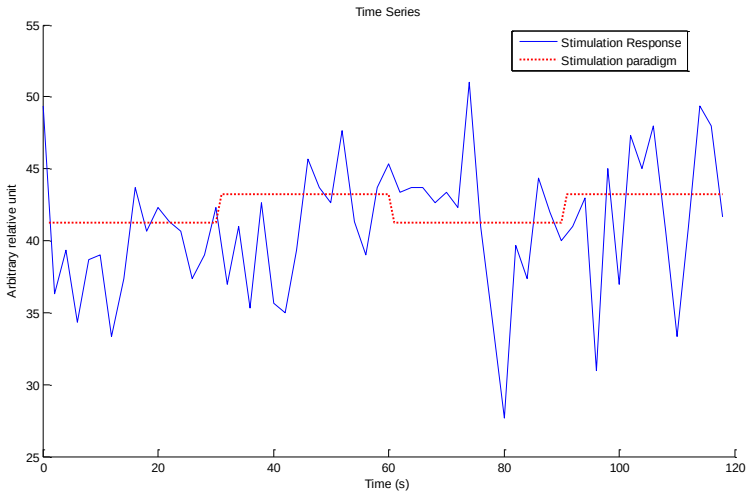

Figure 5. 12: BOLD fMR time series showing the response of an ROI in the visual cortex during visual stimulation at 3.6 Hz (blue trace) and the applied stimulation paradigm (red trace) - typical experimental result with no temporal filtering.

Tables 5.4 presents analyses of all positive results for the BOLD technique using the strobe light to stimulate the visual cortex acquired with a TR of 2000 ms. The table summarises the stimulated frequencies, percentage signal change and SNR. All the experiments were acquired on the 1.5T MR scanner using the BOLD technique with strobe light stimulation frequency in the range of 2.2 - 4.4 Hz. Table 5.5 shows detection of significant strobe responses at a success rate of 73%.

Table 5. 4: Percentage signal change and SNR for the visual cortex experiments at different frequencies acquired at 1.5T

Frequency (Hz)	$\%\lvert\Delta S/S_{eq}\rvert$	SNR
2.2	0.7	4:1
2.3	3	5:1
2.4	1.1	4:1
2.5	1.75	5:1
2.6	0.9	3:1
2.8	1.2	3:1
3.1	0.7	3:1
3.3	1.4	3:1
3.4	0.5	4:1
3.5	0.8	3:1
3.6	1.9	4:1
4.4	1.1	3:1

Table 5. 5: Summarizes the visual cortex experiments using strobe light paradigm at TR =2000 and TE = 25 ms.

Frequency (Hz)	Detected	Not detected
2.2	2	-
2.3	3	1
2.4	2	-
2.5	2	-
2.6	2	1
2.8	2	1
3.1	2	-
3.3	3	1
3.4	4	2
3.5	2	2
3.6	2	1
4.4	1	1

5.6 Comparison of fast fMRI and BOLD fMRI Results

This section compare the results of rapid fMRI and BOLD fMRI in volunteers using a high frequency range (2.2 to 4.4 Hz) to measure responses in the visual cortex. All experiments

were performed at 1.5T using two different TR values, 88 and 2000 ms respectively and using the same Matlab program for analysis. In addition, the same volunteers were involved in both experiments for each case. Different stimulation frequencies produced the same activation response in the BOLD imaging experiments. BOLD could not respond rapidly enough to the stimulation frequencies but only to the stimulation blocks. Spectral response in the rapid fMRI experiments strongly depended directly on the stimulation frequency used. Therefore, for both frequencies used, BOLD responded at the same frequency of 0.016 Hz but the fast fMRI responded at the fast stimulation frequencies as expected. The BOLD response was thus observed at the much lower frequency associated with convolution of the Haemodynamic Response Function with the stimulation paradigm yielding a very low response frequency, as expected.

Clear differences between Fast fMRI and BOLD technique were found during visual cortex activity with the strobe light using a range of frequencies from (2.2 -4.4 Hz). Fast fMRI appears to be detected if sufficient neurons were stimulated, causing about a 0.1% percentage signal change in the magnitude signal. For the BOLD technique, the average percentage signal change was 1.2 ± 0.6% on the GE EPI magnitude images.

5.7 Discussion

In this chapter, more experimental evidence has been provided to demonstrate that direct visual cortex activation can be detected with strobe light stimulation at high stimulation frequencies using fast fMRI with a very short TR = 88 ms. In addition, the BOLD technique was compared using the same frequency response analysis software. No spatial filtering was used in the analysis and the responses appear to be highly localised for the fast fMRI method. Motion detection was performed using cine visualisation. Motion correction was not performed due to the fast MRI scan single slice acquisition usually resulting in very little head motion during the scan. In addition the head was tightly packed into the head coil with foam to restrict motion.

The optimal TE for the highest practical SNR at 1.5T has been investigated using different echo times of 25, 35, 45 and 55 ms. Our study indicated that TE = 25 ms was the most

sensitive sequence at 1.5T. Table 5.1 records results from the four different values of TE for the visual experiments. The results with fast fMRI demonstrate consistent, although weak, visual activations using TE = 25 ms and frequencies >2.0 Hz which most likely originate from neuronal magnetic fields rather than the hemodynamic response due to the high stimulation frequencies used which suppress the BOLD response.

Increased MR sensitivity and stability is required to improve detection sensitivity. This could possibly be achieved using improved (cryogenic) radiofrequency coils or through use of polarisation techniques (Paley, Kaka et al, 2015). No clear responses with SNR > 3:1 were observed using longer TE = 35, 45, and 55ms. However, previous studies have reported that neuronal magnetic field signals should be stronger if the TE is longer (Xue, Chen et al. 2009). This is thought to be the result of a trade-off between having sufficient signal stability for weak signal detection and the length of time required for significant phase modulation to accrue. Image temporal stability (and absolute SNR) is better for the shorter echo time.

Tables 5.2, 5.3, 5.4 and 5.5 summarise the visual cortex stimulation experiments performed at 1.5T using the fast fMRI method. These experiments were acquired with different stimulation frequencies ranging from 2.2 Hz to 4.4 Hz. It appears that a weak direct fMRI response can be detected over the range of frequencies investigated in most volunteer experiments. The 1D Fourier transforms of ROIs from the image time series consistently show significant differences ($p<0.05$) between visually stimulated and non-stimulated experiments. The detection of frequency responses from the strobe light stimulation mostly occurred in visual paradigm experiments (33/38), at a rate of 87%, and not in the non-stimulated (control experiments – 0/19), with a 0% rate within the same chosen ROI. The in vivo experimental data thus support the hypothesis that direct neuronal detection may be possible in the visual system using fast fMRI with a short repeat time to provide a non-aliased sequence frequency response to above 5 Hz. Almost all other reported experiments in the literature to date looking for direct detection effects have used much longer repeat times which can confound the results with the BOLD effect and with aliasing of the fast signal itself.

Statistical image mapping using a Z-score >2.5 helps to identify the ROIs used to calculate the time series and Fourier transform for spectral analysis. However, the Z-score general linear model methodology only analyses at the exact stimulation frequency chosen (and harmonics if included) in the design matrix. Fourier analysis as used in this study allows all contributing physiological signals to be assessed simultaneously.

All fast fMRI acquisitions used a very short TR; therefore the physiological responses (respiration and heartbeat) were detected in most activated voxels in the fast fMRI experiments. The strength of these physiological signals seemed to depend on the ROI distance from obvious major blood vessels such as the sagittal sinus. Using a more conventional BOLD technique, the Fourier transform time series was detectable as a spectral response at very low frequencies (in this study the acquired frequency range was 0-0.25 Hz) due to long TR = 2000 ms. Therefore, the frequency response for respiration and the heartbeat will alias (0.3-0.4 Hz for respiration and 0.9 - 1.2 Hz for heartbeat).

To find the percentage changes in the magnetic field from the percent signal modulation measured, equation 3.1 can be used. This equation assumes a Lorentzian distribution of magnetic fields which makes the phase change vary linearly with modulation field rather than a quadratic dependence as found in other models (Chow 2005, Truong, Wilbur et al. 2006). This study estimated a neuronal modulation field with a mean value of 0.8 nT. As expected, a range of 0.07% - 0.1% signal change was found in this study in selected ROIs, dependent on the voxel size. The average SNR was 3:1. To increase SNR and reduce physiological noise, a time series with a total of 500 images was acquired to improve the statistics due to the low signal and so that stimulation frequencies could be chosen that were away from physiological rates. A low SNR (<= 2:1) was rejected as a negative result.

In previous studies (Chow 2005, Chow, Cook et al. 2006) preliminary results found evidence for detection of transient current in axons due to strobe light stimulation in a range of frequencies from 0.7 - 3.3Hz; the percentage signal change was found to be about 0.07 ± 0.03% for the visual cortex with TE = 30 ms at the same magnet strength (1.5T) that has been used in the present work. The magnetic field generated from this percentage change was (0.54 ± 0.23) nT using the Lorentzian model for the intra-voxel field distribution. Meanwhile, the maximum percentage signal change in the cortex was found to be around

1% using the BOLD technique at around 0.1 Hz. Furthermore, the study found a percentage signal change of about (0.06 ± 0.02)% due to LED stimulation using TE= 32.4 ms at a mean SNR= 4:1, corresponding to a mean predicted axonal field of (0.44 ± 0.12) nT.

A study by Xiong et al. (2003), detected signal change (<1%) from the baseline signal, using a wedge of random dots to stimulate the visual cortex at 1.9T using a long TR = 1000 ms and TE = 100 ms. However, they found that a low temporal resolution of 1000ms and spatial resolution of 3 mm were not optimal for investigating direct neuron detection at the system level(Xiong, Fox et al. 2003). Another study by Huang in 2013 found the signal change to be less than 0.07% under their study conditions and therefore not sensitive enough to be detectable by MRI at 3T using TR = 300ms and TE = 70 ms with small flip angle 36^{o} (Huang 2013). This study used a black-and-white vertically striped pattern with a frequency of 2.5 cycles per degree to stimulate the visual cortex. In addition, Luo et al. in 2011 did not find any significant signal change in magnitude in visual cortex due to transient currents, and they reported that the visual tasks were not detectable under the imaging conditions utilized, TR = 1000 ms and a range of TE = 30 – 100 ms at 3T (Luo, Jiang et al. 2011). In addition, they used an event-related paradigm (wedge of random dots at 100 ms followed by 19.90 s of blank screen) to stimulate the visual cortex. They nevertheless reported the neuronal current signal to be below 0.2% in human visual cortex.

However, neuronal activation also changes blood flow and blood oxygenation. Therefore, a number of BOLD experiments have been performed to compare the results. The stimulation paradigm used was high frequency (2.2 - 4.4 Hz) to allow separation of fast fMRI effects from those produced by BOLD effect.

The BOLD effect was seen at low frequency in all subjects using the same Fourier transform of the time series used for analysis of the fast fMRI experiments (rather than the conventional GLM analysis). The BOLD frequency (0.016 Hz) was the dominant signal. It was difficult to assess contribution of physiological signals on the BOLD response however, due to possible aliasing as discussed above. The mean BOLD effect observed here was ~ 1.2% which is consistent with literature values for this field strength and echo time (Stroman, Krause et al. 2001, Triantafyllou, Wald et al. 2011).

The fast fMRI visual response should provide a more direct measure of underlying neuronal function as the phase integration time involves just the data acquisition window rather than the HRF as found for BOLD and could possibly eventually be used in an advanced Brain Computer Interface (BCI) (Paley, Kaka et al. 2015). However, a SNR of significantly >3:1 would be required for reliable BCI use, so further development will be required. Use of cryogenic coils and polarised substrates may help in this regard.

In summary, reasonably strong experimental evidence has been presented that weak direct electromagnetic modulation effects can be observed in the visual cortex at 1.5T using an eight channel phased array head coil in adult human volunteers. The next chapter will aim to add further validation to these results by studying another brain region, using different tasks to stimulate action potentials.

Chapter 6: Rapid functional MRI measurements of the thalamus and motor-sensory cortex using stimulation of the median nerve

6.1 Introduction

The thalamus is a small structure within the brain with extensive nerve connections to the cerebral cortex and the midbrain. Its main function is to relay motor and sensory signals to the cerebral cortex. In order to investigate brain function, thalamus and motor sensory function response were studied in the brain using median nerve transcutaneous electrical nerve stimulation (TENS). In addition, fast fMRI was used to investigate direct neuron detection in the motor cortex during real and imaginary movements of the right and left hand in healthy volunteers (details of the paradigm are presented in the methodology chapter 2). Studies of imaginary finger tapping of the motor cortex have previously reported signal intensity changes with the BOLD technique due to blood oxygenation changes (Ersland, Rosén et al. 1996, Lotze, Montoya et al. 1999). In this study, we investigated whether brain activity could be detected using both real and imaginary finger tapping experiments using fast fMRI acquisitions with a sensitive 32 channel head coil operating at 3T as well as with an 8 channel head array at 1.5T.

6.2 Fast fMRI experiments with TENS stimulation

Six healthy volunteers were studied using the paradigm given in figure 2.7 in chapter 2. These experiments were performed on the 1.5T MRI system with an eight-channel head coil (details of the methodology and sequence protocols were also explained in detail in chapter 2). There were a total of 33 experiments performed on six male volunteers with an age range from 23 - 57 years for a range of stimulation frequencies (2.2 to 4.4 Hz) using a TENS machine.

A GE-EPI sequence with an oblique axial plane was used for all scans containing the motor sensory cortex. Typical results are shown in Figure 6.1. It shows the stimulation response of the motor sensory cortex using no stimulation at 2.5 Hz and 3.2 Hz with a Z-score of 2.0. For the non-stimulated experiments, there were no significant active pixels with a Z-score

of 2.0 and there was no detected peak in the frequency spectrum (figure 6.1b) from the motor sensory cortex from the typical ROI (figure 6.1a) highlighted in blue.

In the stimulated experiment using 2.5 Hz, a TENS response was detected in the motor sensory cortex in the right hemisphere of the brain as shown on the overlay image. A 2×3 voxel ROI, with voxel size 3.75×3.75×5 mm^3 was selected from the mean GE-EPI magnitude image (blue box). A stimulation response was detected at 2.5 Hz corresponding to the applied TENS frequency. Experiments were also run with different frequencies showing active pixels in the motor-sensory strip (red regions) on the overlay image (figure 6.2c). The image shows result on the left hemisphere of the brain using stimulation of the median nerve on the right hand with TENS stimulation. Figure 6.1f corresponds to the ROI selected in figure 6.1d and there was no response from the same ROI without stimulation.

The response patterns observed at both frequencies were very similar and included the respiration and heartbeat at approximately 0.3 and 1 Hz respectively in the stimulation frequency at 3.2 Hz and the related control experiments, depending on the selected ROI distance from the arteries and vessels.

29 positive responses were observed from 33 stimulation experiments which were significantly different from control spectra according to a Student's t test ($P<0.05$) (IBM SPSS v21.0).

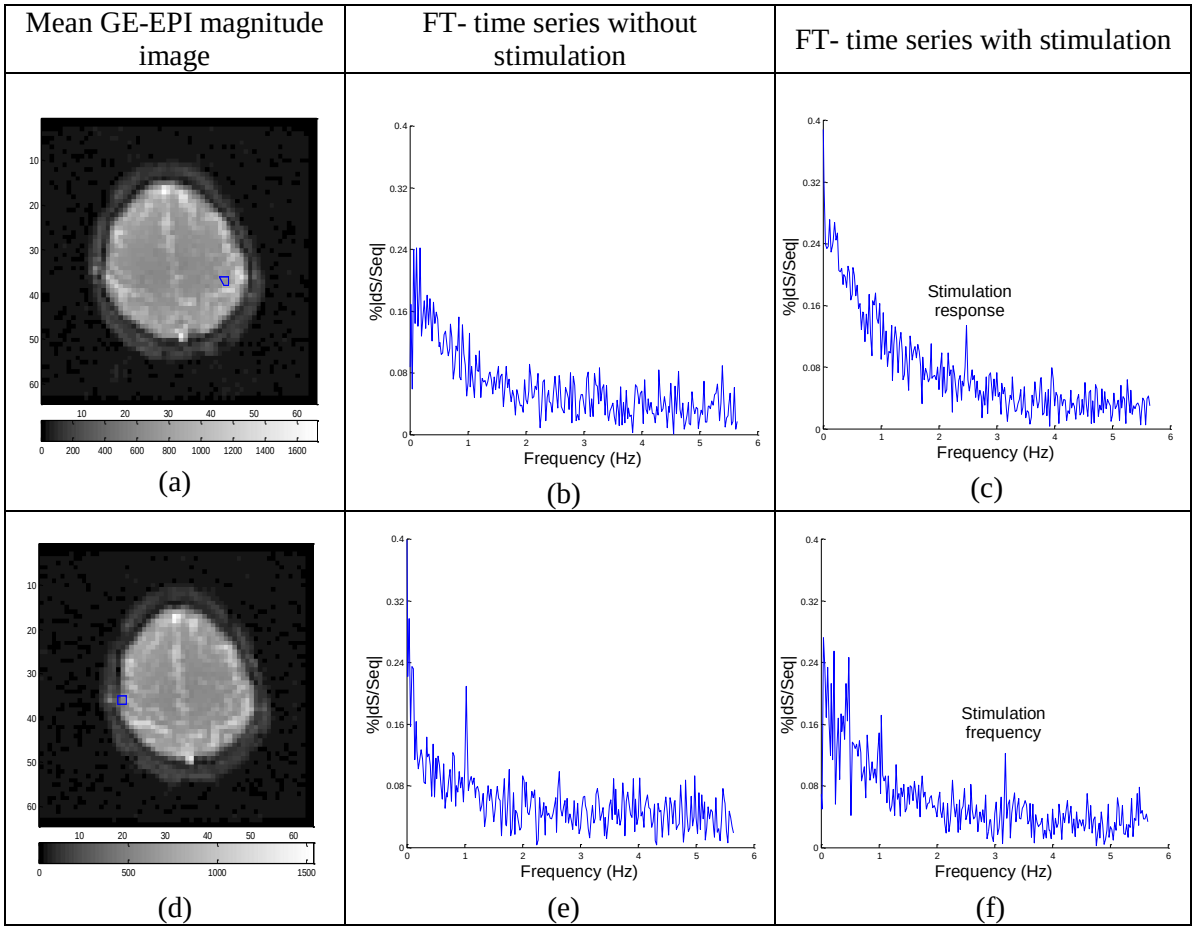

Figure 6. 1: Typical experimental results illustrating control experiments (all OFF blocks) and stimulation with 2.5 Hz and 3.2 Hz using fast fMRI TR = 88 ms with a TENS paradigm applied to the median nerve to stimulate the motor sensory cortex. (a) Mean GE-EPI magnitude image at 2.5 Hz stimulated frequency. (b) Measured frequency spectra shows no significant response in the ROI in the control experiment (c) Measured frequency spectrum shows response at the applied frequency. (d) Mean GE-EPI magnitude image shows ROI selected in the left hemisphere of brain. (e) measured frequency spectrum shows no peaks at the specific frequency in the control experiment however there is also a peak at 1 Hz corresponding to the heartbeat. (f) shows a response at 3.2 Hz as well as peaks due to respiration and heartbeat at 0.3 and 1 Hz respectively.

In these examples, the percentage signal changes were corrected relative to the full equilibrium signal value using a white matter relaxation time in the motor sensory cortex at 1.5T of T1 = 660 ms (Ethofer, Mader et al. 2003, Wright, Mougin et al. 2008). Therefore, the mean measured percentage signal change for the stimulated frequencies 2.5 and 3.2 Hz were 0.079 ± 0.016% and 0.08 ± 0.009% respectively, with a mean SNR = 4:1. According to equation 3.1 and the associated curve shown in figure 5.9, using TE = 25 ms, the corresponding axonal fields were ΔB_{ms} of 0.74 ± 0.15 and 0.8 ± 0.09 nT respectively.

SPM was used to identify activated regions with a z-score of 2.0, shown in figure 6.2.

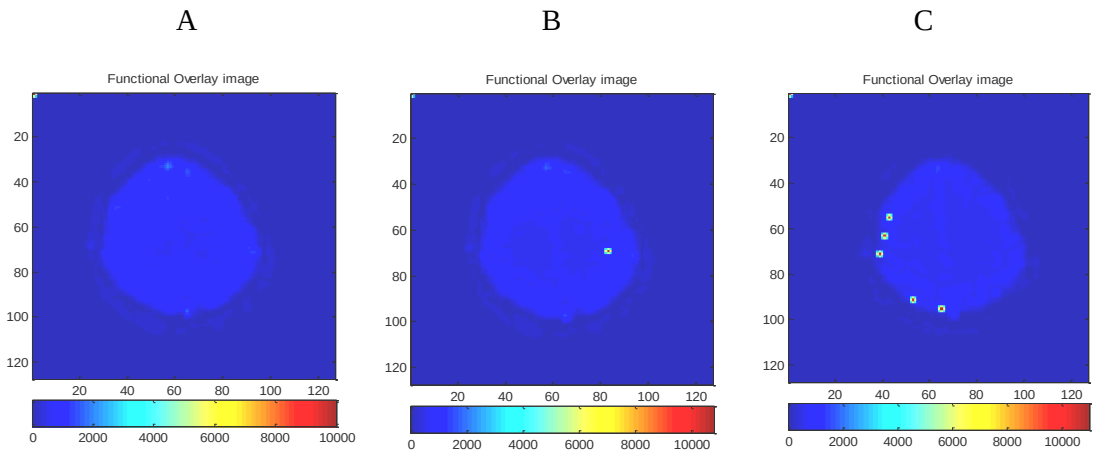

Figure 6. 2: Overlay images for typical control experiments without stimulation (all OFF blocks) and TENS stimulation applied to the median nerve to stimulate the motor sensory cortex with 2.5 Hz and 3.2 Hz stimulation frequencies using fast fMRI TR = 88 ms, TE = 25 ms with an eight-channel head coil The hand used for data acquisition was chosen randomly. (a) Overlay image for a typical control experiment with a Z-score of 2.0 showing no significant response in the motor sensory cortex. (b) Overlay image with a Z-score of 2.0 shows significant response (highlighted in red) in the ROI in the right hemisphere of the brain with 2.5 Hz stimulation (c) Overlay image showing response with 3.5Hz stimulation in the left hemisphere of the brain.

Figure 6.2 shows significant responses in the motor sensory cortex for both frequencies, 2.5 and 3.2 Hz, using TENS stimulation of the median nerve and these responses did not occur

in the non-stimulated experiments using the same Z-score. However, there are some other significant red pixels in the visual cortex of the 3.2 Hz experiments, which could be due to simultaneous tasks undertaken by the subject related to activation of the visual cortex. It is possible that one of the brain hemispheres is dominant based on personality and cognitive style, or that higher activity tends to activate both sides of the brain. Thus, more investigation is required for future study using fast fMRI with specific tasks.

Table 6.1 records the overall results for the median nerve TENS stimulated motor-sensory cortex experiments. Table 6.2 summarizes the motor sensory cortex experiments for the TENS stimulation paradigm. The mean percentage signal change was $\%|\Delta S/S_{eq}| = (0.077 \pm 0.012)\%$ corresponding to a mean axonal magnetic field $\Delta B_{ax} = (0.73 \pm 0.1)$ nT. The mean SNR = 3:1. A positive detection rate of 91% was found. This detection rate was similar to that found for the visual cortex using strobe light stimulation, as described in the previous chapter.

Table 6. 1: Motor sensory cortex experiments using a range of stimulation frequencies between (2.3 to 3.8 Hz) at 1.5T - $\%|\Delta S/Seq|$, ΔB_{ax} (nT), and SNR

Stimulation frequency (Hz)	$\%\|\Delta S/S_{eq}\|$	ΔB_{ax} (nT)	SNR
2.3	0.086	0.81	3:1
2.4	0.081	0.76	4:1
2.5	0.08	0.74	4:1
2.6	0.043	0.4	3:1
2.8	0.083	0.78	3:1
2.9	0.08	0.76	3:1
3.2	0.085	0.8	3:1
3.3	0.066	0.62	3:1
3.4	0.077	0.72	3:1
3.5	0.085	0.8	3:1
3.6	0.093	0.89	3:1
3.7	0.067	0.63	3:1
3.8	0.083	0.78	3:1

Table 6. 2: Summary of the motor sensory cortex experiments using TENS paradigm at 1.5T

TENS frequency (Hz)	Detected	Not detected
2.3	2	
2.4	2	1
2.5	2	-
2.6	2	-
2.8	2	-
2.9	2	-
3.2	1	1
3.3	3	1
3.4	2	-
3.5	4	-
3.6	3	1
3.7	2	-
3.8	2	-

6.3 Fast fMRI experiments using TENS and Finger tapping simultaneously

6.3.1 Acquisition methodology

Simultaneous TENS machine and finger tapping experiments were performed on the 1.5T MRI system with an eight-channel head coil as described in Chapter 2.

6.3.2 Experimental results

Individual results for motor sensory area activation using simultaneous TENS stimulation and a finger tapping task are summarized for different stimulation frequencies in Table 6.3. The subjects' tapping rate was self-selected and the TENS machine frequency was set to avoid cardiac and respiration peaks. Figure 6.3 shows typical experiments on the motor

sensory cortex with stimulation at two different frequencies simultaneously. The FT of the time series from the ROI, shown in blue, shows responses from the two different stimulation frequencies.

Equation 3.1 was used to calculate the percentage signal change $\%|\Delta S/S_{eq}|$ relative to the fully relaxed equilibrium signal as described previously. A 0.068% finger tapping response with SNR = 3:1 was detected at 1.5 Hz and a 0.064% TENS response with SNR = 3:1 was detected at 2.5 Hz from the motor sensory cortex (figure 6.3c). A 0.064% response with SNR = 3:1 and a 0.073% response with SNR = 3:1 were also detected at 1.7 Hz and 3.6 Hz for both finger tapping and TENS stimulation respectively from the motor sensory cortex in another subject (figures 6.3d and 6.3f). These signal changes correspond to axonal magnetic fields ΔB_{ax} of 0.64 and 0.7 nT respectively using equation (3.1) according to the Lorentzian field model in figure (5.9) at TE = 25 ms. Using Student's t-test, the method detected a significant difference ($P<0.05$) between stimulation and control experiments. In addition, peaks were also detected at the heartrate (1 and 1.1 Hz) and 0.35 and 0.3 Hz for respiration for the two subjects respectively.

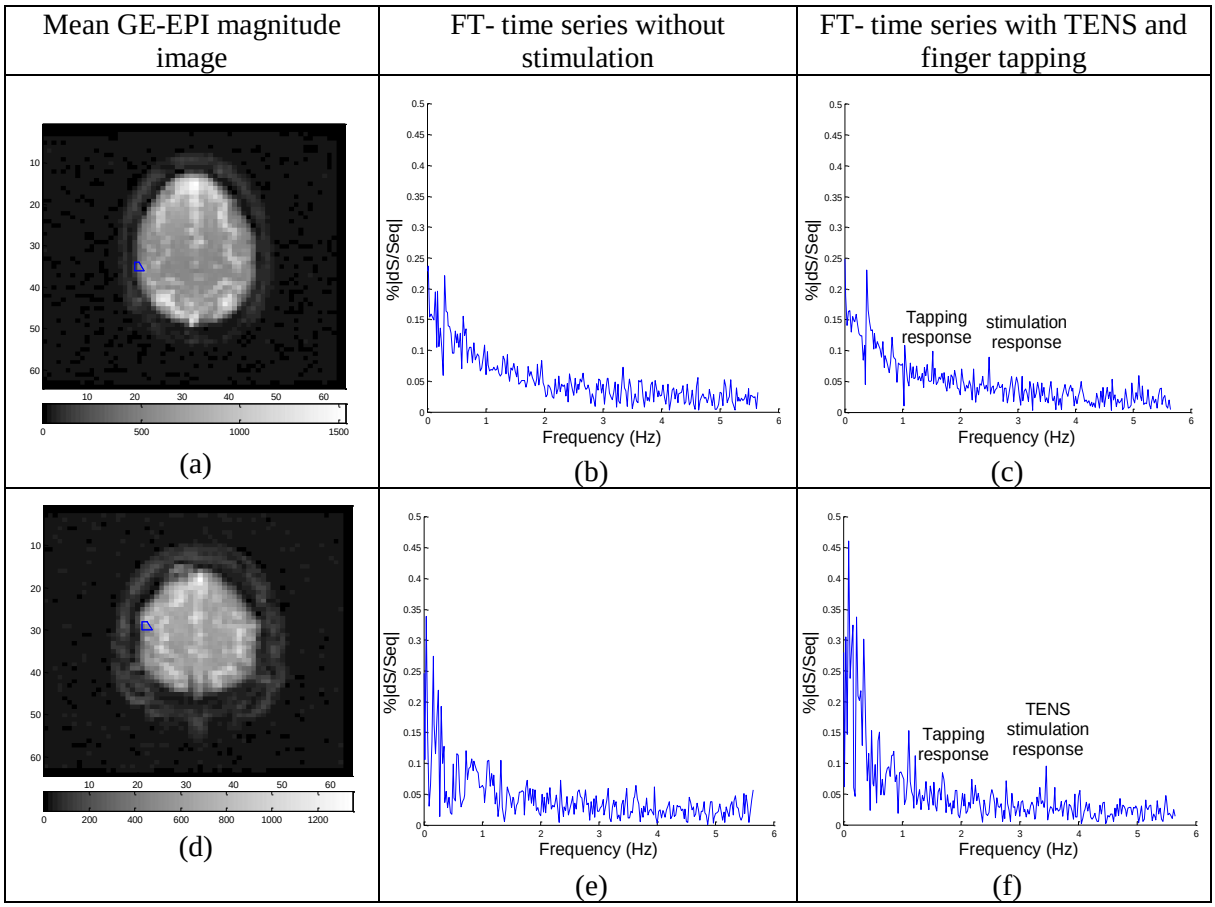

Figure 6. 3: Simultaneous finger tapping and TENS stimulation. The figure shows control experiments without stimulation (all OFF blocks), finger tapping rate and TENS stimulation applied to the median nerve on the contra-lateral hand to stimulate the motor sensory cortex using fast fMRI with TR = 88 ms. (a) Mean GE-EPI magnitude image (b) Measured frequency spectrum from control experiment showing no significant response in the ROI. (c) Measured frequency spectrum showing response with a 2.5 Hz TENS stimulation frequency and a finger tapping rate of 1.5 Hz (d) Mean GE-EPI magnitude image (e) Measured frequency spectrum from control experiment showing no response peaks at specific frequencies. (f) Measured frequency spectrum showing responses at 3.6 Hz from the TENS stimulation and at 1.7 Hz from the finger tapping.

Figure 6.4 shows statistical mapping results for the motor sensory cortex. The Z-score used was 2.0. The left hemisphere of the brain shows correlated pixels. There was (a) no significant response in the motor sensory cortex during control experiments (b) and (c) show significant responses (highlighted in red) in the ROI in the left hemisphere of the brain from simultaneous stimulation by finger tapping and median nerve TENS electrical stimulation.

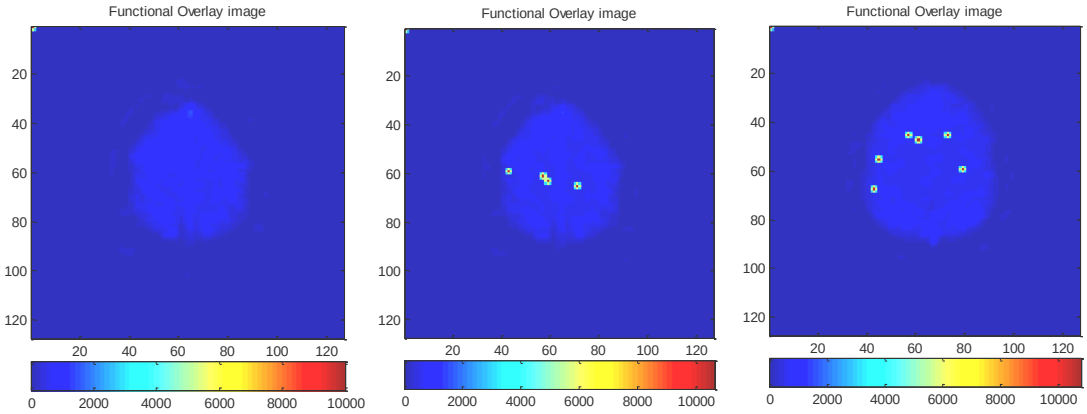

Figure 6. 4: Overlay image for typical control experiments without stimulation and two different frequencies applied to the median nerve with simultaneous finger tapping to stimulate motor sensory cortex using same Z- score and paradigm that was presented in chapter 2. a) Overlay image for a typical control experiment , b) Overlay image for TENS frequency at 2.5 Hz and a finger tapping rate of 1.5 Hz and c) Overlay image for stimulated frequency at 3.6 Hz from the TENS machine and finger tapping at 1.7 Hz for a different subject.

6.3.3 Summary

Tables 6.3 and 6.4 summarise all the motor sensory cortex experiments using simultaneous finger tapping and TENS stimulation tasks. The mean percentage signal change was $\%|\Delta S/S_{eq}| = (0.07 \pm 0.004)\%$ corresponding to a mean axonal magnetic field $\Delta B_{ax} = (0.72 \pm 0.1)$nT for the TENS stimulation frequencies and $\%|\Delta S/S_{eq}| = (0.06 \pm 0.01)\%$ with $\Delta B_{ax} = (0.56 \pm 0.1)$nT for the finger tapping. A mean SNR = 3:1 was found. The results show a detection rate of 90% for TENS stimulation and 30% for finger tapping.

Table 6. 3: Percentage signal change for responses from the motor sensory cortex experiments and corresponding axonal magnetic fields and SNR values using finger tapping and TENS machine stimulation paradigms

TENS stimulation frequency (Hz	$\%\lvert\Delta S/S_{eq}\rvert$	ΔB_{ax} (nT)	SNR	Finger tapping rate (Hz)	$\%\lvert\Delta S/S_{eq}\rvert$	ΔB_{ax} (nT)	SNR
2.5	0.064	0.61	4:1	1.5	0.068	0.64	3:1
3.5	0.07	0.86	3:1	1.6	0.047	0.44	3:1
3.6	0.073	0.69	3:1	1.7	0.064	0.6	3:1

Table 6. 4: Summary of the motor sensory cortex experiments using finger tapping and TENS machine stimulation paradigms at 1.5T with TE = 25 ms

Stimulation frequency (Hz) Tapping and TENS	Finger Tapping		TENS stimulation	
	Detected	Not detected	Detected	Not detected
1.5 and 2.5	1	3	3	1
1.6 and 3.5	1	1	1	1
1.7 and 3.6	1	3	3	1

6.4 Investigation of possible fast fMRI responses from the thalamus

6.4.1 Acquisition methodology

Fast fMRI experiments were performed to assess responses from the thalamus A 1.5T MRI system was used with an eight-channel head coil for acquisitions from four subjects with no known neurological pathology using a TENS machine to stimulate the median nerve. The hand side was chosen randomly. The methodology was the same as that used for the motor sensory testing using the TENS machine (chapter 2, section 2.3.2.1). However, in these

experiments the two slice planes were sagittal and axial and a Z-score = 2.0 was used for analysis.

6.4.2 Experimental results (sagittal plane)

Two typical data sets are shown in Figure 6.5 revealing a significant fast fMRI response from the thalamus with applied frequencies of 2.6 and 3.8 Hz in the same subject using sagittal slices shown and recorded in Figure 6.5, Table 6.5 respectively. The voxel size was $3.75\times3.75\times5$ mm^3 for all experiments. The TENS stimulus responses had a percentage signal change of 0.1%, with SNR = 6:1 and 0.09% with SNR = 4:1 for 2.6 Hz and 3.8 Hz frequencies, respectively. These results correspond to axonal magnetic fields of 0.94 nT and 0.86 nT.

Response peaks from the selected ROI during stimulation differed significantly using a Student's t-test ($p<0.05$) from non-stimulated experiments for each frequency (IBM SPSS v21.0). Comparing the results with the motor sensory cortex, the response from the thalamus was about 0.03% higher and the SNR was also better.

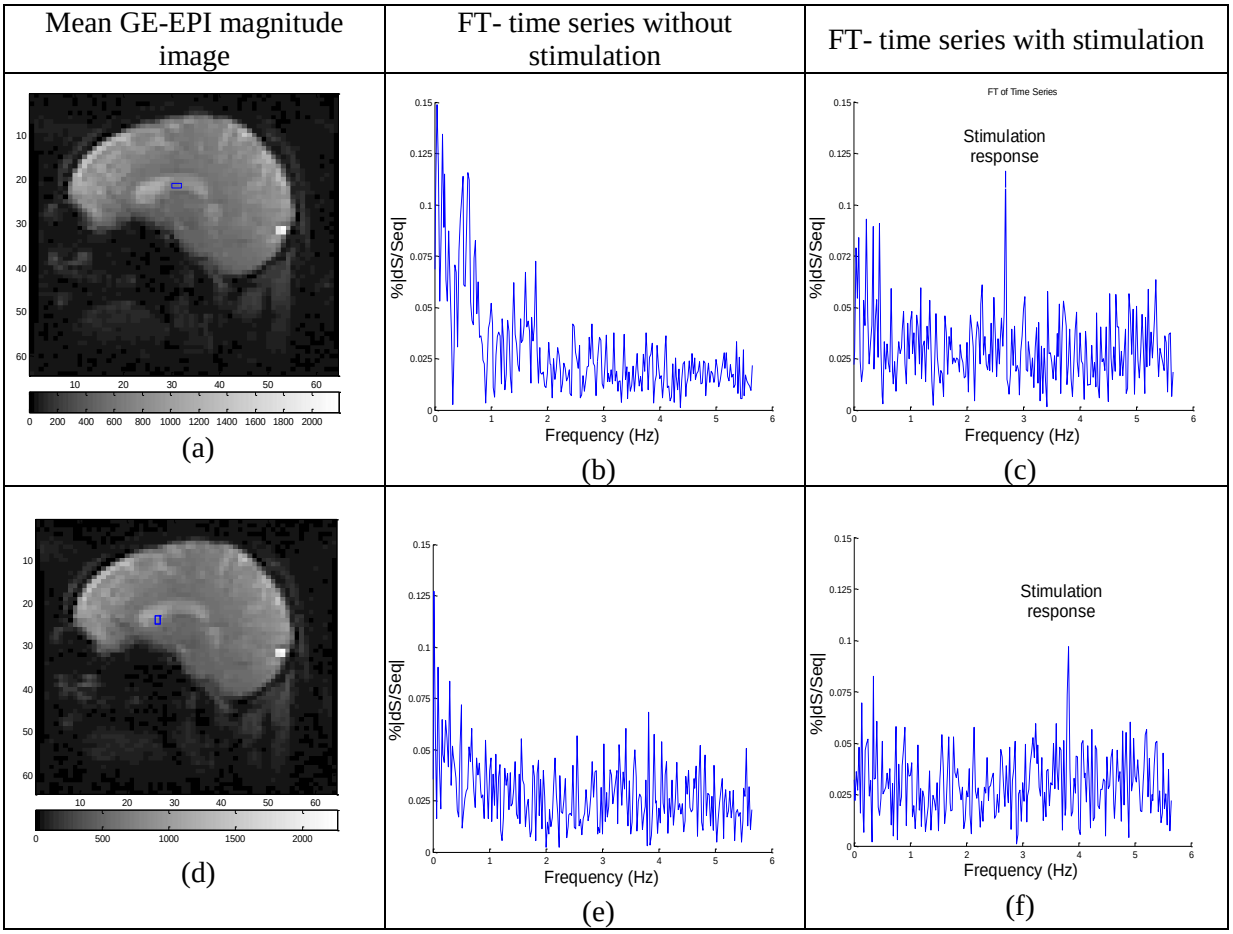

Figure 6. 5: Two typical experiments with TENS stimulation. The figure shows control experiments without stimulation (all OFF blocks) and stimulation at 2.6 Hz and 3.8 Hz applied to the median nerve to stimulate the thalamus. (a) Mean GE-EPI magnitude showing selected ROI. (b) FT of the time series showing no significant response in the ROI during control experiments. (c) Measured frequency spectrum showing a response at the applied frequency of 2.6 Hz (d) Mean GE-EPI magnitude image (e) FT of the time series showing no response during control experiment (f) Measured frequency spectrum showing a response at the applied frequency of 3.8 Hz

Figure 6.5 shows the results of typical experiments using two different frequencies (2.6 and 3.8 Hz) and control experiments on the thalamus. Control experiments did not show significant pixels. There were many significant pixels (highlighted in red) in the thalamus, resulting from median nerve TENS stimulation of the motor sensory cortex at 2.6 Hz as shown in figure 6.6b. In addition, there were significant pixels in other regions that could be related to blood vessels observed at both frequencies.

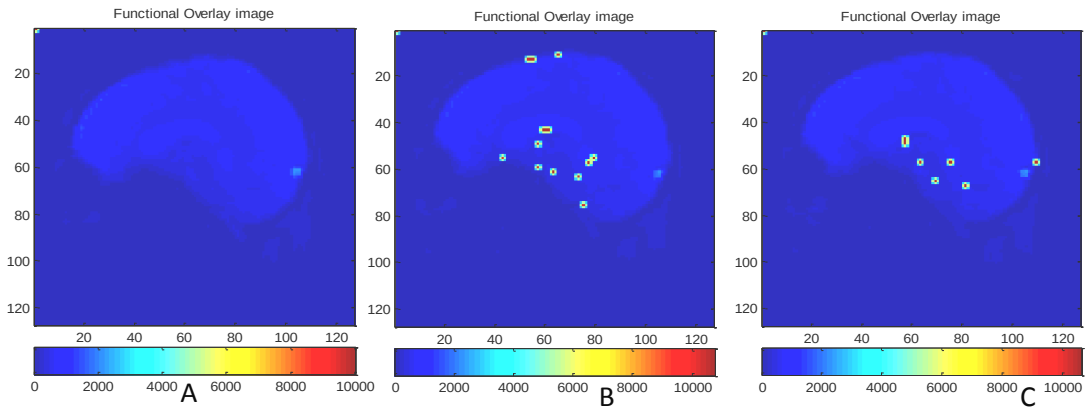

Figure 6. 6: Statistical mapping for the thalamus experiments showing significant pixels related to the TENS stimulation. Note: no active pixels were seen during control experiment without stimulation (all OFF blocks), whereas many active pixels were seen with median nerve stimulation at 2.6 Hz (b) and 3.8 Hz (c).

6.4.3 Experimental results (axial plane)

The methodology used was the same as in the previous section except that the slice was changed to the axial plane. Fast fMRI activity was significantly greater in the thalamus than other brain regions with TENS stimulation.

Figure 6.7 presents fast fMRI signal responses at 2.5 and 3.7 Hz. The non-stimulated control experiments are shown in figures 6.7b and 6.7e). The mean percentage signal

change was 0.07 ± 0.01% and the corresponding axonal magnetic field was 0.6 ± 0.02 nT with a mean SNR = 3:1. The voxel size was 3.75×3.75×5 mm^3.

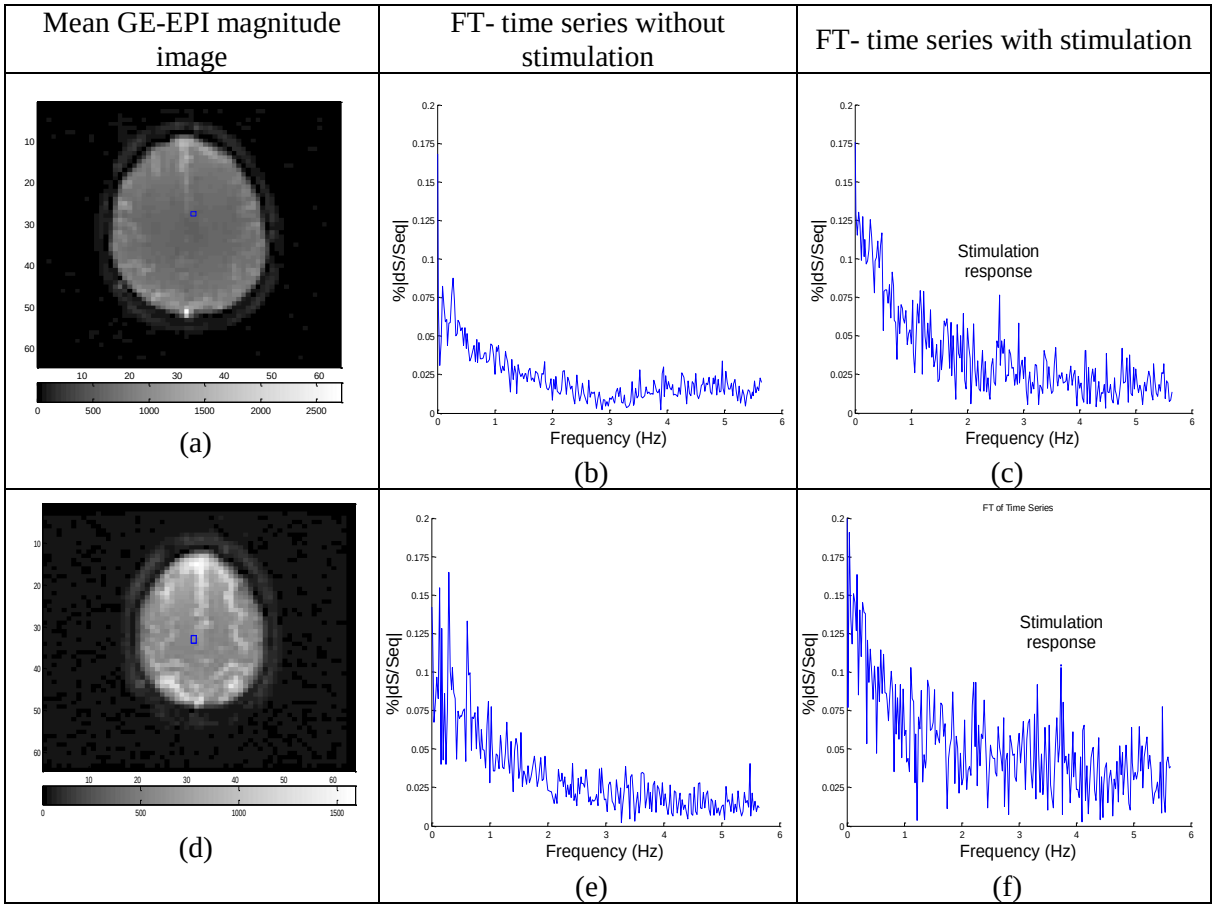

Figure 6. 7: Two typical experiments using axial slices and the TENS stimulation paradigm. The figure shows control experiments (all OFF blocks) and TENS stimulation applied at 2.5 Hz and 3.7Hz to stimulate the thalamus. (a) Mean GE-EPI magnitude (b) FT of the time series showing no significant response in the ROI during control experiments. (c) Measured frequency spectrum showing a response at the applied frequency of 2.5Hz (d) Mean GE-EPI magnitude image (e) FT of the time series showing no significant responses in the control experiment (f) FT of the time series showing a stimulated frequency response at 3.7Hz.

Figure 6.8 illustrates statistical mapping at 2.5 Hz and 3.7 Hz using a Z-score of 2.0. There were no significant pixels in the non-stimulated control experiments whilst there were active pixels for both stimulation frequencies (2.5 and 3.7 Hz). The number of significant pixels depends on the Z-score.

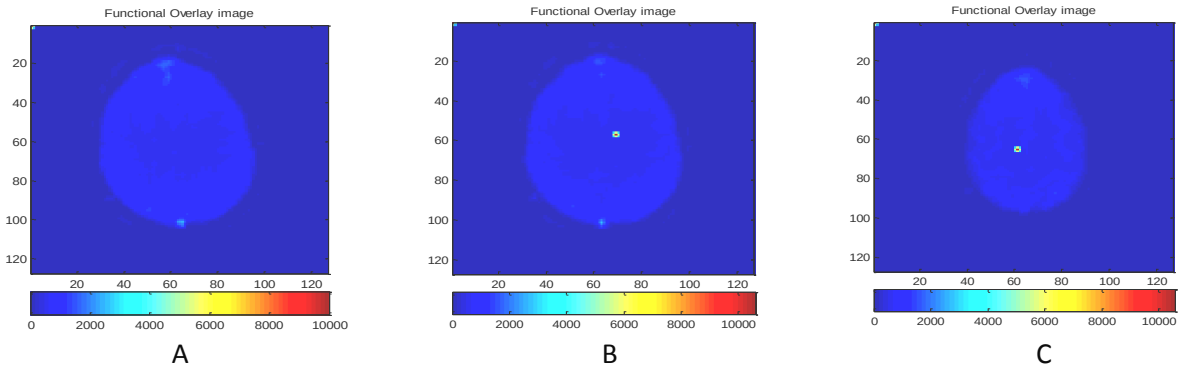

Figure 6. 8: Shows axial plane statistical mapping for the thalamus experiments acquired in the axial plane showing significant pixels that are related to the TENS stimulation using a Z score of 2.0 and TR = 88 ms. a) Overlay image showing no significant response in the thalamus without stimulation. (b) Overlay image shows significant response (highlighted in red) in the thalamus due to the stimulated frequency of 2.5 Hz and (c) Overlay image showing response of the thalamus with a stimulated frequency of 3.5 Hz.

Tables 6.5 and 6.6 summarises all of the experiments performed with thalamus activation in the sagittal and axial planes. They record the detectable mean percentage magnitude signal changes, axonal magnetic field and SNR using the TENS stimulation paradigm.

Table 6. 5:Summary of acquisitions in the sagittal and axial planes with a range of stimulation frequencies and percentage signal changes for the thalamus experiments with corresponding axonal magnetic fields and SNR.

Slice plane	Stimulated frequency (Hz)	$\%\lvert\Delta S/S_{eq}\rvert$	ΔB_{ax}	SNR
Sagittal	2.6	0.1	0.94	6:1
	3.8	0.09	0.86	4:1
Axial	2.3	0.08	0.79	3:1
	2.5	0.076	0.072	3:1
	2.8	0.08	0.76	3:1
	3.3	0.06	0.62	3:1
	3.4	0.057	0.53	3:1
	3.7	0.075	0.7	3:1

Table 6. 6: Summarizes the thalamus experiments using TENS machine paradigm frequencies at 1.5T with TE = 25 ms, (N means the experiment was not performed)

Stimulation frequency (Hz) Tapping and TENS	Sagittal plane		Axial plane	
	Detected	Not detected	Detected	Not detected
2.3	N	-	2	-
2.5	N	-	2	-
2.6	2	-	1	-
2.8	N	-	1	1
3.3	N	-	2	-
3.4	N	-	2	1
3.7	N	-	1	1
3.8	2	-	N	-

6.5 A fast functional magnetic resonance imaging study of motor and sensory cortex activation using finger tapping tasks at 1.5T and 3T

6.5.1 Acquisition methodology

Regions of the sensorimotor cortex that were activated by finger tapping were previously identified using BOLD functional MRI methodology (Friedman, Glover et al. 2006, Mostofsky, Rimrodt et al. 2006). This section investigates whether responses to finger tapping can be detected using the fast fMRI method. A fast fMRI FT time series was acquired from echo-planar image (EPI) at 1.5T with an eight-channel head coil and at 3T with a 32 channel head coil (as described in chapter 2, sections 2.5.1 and 2.5.2).

6.5.2 Experimental results at 1.5T

All imaging results were based on individual finger tapping rates, with slightly different durations for each subject. As can be seen in figure 6.9c, there was a significant tapping response from the chosen 2×2 voxel ROI in the right hemisphere of the brain in the motor sensory cortex (voxel size 3.75×3.75×5 mm^3). In this experiment the finger tapping response was at 1.6 Hz (the volunteer tapping rate). In another volunteer the observed frequency was at 1.7 Hz (figure 6.9f), while there was no response during the control conditions. Thus activations relative to finger tapping were as expected. However, physiological responses were observed in the 1D frequency spectra in both subjects due to the heartbeat and respiration at 1.1 and 0.3 Hz respectively. The mean measured percentage

signal change at 1.6 and 1.7 Hz was 0.07%, corresponding to a predicted axonal field of 0.7 nT with SNR = 3:1.

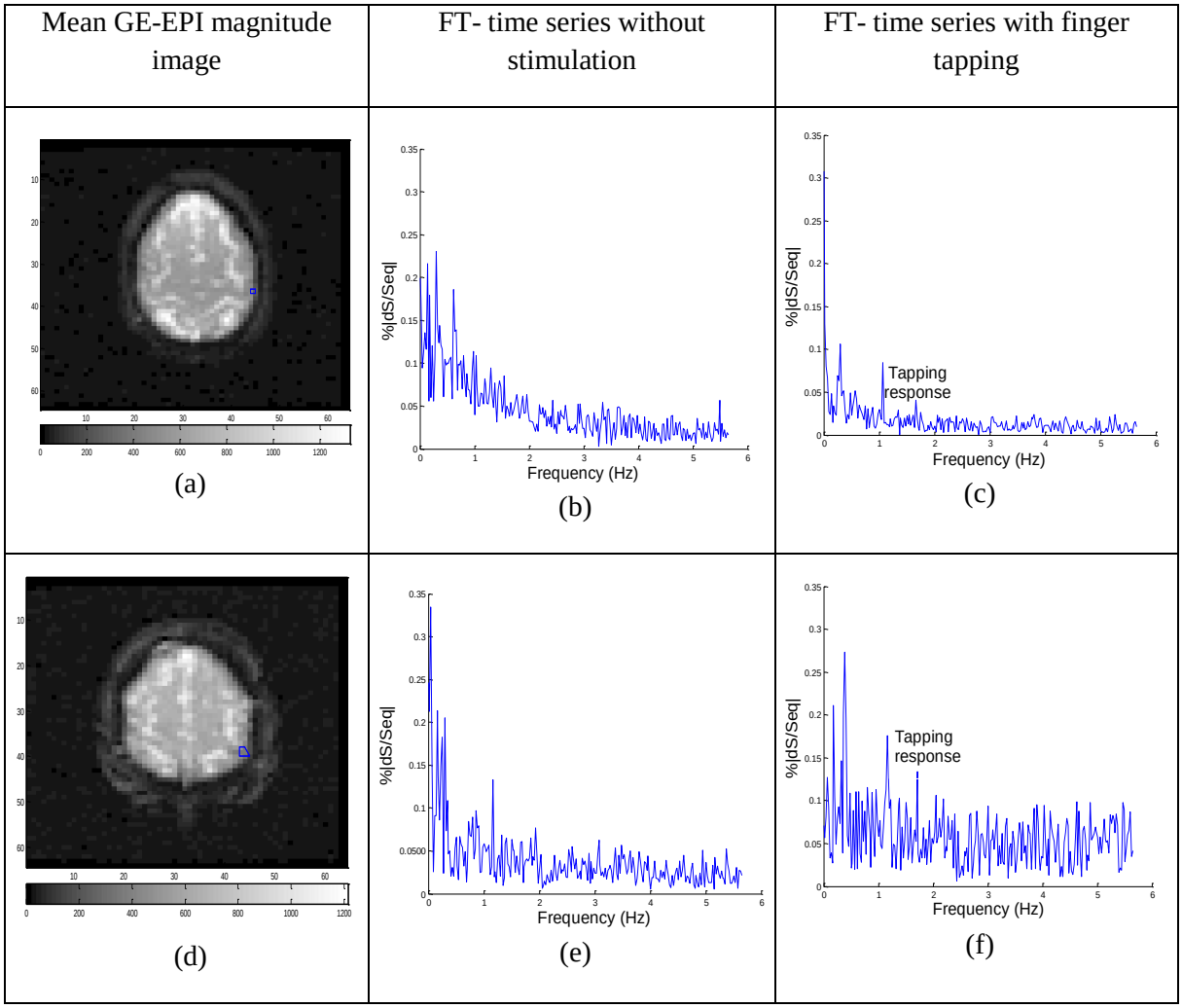

Figure 6. 9: Two typical experiments with a finger tapping paradigm using an eight-channel head coil at 1.5T. It shows two different subjects with control experiments (all OFF blocks), and two different tapping rates of 1.6 and 1.7 Hz. (a) Mean GE-EPI magnitude image (b) FT of the time series showing no significant response during control experiments. (c) Measured frequency spectrum showing a response at the applied frequency of 1.6 Hz. (d) Mean GE-EPI magnitude image. (e) FT of the time series shows no peaks at the specific frequency in the control experiment (f) FT of the time series showing a tapping response at 1.7 Hz

Figure 6.10 shows statistical mapping with a Z-score of 2.0 for these two experiments. Significant activation (highlighted in red) in response to finger tapping at 1.6 and 1.7 Hz is shown in figures 6.10b and 6.10c respectively. The finger tapping condition revealed fast fMRI responses in the right motor sensory strip, while there was no activation in this area during the control condition.

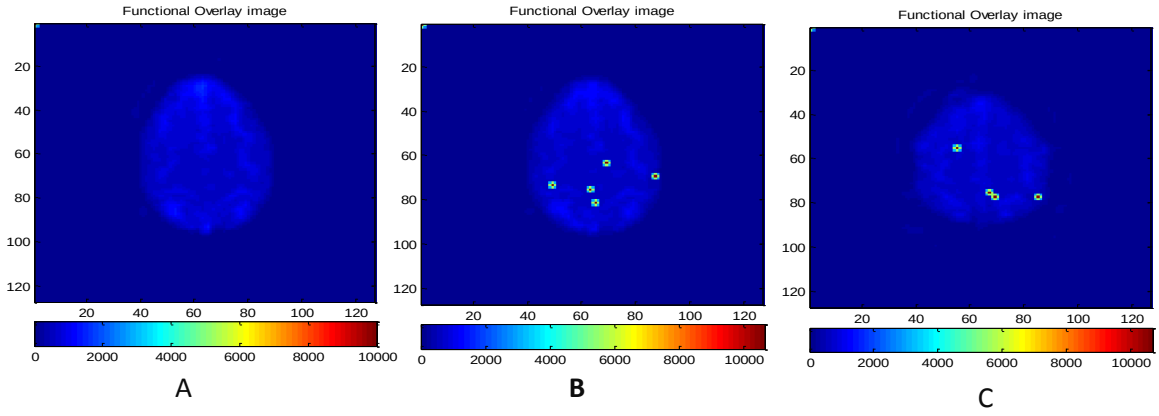

Figure 6. 10: Shows statistical maps from two different subjects in the axial plane with finger tapping. Significant pixels are highlighted in red using a Z score of 2.0 and TR = 88 ms. a) No active pixels were seen during control experiments b) Overlay image shows significant response (highlighted in red) in the ROI of the motor sensory and other unknown regions due to finger tapping at 1.6 Hz and (c) Overlay image showing response with a finger tapping rate of 1.7 Hz.

6.5.3 Experimental results at 3T

The motor sensory cortex results for two typical finger tapping experiments are given in figure 6.11. For the first experiment the tapping response was nominally detected at 1.8 Hz at the finger tapping frequency (figure 6.11c). The peak corresponds to the selected 2×2 voxel ROI (figure 6.11a) in the left hemisphere of the brain in the motor sensory cortex (voxel size 1.875×1.875×5 mm^3) acquired using a 32 channel head coil. The measured percentage signal change was 0.1%, corresponding to an axonal field ΔBax = 0.97 nT with SNR = 5:1. For the second experiment, the resultant 0.087% percentage signal change is related to a 0.82 nT axonal field with SNR = 4:1. There were significant differences

between the data sets obtained from the finger tapping and control experiments according to a Student's t-test ($p<0.05$) (IBM SPSS v 21.0). A peak was observed in the second experiment due to the heartbeat at 1.1 Hz.

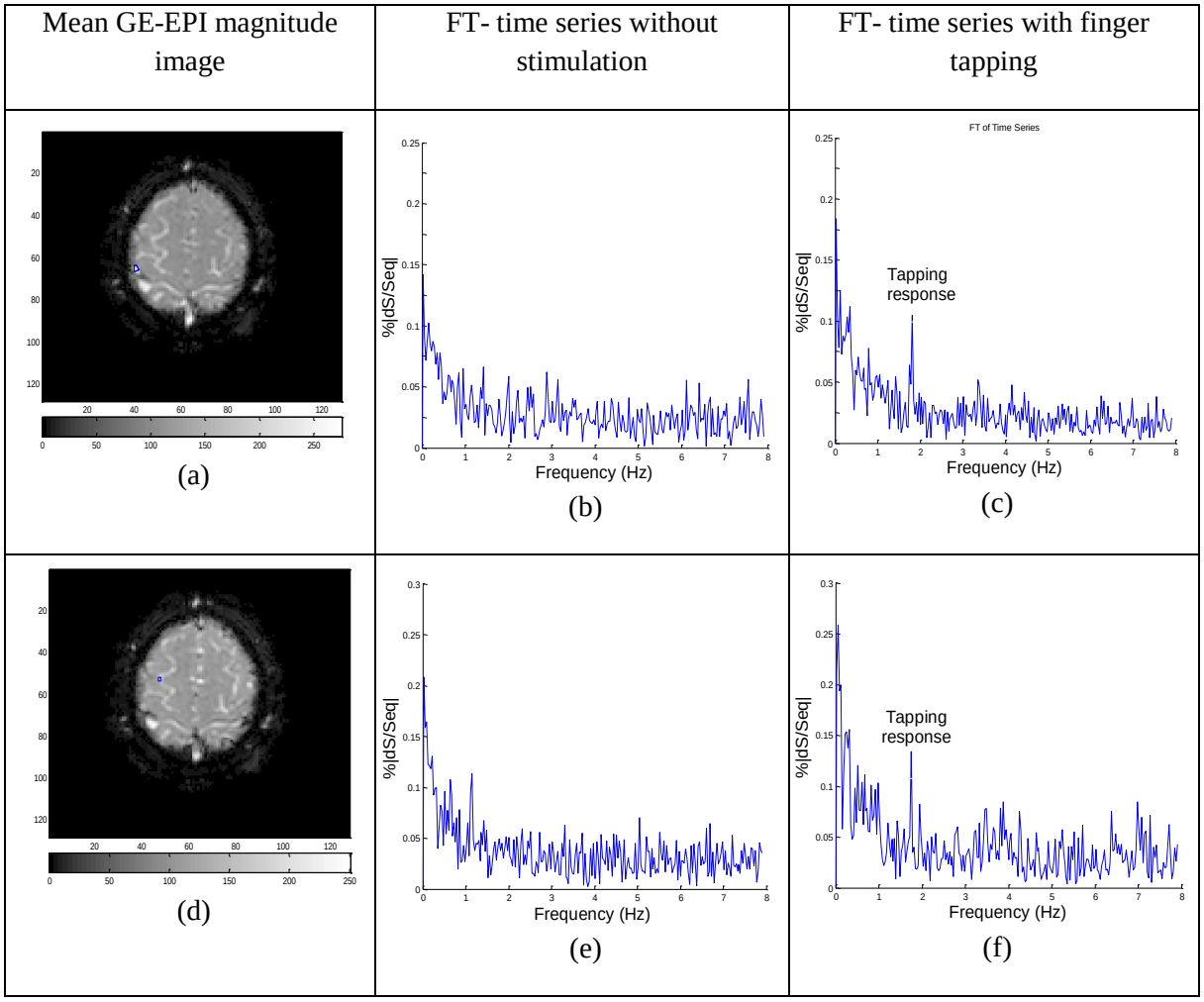

Figure 6. 11: Two typical examples of a finger tapping paradigm using a 32 channel head coil at 3T with two different tapping rates of 1.7 and 1.8 Hz. (a) Mean GE-EPI magnitude (b) FT of the time series showing no significant response in the ROI during control experiments (c) Measured frequency spectrum showing a response at the tapping frequency of 1.8Hz. (d) Mean GE-EPI magnitude (e) FT of the time series from the control experiment showing no response peaks but a peak at 1.1 Hz due to the heartbeat. (f) FT of the time series showing a response at the stimulated frequency of 1.7 Hz.

Statistical mapping analysis at 3T used a different Z-score (Z = 2.5) to suppress physiological artifacts. Figure 6.12 shows results from the motor sensory cortex for the same dataset shown in figure 6.10. No significant pixels were seen in the control experiments but significant pixels were seen with finger tapping at 1.8 and 1.7 Hz, highlighted in red in figures 6.12B and 6.12C respectively.

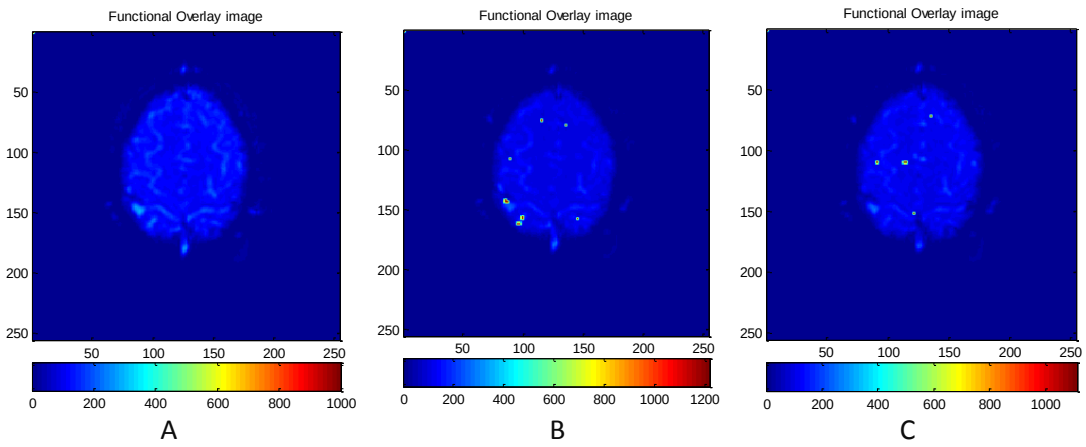

Figure 6. 12: Shows two different experiments performed at 3T with a finger tapping task in the axial plane using a Z score of 2.5. The overlay image in (a) shows there is no active pixel during the control experiment b) responses are seen in the left hemisphere of the brain during right finger tapping at a rate of 1.8 Hz and c) Finger tapping at 1.7 Hz. All images acquired using fast fMRI with TR = 63 ms and TE = 25 ms

Experimental results for the motor sensory cortex finger tapping experiments performed at 1.5T and 3T are summarised in tables 6.7 and 6.8. For datasets acquired at 1.5T, the correct frequency was observed in five out of twelve experiments on the six volunteers. Therefore, the detection rate was 42% with a mean percentage signal change of 0.07 ± 0.01% corresponding to a predicted axonal field of 0.7 ± 0.012 nT, with SNR = 3:1. At 3T, 6 out

of 10 experiments were successful on the five volunteers with a 60% detection rate. The mean signal change was 0.1 ± 0.02% corresponding to a mean predicted axonal field of 0.9 ± 0.02 nT with SNR = 4:1.

Table 6. 7: Finger tapping rate and percentage signal changes for the motor sensory cortex finger tapping experiments and corresponding axonal magnetic field and SNR at 1.5T and 3T.

Field Strength	Stimulated frequency (Hz)	$\%\lvert\Delta S/S_{eq}\rvert$	ΔB_{ax} (nT)	SNR
1.5T	1.5	0.07	0.068	3:1
	1.6	0.08	0.79	3:1
	1.7	0.07	0.69	3:1
3T	1.6	0.07	0.86	3:1
	1.7	0.09	0.82	4:1
	1.8	0.1	0.97	5:1

Table 6. 8: Summarizes the motor sensory cortex experiments using finger tapping paradigm at TE = 25 ms.

Stimulation frequency (Hz) Tapping and TENS	1.5T		3T	
	Detected	Not detected	Detected	Not detected
1.5	1	3	N	-
1.6	3	1	1	3
1.7	1	3	2	1
1.8	N	-	2	1

6.6 Motor sensory cortex responses with imaginary finger tapping using fast fMRI at 3T

6.6.1 Acquisition methodology

Motor sensory activation was measured by fast fMRI during imagined finger tapping and compared to control experiments. These experiments were performed at 3T using a 32 channel head coil with TE = 25 ms and TR = 63 ms, and matrix size = 128×128. Five subjects with no history of neurological or orthopaedic conditions were involved in this experiment (see section 2.3.2.3 in chapter two for more details on these tasks).

6.6.2 Experimental results

The effect of imaginary tapping was easily seen in fast fMRI studies of motor sensory activation using simple tasks such as imagining the left or right hand tapping fingers. Figure 6.13 shows two results from typical experiments.

A significant response was observed for left hand imaginary tapping at the tapping rate of 1.7 Hz. The selected ROI was a 2×2 voxel (voxel size = 1.875×1.875×5 mm^3) shown on the GE-EPI magnitude image (figure 6.13a) in the right hemisphere. The percentage signal change resulting from the stimulus response was calculated as 0.08%, which corresponds to an axonal magnetic field of 0.76 nT with SNR = 4:1. The response to imaginary tapping by the right hand at 1.8 Hz was slightly lower than the percentage change in the left hand by 0.04% with an axonal magnetic field of 0.4 nT and SNR = 3:1 (figure 6.13f).

By comparing results for experiments during imaginary tapping with control experiments it can be concluded that the responses are most likely from the applied tasks. There was a significant difference ($p<0.05$) between control and applied task experiments using Student's t-test (IBM SPSS v 21.0). It can be seen that there are other spectral peaks present; at ~0.3 Hz this most likely represents respiration and at ~1 Hz it represents the cardiac frequency due to veins present in close proximity to the selected ROI.

The statistical map from the non-stimulated control experiment did not show any significant pixels using a Z-score of 2.5 (figure 6.14A). There were significant pixels activated with the imaginary finger tapping with the left hand highlighted in red in right brain hemisphere at 1.7 Hz (figure 6.14B). A few other active pixels in other regions most likely represent pulsation due to capillaries in the selected slice. Figure 6.14C shows a fast response due to imagined right hand finger tapping at 1.8 Hz; a significant pixel can be seen in the left hemisphere. Furthermore, there were two significant pixels in the frontal lobe and right side of the motor sensory cortex. More investigation is required regarding these other active pixels.

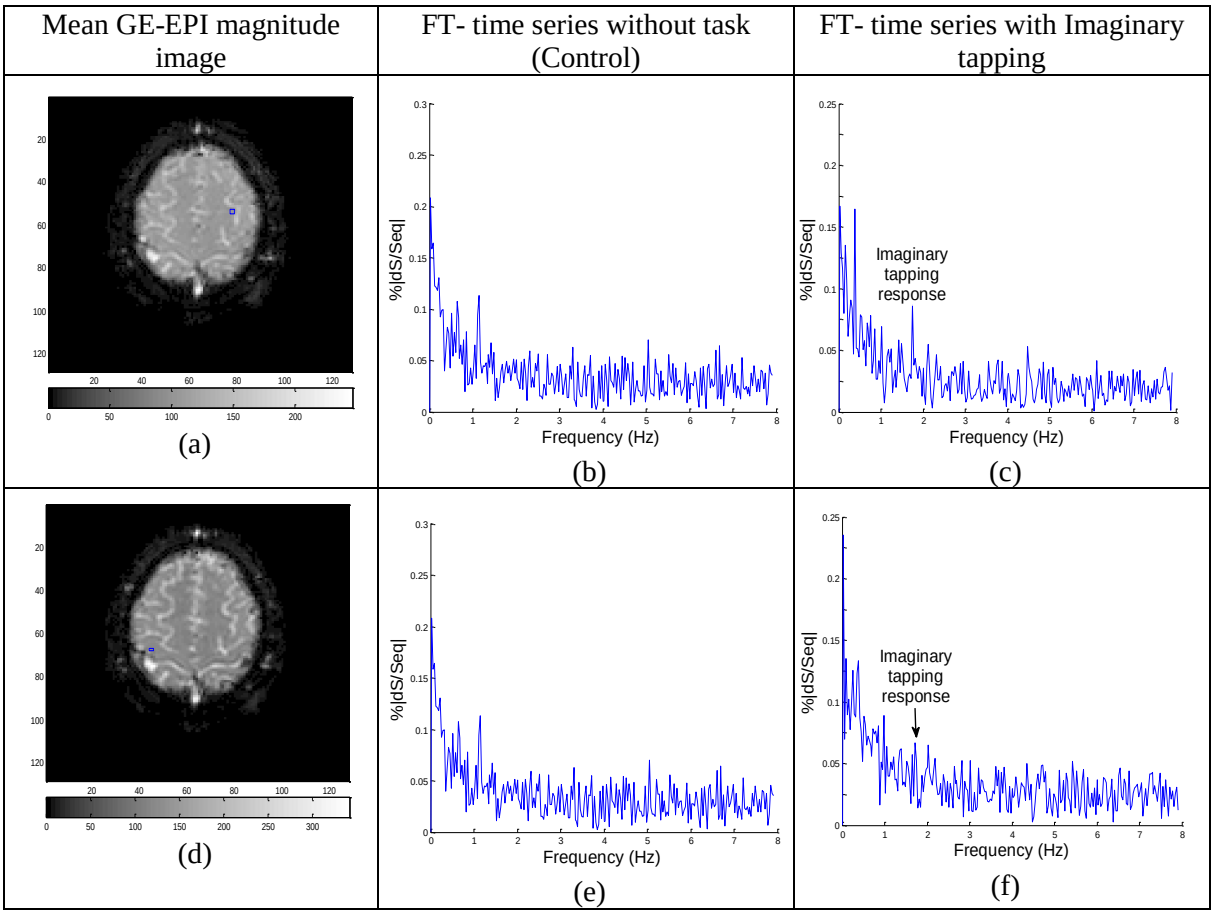

Figure 6. 13: Two typical imaginary finger tapping experiments using a 32 channel head coil at 3T with left and right hand tapping (a) Mean GE-EPI magnitude image and ROI selected (blue box) for the imagined left hand tapping (2×2 voxel ROI- voxel size $1.875 \times 1.875 \times 5\ mm^3$) (b) FT of the time series showing no significant response in the ROI during the control experiment and (c) response during the imagined task at 1.8 Hz (d) Mean GE-EPI magnitude image for imagined right hand tapping (1×2 voxel) (e) FT of the time series showing no response peak in the control experiment (f) a response peak is seen at 1.7 Hz.

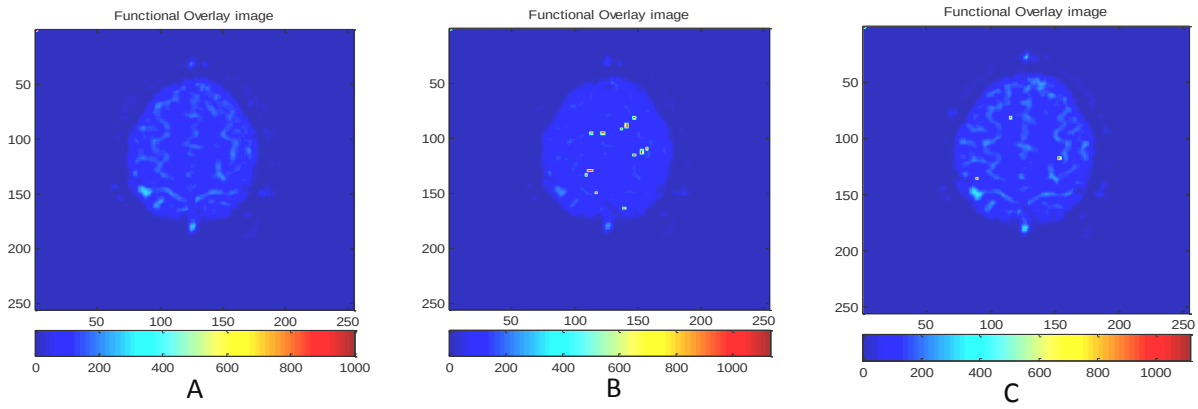

Figure 6. 14: Statistical maps for two typical imaginary finger tapping paradigms in the motor sensory cortex at 3T using a Z score of 2.5 showing the differences between rest and left and right hand imaginary finger tapping. The active pixels are highlighted in red. a) No active pixels were seen in control experiments, b) left hand imagined tapping with rate of 1.7 Hz and c) right hand imagined tapping with rate of 1.8 Hz.

The BOLD technique was also used to see whether the functional areas overlapped. Figure 6.15a shows significant active motor sensory cortex with BOLD data acquisition in figure (6.15b) at 1.5T. Figure 6.16 is from the same subject. These experiments were performed for comparison with the fast fMRI results.

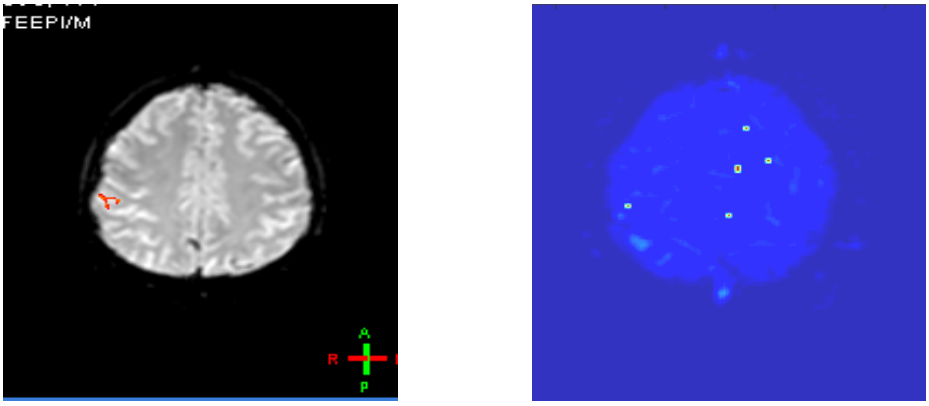

Figure 6. 15: shows two different techniques are used to compare and find the active pixels on the same subject, left image shows BOLD response during imaginary finger tapping task at 3T with a Z score of 2.0 while the right image shows a fast fMRI overlay image during imaginary finger tapping using the same Z score of 2.0 showing a correlation with the BOLD result.

A summary of the imaginary finger tapping data of all five subjects who participated in the experiment is recorded in tables 6.9 and 6.10. Table 6.9 shows the imagined finger tapping mean percentage signal change $\%|\Delta S/S_{eq}| = 0.05 \pm 0.02\%$, corresponding to a mean axonal field $\Delta B = 0.56 \pm 0.16$ nT with mean SNR = 3:1. Positive results similar to those shown below were observed for 40% of participants (i.e. four out of ten experiments on the five volunteers).

Table 6. 9: The imaginary finger tapping rate with percentage signal change, calculated axonal field and SNR from the motor sensory cortex experiments at 3T with TR = 63 and TE = 25 ms

Imagination finger tapping	Stimulated frequency (Hz)	$\%\|\Delta S/S_{eq}\|$	ΔB_{ax}	SNR
Left hand	1.6	0.068	0.64	3:1
	1.7	0.083	0.76	4:1
Right hand	1.7	0.04	0.4	3:1
	1.8	0.047	0.44	3:1

Table 6. 10: Experiments on imaginary finger tapping to stimulate the motor sensory cortex at 3T

Stimulation frequency(Hz) Tapping and TENS	Left hand		Right hand	
	Detected	Not detected	Detected	Not detected
1.5	-	1	-	1
1.6	1	-	-	1
1.7	1	1	1	-
1.8	-	1	1	1

6.7 Discussion

This chapter reports attempts to detect fMRI responses of brain neuronal activity using a range of different stimulation tasks. Successful detection requires an approach that takes into account discrimination between task responses and artefacts. The motor sensory cortex and thalamus were stimulated at the threshold of action potential generation using TENS at the median nerve, TENS and finger tapping simultaneously, motor and sensory cortex activation using a simple finger tapping task (for comparison with BOLD) and imaginary finger tapping. In addition, direct detection by fast fMRI was also attempted at a different MR field strength (3T) with a very sensitive 32 channel array coil in an attempt to improve signal to noise ratio.

These experiments provide support that fast fMRI can directly detect electromagnetic responses in the brain. All experiments gave approximately the same percentage signal changes and thus calculated axonal fields. However, the imaginary finger tapping had the lowest overall detection rate (40%). Evidence of fMRI responses in the motor sensory cortex during wrist stimulation by TENS was observed at the relatively high stimulation frequency range of 2.3 to 3.8 Hz. These results were observed at the correct frequency in 29 out of 33 experiments on the six volunteers with a significant detection rate of 91%. The response of the motor sensory cortex using TENS stimulation were very similar to those found from the visual cortex using strobe light stimulation in the previous chapter with the mean %|S/Seq| = (0.08 ± 0.01)% corresponding to the mean axonal magnetic field ΔB_{ax} = (0.7±0.1) nT with SNR = 3:1. There are some other significant pixels in the visual cortex from the functional overlay image of the 3.2 Hz experiments, which could be another task activated by the subject in the visual cortex. It is possible that one of the brain hemispheres is dominant based on personality and cognitive style, or that higher activity tends to activate both sides of the brain(Nielsen, Zielinski et al. 2013). Thus, more investigation is required for future study using fast fMRI with specific tasks.

Several recent studies using direct neuronal detection fMRI have reported motor sensory activation during rapid median nerve stimulation paradigm (Xue, Chen et al. 2009). The activation was observed with a percentage signal change of 0.2% - 0.3%, but it was

detected 80 ms after stimulation onset. Xiong et al. detected about a 1% change of the baseline signal in the motor cortex with a temporal resolution of 100 ms (Xiong, Fox et al. 2003).

Regarding simultaneous TENS stimulation and finger tapping tasks in the motor sensory cortex, responses were found at both frequencies (seen in figures 6.3c and 6.3f) in the expected region, and in other cortical regions such as the thalamus, the cerebellum and corpus callosum in the first subject (figure 6.4b) and subcortical motor areas and frontal lobe in the second subject (figure 6.4c). The spectral responses measured in the motor sensory cortex are detected away from hemodynamic, cardiac and respiratory responses through use of relatively high stimulation frequencies. As anticipated, detection rates were higher overall for the TENS stimulations than for the finger tapping experiments.

Mean percentage signal change was higher for TENS than for finger tapping, with (0.07 ± 0.004)% corresponding to a mean axonal magnetic field ΔBax = (0.72 ± 0.1) nT and $\%|\Delta S/Seq|$ = (0.06 ± 0.01)% with ΔBax = (0.56 ± 0.1) nT with SNR = 3:1 respectively. The rates of detection were 90% for the TENS stimulation and 30% for the finger tapping. This means that the TENS stimulation may be the dominant task as might be expected for a direct electric shock. In addition, interference may occur when a human attempts to perform two concurrent tasks and the second task may be deprioritized compared to the main task (Schubert and Szameitat 2003).

It is believed that the relatively strong responses demonstrated from the thalamus are due to direct neuronal detection and not due to hemodynamic responses. Previous studies on conventional functional MRI study of the thalamus (Davis, Kwan et al. 1998, Rauch, Whalen et al. 1998, Hazlett, Buchsbaum et al. 2001, Greicius, Flores et al. 2007) reported activation in the thalamus but so far there has been no study using direct detection methodology. However, a direct detection investigation on the corpus callosum was performed at 3T by Chow et al. which reported a low signal percentage change of 0.015 ± 0.005% corresponding to the mean axonal field of 0.12 ± 0.04nT using TR = 73 ms and TE = 35 ms (Chow 2005).

Evidence of fast fMRI responses in the thalamus (the brain's switching relay area) during wrist stimulation by TENS was observed at this relatively high stimulation frequency. These results correlated with the applied frequencies and were observed at the correct frequency with a significant detection rate of 83%, representing 15 out of 18 experiments on the four volunteers. The mean percentage signal change was 0.7 ± 0.01%, corresponding to an axonal magnetic field 0.65 ± 0.2 nT, which is approximately the same as motor sensory detection using the same stimulation paradigm. However, the sagittal plane showed higher percentage signal changes than the axial plane.

Finger tapping tasks are one of the most common paradigms used to study the human motor system in conventional functional neuroimaging studies (BOLD fMRI). Clear connectivity between finger tapping and activation within the sensorimotor cortices, supplementary motor area, premotor cortex, inferior parietal cortices, basal ganglia, and anterior has been found (Dalen and Hugdahl 1986, Shimoyama, Ninchoji et al. 1990, Levit-Binnun, Handzy et al. 2007, Witt, Laird et al. 2008). In the present study we performed neuronal stimulation using two different MRI scanners, 1.5T and 3T. Results from both field strengths support the hypothesis of direct neuronal detection. The percentage signal change 0.07±0.01% corresponds to a predicted axonal field of 0.7 ± 0.012 nT and 0.1 ± 0.02%, corresponding to a mean predicted axonal field of 0.9 ± 0.02 nT for 1.5T and 3T respectively. This evidence for both the slow BOLD effect and direct primary sensory activation with imaginary finger tapping at the tapping rate in fast fMRI statistical maps was observed using the 3T scanner. The mean percentage signal changes were 0.06 ± 0.01% and ΔB = 0.56 ± 0.16 nT with SNR = 3:1. There were far fewer voxels activated in the fast experiments compared to the BOLD experiments.

Overall, the results showed that fast MRI technique has potential to increase the spatial and temporal accuracy in detecting neuronal function, if improved sensitivity can be achieved.

Chapter 7: Conclusion and future work

7.1 Introduction

In this study, it was investigated whether ionic currents can generate fields which can affect the main magnetic field of an MRI system and studied the feasibility of detecting the electrical activity of neurons. Carefully controlled and extensive experimental measurements have been made to establish a correlation between the stimulated frequency and analysis response in the Fourier transform from a time series of rapid MR images acquired in vivo. Many experimental designs presented here have used the very short EPI repetition times of 88 ms and 63 ms at 1.5 and 3T respectively to provide access to direct measurement of high stimulation frequencies, to avoid the BOLD effect. A TENS machine has been used to produce stimulation for both phantom experiments and for measurements in vivo. The results support the hypothesis that fast fMRI can provide higher temporal resolution and better spatial resolution than the well established BOLD effect, although the sensitivity is currently at least an order of magnitude lower.

Firstly, we applied external currents to generate magnetic fields to conducting phantoms to investigate whether the generated fields have a detectable effect on MR images, and have a correlation with the applied frequency. The currents were adjusted to simulate neuronal activity which was demonstrated with fields as low as 0.3 nT.

Secondly, to verify the possibility of direct detection of ionic currents in vivo, we carried out direct detection activation experiments using the median nerve, visual cortex, thalamus and motor sensory cortex with generally positive results. This chapter presents a summary of the outcomes presented in previous chapters and future work needed to improve the feasibility of advanced fMRI

7.2 Conclusion

Evidence of fast fMRI was observed with TENS applied at relatively high stimulation frequencies. No spatial filtering was used in the analysis and the responses appear to be highly localised. The TENS pulses patterns were used to estimate the percentage signal change during phantom experiments. The minimum detected percentage signal changes

were comparable to estimated neuronal magnetic fields in vivo. These results were thus encouraging for us to move on to perform extensive experiments in vivo.

Applying electrical stimulation using the TENS machine to the median nerve, we observed clear evidence of fMRI responses with positive results observed in 29 out of 34 experiments yielding a success rate of 85%. The corresponding mean local magnetic field was estimated at 0.7 ± 0.1 nT Which was typical of most in vivo experiments.

Successful fast fMRI responses in the visual cortex during visual system stimulation by strobe light was observed at high stimulation frequencies >2.2 Hz using both fast fMRI and the BOLD technique. Responses with SNR >4:1 were observed at the stimulation frequency in 33 out of 38 experiments on the four volunteers corresponding to a mean axonal field of 0.8 ± 0.1 nT.

fast fMRI appeared to detect weak responses to median nerve stimulation in the motor sensory experiments. There was also exciting new evidence of stimulation related direct responses within the thalamus which is the brain's switching relay area. In addition, there was positive evidence that motor sensory cortex activation can be directly detected using real and imaginary finger tapping performed at both 1.5T and 3T.

Use of a TENS system to directly stimulate the motor-sensory system and other areas may help elucidate brain function with fast fMRI as an alternative to conventional BOLD experiments, if these results can be successfully repeated in other studies.

Advanced fMRI has great potential to increase the spatial and temporal accuracy in detecting neuronal function with improved sensitivity. We conclude that this technique could eventually be useful in early diagnosis of certain diseases such as multiple sclerosis which affects the myelin sheath and thus conductivity of axons, in pre-surgical planning to allow surgeons to avoid nerves and possibly in assessing damage and possible repair options in cases of spinal cord and peripheral nerve trauma.

7.3 Future work

The challenge to advanced fMRI is the ultimate sensitivity and stability of the MRI system itself. Therefore, MRI hardware, imaging sequence and experimental paradigm design will

all play a major role during attempts to improve direct detection. Use of electrical stimulation devices such as the TENS system provides exciting new opportunities for studying the central nervous system and it is encouraging that the response success rates for experiments using the TENS device were very high compared to, for example, finger tapping experiments. More sophisticated TENS arrays (TENSA) could be developed to stimulate multiple regions of the body simultaneously, perhaps with different frequencies and stimulation patterns to avoid overlap. With improved sensitivity through use of cyrogenic RF coils and hyperpolarised nuclei, direct neuronal detection is within the clear grasp of the next generation of MRI scientists.

Due to low SNR and noise accompany the results of the fast fMRI, there is some controversy about the use of this technique. Therefore, in the future it will be important to incorporate such constraints into more detailed and use other assistant technique. In addition, the potential distortion due to these mismatches or uncertainties should be considered in advanced fMRI source analysis. In fast fMRI may result in a significant estimation error if not the selected ROIs specified at the foci of the source. This problem could address by an extra neuroimaging tools such as MEG to improve the reliability of source imaging against the possible signal from other sources. Therefore, combining MEG with advanced fMRI holds promise to significantly increase the accurate sources of the neurons activity, and at the same time, allows tracing the rapid neural processes and information pathways within the activated regions, which cannot be achieved easily using these modalities in isolation. However, it is impossible or it is very difficult simultaneous acquisition of MEG and fast fMRI. This would probably require the extensive experimental studies by use of advance fMRI and invasive cortical and/or subcortical electrical recordings in volunteers.

The availability of high field 7T MR scanner can be further utilised by performing in vivo advanced fMRI experiments. Hence, future work could be based on acquiring MR and MEG data using a TENS stimulation, and thereby directly detecting perturbations of the local neuronal fields using this technique.

Appendix A

A.1 Pulse Sequences

A pulse sequence is a series of combined radiofrequency and gradient pulses leading to a complex cascade of events used to acquire the data to form Magnetic Resonance images. There are many different types of pulse sequences available for imaging; they are chosen to best suit the designed application. Following are the main types of pulse sequence categories used in MRI. However, there are two main sequences (Gradient echo and spin echo), and the others are modified from these with the addition of some parameters (Haacke, Brown et al. 1999, Bitar, Leung et al. 2006, Chavhan 2007).

1- Gradient echo sequence (GRE)
2- Spin Echo (SE)
3- Inversion Recovery (IR)
4- Fast Spin Echo(FSE)
5- Ultrafast Sequence
6- Conventional Spin Echo

In the experiments used for this report a gradient echo sequence was used, which is commonly used for fMRI. Therefore, a brief introduction to discuss and describe this sequence now follows.

The gradient echo sequence is used in a wide variety of imaging techniques, particularly when fast imaging is required. However, it has the simplest pattern and is an essential base for many imaging methods. The basic and widely used gradient echo sequence is shown as a diagram in Figure (A.1), and it contains several sequence lines that illustrate the pulse instructions. The first line is a radiofrequency pulse, which describes the size of the flip angle. This represents the angle by which the net magnetization vector is rotated towards the transverse plane. It is a variable angle $<=90^{o}$. These excitation pulses (RF pulse) are repeated as a series every TR. The second line represents the gradient slice selection and depends on the image plane required. The gradients are represented as Gx, Gy and Gz and

they are related to the slice orientations sagittal, coronal and axial which are generated by applying slice, read and phase gradient to different physical channels as in the table below.

Table (1): Imaging plane related to the gradient encoding

Imaging plane	Gradient used for Encoding		
	Slice selection	Phase	Frequency
Coronal	Gy	Gx	Gz
Axial	Gz	Gy	Gx
Sagittal	Gx	Gy	Gz

Another line in the sequence is called the phase encoding gradient, which is applied to alter the phase in a vertical direction for a limited time period. It results in the proton having different phases but precession takes place at the same frequency and this process is repeated many times with different phase encoding gradient strengths, dependent on the matrix size. Each phase encoding step represents a line in the raw data matrix that is stored to make up the full k-space (Ridgway 2010).

The next line represents frequency encoding applied for spatial encoding in an orthogonal axis. Different frequencies contribute to the signal to create the image. Each point in space is given a unique phase and frequency through phase and frequency encoding combined.
Finally, the last step is Analogue to Digital Conversion (ADC) of the MR signal which occurs simultaneously with frequency encoding.

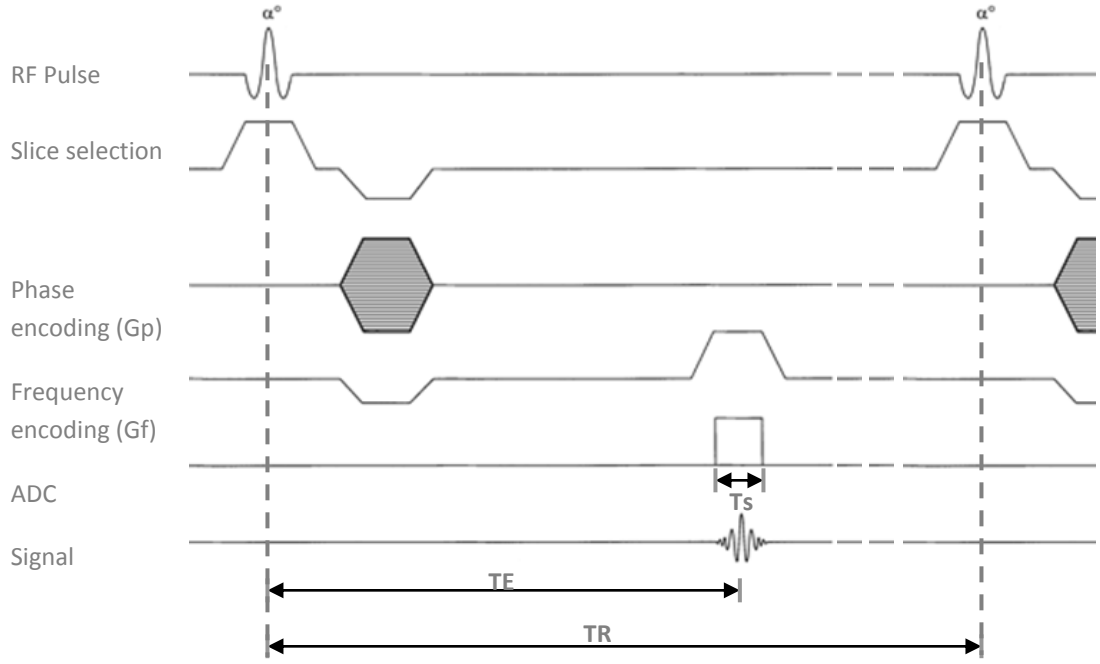

Figure A.1: Simple Gradient Echo Sequence (Brown and Semelka 1999).

The above diagram shows the standard Gradient echo sequence, whilst the sequence most commonly used in the functional experiments reported here was Echo planar imaging (EPI).

A.2 Echo Planar Imaging (EPI)

EPI is a technique used to obtain a faster gradient echo image. It is a method that can complete the image in a single shot as all the lines in the k-space are acquired from a multiple data readouts in a single TR period during one T2* decay which produces an image that is heavily T2*- weighted. The rapid filling of k-space lines results from the very fast switching on and off of the phase encoding and frequency encoding gradients (Ridgway 2010). Therefore, the T2* weighted images have limited spatial resolution (Biglands, Radjenovic et al. 2012). This technique is more susceptible to signal loss from T2* effects, because of the long period of data acquisition during the single shot. This type

of sequence is used in Functional MRI and experiments that require very short imaging times to freeze motion. The diagram below shows the EPI sequence, figure (A.2).

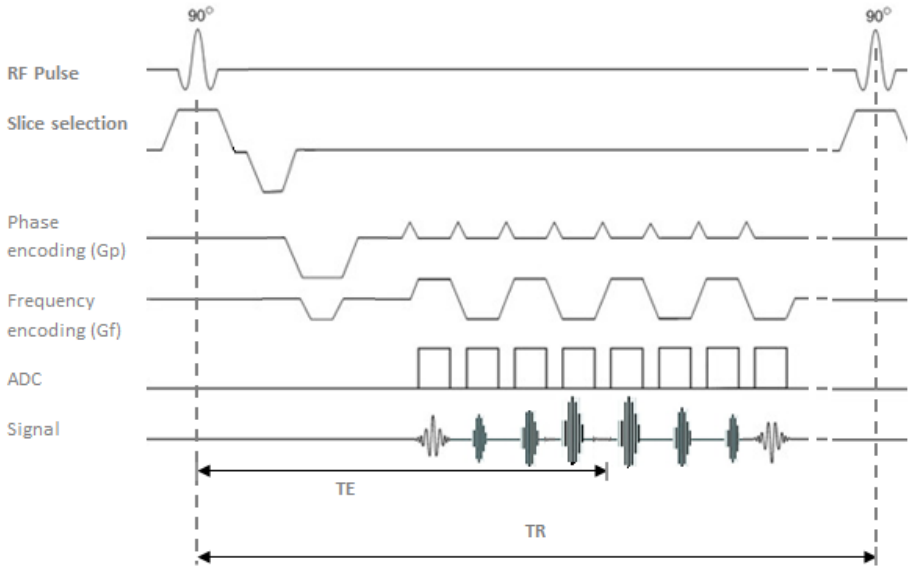

Figure A.2: Echo Planar Imaging sequence EPI

A.3 A brief comparison between BOLD effect and direct neutron detection DND

Figure (A.3) below show two different fMRI techniques, namely, Blood Oxygenation Level Dependent contrast (BOLD) and Direct Neuronal Detection (DND).The first technique is widely used in various fields of brain activity, while direct neuronal detection and the related activity is a matter of debate and recent investigation. BOLD technique is an indirect measure that relies on assessment of oxygen levels in blood and blood flow, whereas the DND method involves direct detection of axon firing. Due to the presence of the magnetic component of the neuronal magnetic field parallel to the main field, modulation of the MR signal occurs. Figure (5) shows that the BOLD response is slow for about 6 seconds and returns to resting state in approximately 24 seconds, whilst DND has a fast response at about 1-3 ms and rests at about 4-5 ms, as shown in figure(7). The BOLD technique induces 0.5% - 3% changes in the MR signal, however, DND causes a <0.2% change in the MR signal(Chow, Dagens et al. 2008). Therefore, the magnetic field in the BOLD contrast is greater than the magnetic field inDND, which is about 0.14 nT.

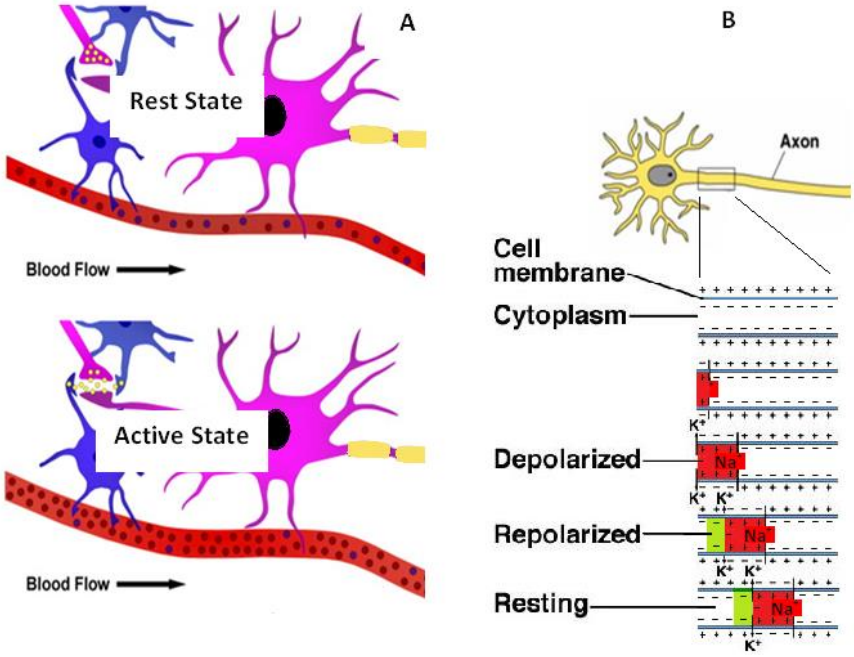

Figure A.3: Two fMR methods: A, BOLD technique and B, DND method

Appendix B

Table B.1: Visual cortex GE-EPI magnitude image and the percentage signal change in the frequency spectra that resulted from an applied frequency range (2.2 – 2.8 Hz), acquired at 1.5T using 8 channel head coil with TE = 25ms

Stimulated frequency (Hz)	GE-EPI magnitude image	Measured frequency spectra	$\%\lvert\Delta S/S_{eq}\rvert$
2.2	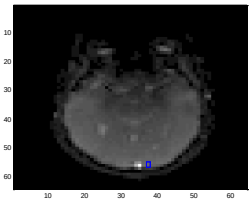	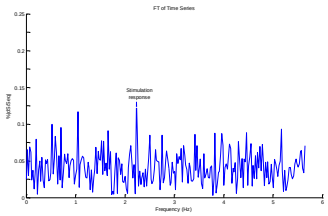	0.09
2.3	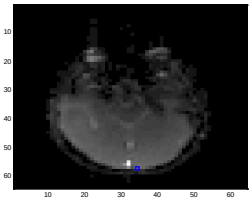	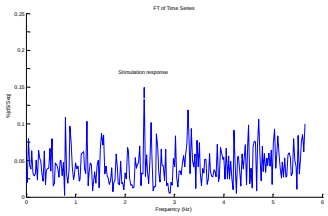	0.09
2.4	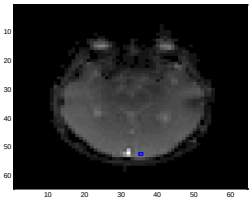	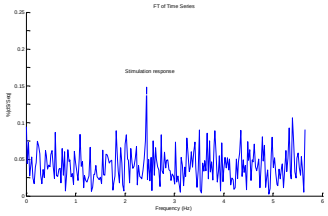	0.09
2.5	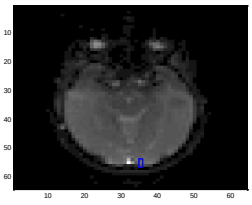	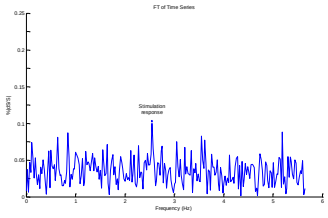	0.08
2.8	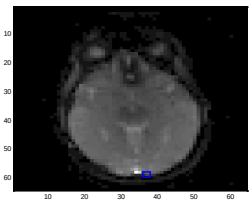	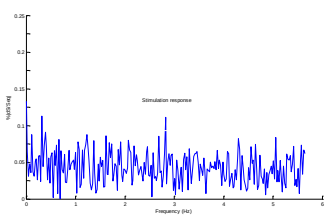	0.08

Table B.2 Visual cortex GE-EPI magnitude image and the percentage signal change in frequency spectra that resulted from applied frequency range (3.1 – 4.4 Hz), acquired at 1.5T using head coil with TE=25ms

Stimulated frequency (Hz)	GE-EPI magnitude image	Measured frequency spectra	$\%\lvert\Delta S/S_{eq}\rvert$
3.1	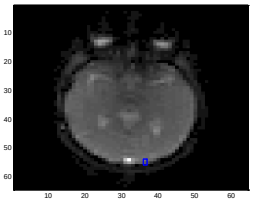	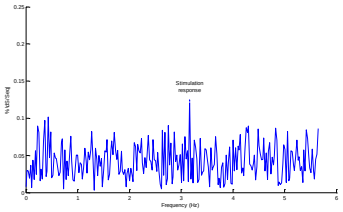	0.08
3.3	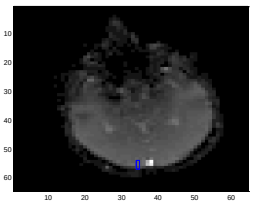	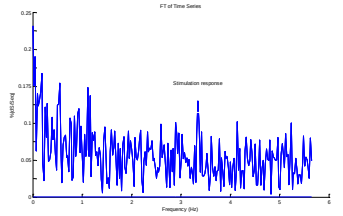	0.07
3.4	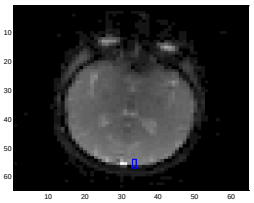	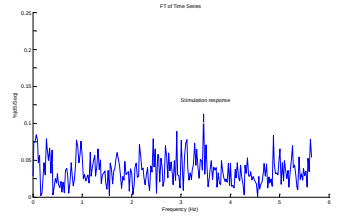	0.08
3.5	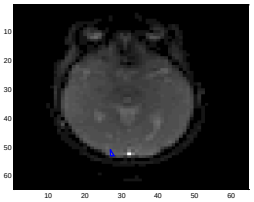	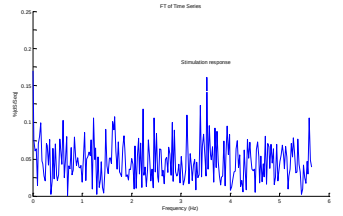	0.09
4.4	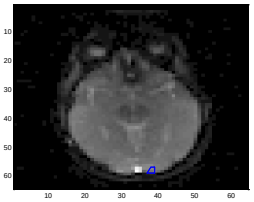	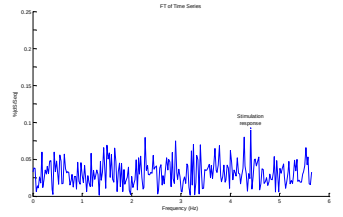	0.08

Table B.3: Record of different experiments with a range of stimulation frequencies (2.3-3.6), GE-EPI magnitude image, 1D Fourier transformation time series, and %|ΔS/S|

Stimulated frequency (Hz)	GE-EPI magnitude image	Measured frequency spectra	%|ΔS/S|
2.3	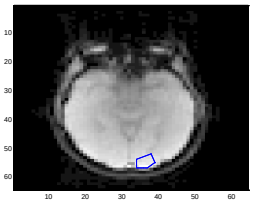	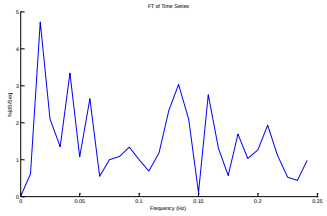	3.5
2.4	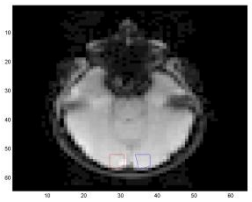	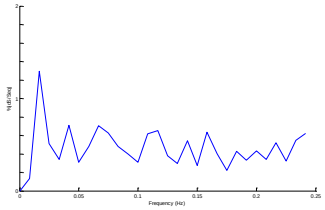	1.3
2.5	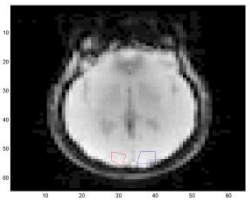	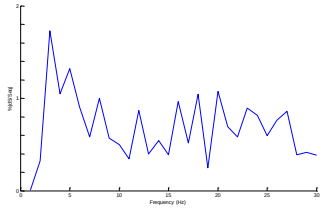	1.7
3.4	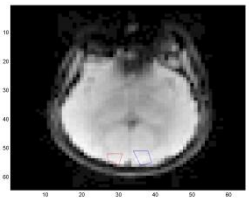	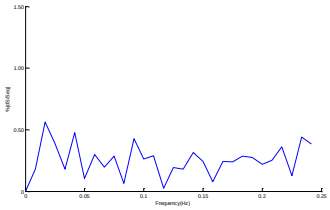	0.5
3.6	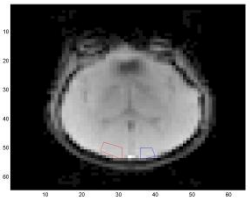	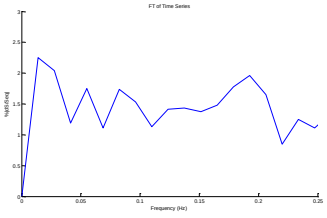	2.3

Table B.4 Records Median nerve experiments peaks calculation for range of frequencies (2.2 to 2.9)

f (Hz)	Std	SNR	Fast response(a.u)	BOLD effect(a.u)	Heartbeat (a.u)	Respiration (a.u)
2.5	125.465	4:1	750.1	1320	900	980
2,8	17.96	5:1	116.6	108.2	70.18	75.23
2.77	10.5	6:1	84.03	31.89	39.98	43.81
2.72	10.9	6:1	89.2	36.5	40.2	67.8
2.84	8.98	4:1	51.1	70.9	26.98	64.17
2.81	18.4	5:1	113.2	65	66	64.1
2.2	33.22	4:1	162.9	151.1	169.3	212.5
2.45	40.09	3:1	133.2	209.5	115.9	199.5
2.93	15.27	5:1	113.2	45.6	56.68	83.62
2.71	96.9	3:1	206.8	265.6	287.3	298.7
2.6	75.8	3:1	280.3	420.1	231.8	408.5
2.8	13.6	6:1	111.5	45.6	50.25	85.2
2.73	9.765	6:1	78.14	29.65	38.18	44.81
2.6	89.6	4:1	430.9	671.8	711.4	890.1
2.6	18.76	5:1	113.8	132,8	149.3	135.6

Table B.5: Records Median nerve experiments peaks calculation for range of frequencies (3.3 to 3.8)

f (Hz)	Std	SNR	Fast response	BOLD effect	Heartbeat	Respiration
3.75	12.15	6:1	92.87	60.57	56.82	59.34
3.7	22.16	5:1	145.6	450	210	400
3.7	10.96	5:1	81.22	139.7	99.9	111.1
3.62	15.92	5:1	117.5	66.09	51.55	90.77
3.39	15.38	4:1	71.46	169.5	106	168.1
3.61	22.3	6.3	142.4	59.8	73.2	86.4
3.75	11.94	6:1	137.3	37.73	34.59	53.48
3.73	73.22	3:1	153.3	380.2	180.2	338.1
3.54	13.76	6:1	131.8	27.06	41.7	83
3.72	30.1	6:1	250.3	76.3	70.3	108.6
3.72	98.3	3:1	306.5	530.2	355.4	670.1
3.72	24.6	5:1	154.6	504.3	418.7	516.4
3.72	16.6	5.38	89.34	126.9	132.6	142.7
3.76	35.69	6.47	231.4	261.8	376.7	369.6

Appendix C

MATLAB Codes

Fast fMRI analysis code

```
% fMR analysis for IMRI dicom files
% MP rejigged Mar2011


clear all;
close all;

rect1=[35,50,750,500];
%rect_roi = [40 40 80 75];     %for resolution 128x128      [xmin ymin width height]
rect_roi = [20 20 40 38];      %for resolution 64x64

[filename,dir] = uigetfile('C:\mediface\database\image\20121008\E0000316\I0654257.dcm','EPI Analysis - Select Image',10,100);
pathname = [dir, filename];

if filename ~= 0

   prompt = {'Number of frames','Width','Height', 'Frequency', 'Time (s)','#Slices', 'StartSlice','Z score', 'TR (s)'};
   def = {'499','64','64','2.5','44', '1','0','2.5','0.088'};
   answer = inputdlg(prompt, 'Enter details', 1, def);

   if not(isempty(answer))

      num = eval(answer{1});
      width = eval(answer{2});
      height = eval(answer{3});
      frequency=eval(answer{4});
      time =eval(answer{5});
      slices = eval(answer{6});
      startslice = eval(answer{7});
      zscore = eval(answer{8});
      TR = eval(answer{9});
      [fid, message] = fopen (pathname, 'r','b');
      if(fid<1)
         disp(message);
      end

      fname = strrep(filename,'I','');
      fname = strrep(fname,'.dcm','');

      lcount=0;
      %Get all the files
      for k=startslice:slices:slices*num-1
         lcount=lcount+1;
```

```
        iNext = str2num(fname) + k;         %integer
        sNext = num2str(iNext);             %string
        [a length]=size(sNext);
        zero_pad = 7-length;
        for z=1:zero_pad
           sNext = strcat('0',sNext);
        end

        fname_next = strcat('I',sNext);
        fname_next = strcat(fname_next,'.dcm');
        name(k+1,:) = fname_next;
        pathname_next = [dir, fname_next];
        [fid_next, message] = fopen (pathname_next, 'r');
        if(fid_next<1)
           disp(message);
        end

        fseek(fid_next, -width*height*2, 'eof');
        buffer = fread(fid_next, width*height, 'int16');
        image(k+1,:)= buffer';
        fclose(fid_next);

        oImage = reshape(image(k+1,:),width,height);

%           % reduce resolution to 64x64 by discarding every other pixel
%           for zi=1:64
%              for zj= 1:64
%                 img64(zi,zj) = oImage(:,:);
%              end
%           end
%           image64(k+1,:,:)= img64;          % 3D array
%           roimgseq(:,k+1)= img64(:);        % 2D array - size: no.pixels x no.frames

image64(lcount,:,:)=oImage;
roimgseq(:,lcount)=oImage(:);
% if (k==startslice)
%   figure;
%   imagesc(oImage);
%   colormap(gray);
% end
end
%Paradigm of stimulus (OFF-ON)
      cycles = time*frequency;
      flag = 0;
      [G, Cs, Cc] = stim_paradigm(num, cycles, flag);
     % figure, plot(G), title('Paradigm of stimulus'), xlabel('Frames');

      %%%%%%%%%% Principal component analysis %%%%%%%%%%

      eval(['[V, D] = pca(roimgseq, 64, 64);'])

      %%%%%%%%%% GLM %%%%%%%%%%

      K = 1;
```

```
      [pa, sigma, Q] = spm_m(roimgseq, G, K);  %Statistical Parametric Mapping (SPM)

      C = Cs;
      sigs = C*pa./sqrt(sigma*(C*Q*C'));
      C = Cc;
      sigc = C*pa./sqrt(sigma*(C*Q*C'));
      sig = sqrt(sigs.*sigs + sigc.*sigc);
      imz = reshape(sig, 64, 64);

       pmapfig = figure;  %  a handle for the figure to pick the roi
       colorbar;
       imagesc(oImage');
       colormap(gray);
       brighten(0.4);
      % Threshold for z score and noise
      %zscore = 4.0;
      noisethreshold = 100.0;
%        figure;
%        imagesc(imz'>zscore);
      imz2 = zeros(64,64);
      imsum=zeros(64,64);
      for zi=1:64
         for zj=1:64
            if (imz(zi,zj)> zscore & oImage(zi,zj)> noisethreshold)
               imz2(zi,zj) = 10000.0;                          % Noise threshold
            else
                           imz2(zi,zj)= 0;
                            imz2(1,1)=10000.0;
            end
            imsum(zi,zj) = (imz2(zi,zj)+oImage(zi,zj));
         end
      end

%        pmapfig = figure;  %  a handle for the figure to pick the roi
%        imagesc(interp2(imsum'));
%        colorbar;
%
%        colormap(gray);
%        brighten(0.4);
%        % Interpolate overlay image back to 128 x 128
%         imsum64128 = zeros(128,64);
%         imsum128 = zeros(128,128);
% %
%         for zi=1:64
%            imsum64128 = interp(imsum,2);
%         end
% %
%         for zi=1:128
%            imsum128(zi,:) = interp(imsum64128(zi,:),2) + oImage(zi,:);
%         end

      figure('Position',rect1);
   %    subplot(1,2,1), imagesc(oImage),title('Original image'), axis image, colorbar('horiz');
       subplot(1,1,1), imagesc(interp2(imsum)'),title('Functional Overlay image'), axis image, colorbar('horiz'),
pixval on;
```

```
      %subplot(1,4,3), imagesc(imz'),title('Functional image'), axis image, colorbar('horiz'), pixval on;
      %subplot(1,4,3), imagesc(imz2),title('Significant Functional image'), axis image, colorbar('horiz'), pixval
on;

      % Time series
    %  answer = questdlg ('Timeseries?','Timeseries','Yes', 'No','Yes');
          % if strcmp(answer, 'Yes')
        % loop around to get the time series from selected regions...

        colormap(jet);

        tsfig = figure; % generates figure for time series
        title('Time Series')
        ftfig=figure;
        title('FT of Time Series')
        roiflag = 1;
        k = 0;
        color = ['b', 'r', 'g', 'c', 'm', 'k' 'b', 'r', 'g', 'c', 'm', 'k' 'b', 'r', 'g', 'c', 'm', 'k' 'b', 'r', 'g', 'c', 'm', 'k'];
        a = [];

        y=[0:num-1];
        ys=y*TR;


        while roiflag
           C = questdlg('Draw a ROI for time series and FT', 'ROI', 'Yes', 'No', 'Yes');
           if strcmp(C, 'Yes')
              k = k+1;
              figure(pmapfig);
              [bw1, x1, y1] = roipoly_h(imz, 'b');
              buff = roimean_h(roimgseq, bw1);
              a = [a, buff(:)];
              for n = 1:k
                 figure(pmapfig); hold on; plot(x1, y1, color(n) );
                 figure(tsfig); hold on; plot(ys,a(:, k), color(n) );
                 ft5=abs(fftshift(fft(detrend(a(:,k)))))
                % wt5 = sgolayfilt(ft5 ,0, 3); %  Savitzky-Golay filtering of FT
                 for i=1:num
                  xscal(i)=   (((i-1)./(TR))/num);
                 end
                figure(ftfig);hold on;plot(xscal(1:num/2),ft5(num/2+1:num),color(n));

              end
          yt= mean(ys(50:450))
           st = std ((ys(50:450)))
          TSNR= yt/st
           ym= max(ft5(50:450))
           s= std ((ft5(450:499)))
          SSNR= ym/s

       else
              roiflag = 0;       %finish
           end
        end
```

```
        end
%
end
%end
```

References

Andrä, W. and H. Nowak (2007). Magnetism in medicine: A handbook, Vch Verlagsgesellschaft Mbh.

Anwar, S., et al. (2010). Modelling of axonal B fields for Direct Neuronal Detection (DND) using MRI. Antennas and Propagation Conference (LAPC), 2010 Loughborough, IEEE (pp. 549-552).

Anwar, S., et al. (2010). A theoretical Direct Neuronal Detection study to estimate percentage local field perturbations. ISMRM-ESMRMB Annual Meeting (p. 2248).

Anwar, S. M. (2011). Direct Detection of Neuronal fields (DND) using Magnetic Resonance Imaging (MRI). Electronic and Electrical Engineering. Sheffield, Sheffield. PhD**:** 207.

Anwar, S. M., et al. (2011). Hybridized axonal field model for signal estimation in magnetic resonance imaging. Antennas and Propagation (EUCAP), Proceedings of the 5th European Conference on, IEEE (pp. 1300-1303).

Bear, Mark F., Barry W. Connors, and Michael A. Paradiso, eds. Neuroscience. Vol. 2. Lippincott Williams & Wilkins, 2007.

Belliveau, J., et al. (1991). "Functional mapping of the human visual cortex by magnetic resonance imaging." Science **254**(5032): 716.

Belo, D., et al. (2011). "Topographic EEG brain mapping before, during and after obstructive sleep apnea episodes." Pattern Recognition and Image Analysis: 564-571.

Bianciardi, M., et al. (2004). "Combination of BOLD-fMRI and VEP recordings for spin-echo MRI detection of primary magnetic effects caused by neuronal currents." Magn Reson Imaging **22**(10): 1429-1440.

Biglands, J. D., et al. (2012). "Cardiovascular magnetic resonance physics for clinicians: part II." Journal of Cardiovascular Magnetic Resonance **14**(1): 66.

Bitar, R., et al. (2006). "MR Pulse Sequences: What Every Radiologist Wants to Know but Is Afraid to Ask1." Radiographics **26**(2): 513-537.

Blagoev, K., et al. (2005). MRI of neural currents: numerical study. Proc Int Soc Magn Reson Med (Vol. 13, p. 1425).

Blagoev, K., et al. (2007). "Modelling the magnetic signature of neuronal tissue." NeuroImage **37**(1): 137-148.

Blake, P., et al. (2003). "Positron emission tomography (PET) and single photon emission computed tomography (SPECT): clinical applications." Journal of neuro-ophthalmology **23**(1): 34.

Bodurka, J. and P. A. Bandettini (2002). "Toward direct mapping of neuronal activity: MRI detection of ultraweak, transient magnetic field changes." Magnetic resonance in medicine **47**(6): 1052-1058.

Bodurka, J., et al. (1999). "Current-induced magnetic resonance phase imaging." Journal of Magnetic Resonance **137**(1): 265-271.

Brown, M. A. and R. C. Semelka (1999). "MR Imaging Abbreviations, Definitions, and Descriptions: A Review1." Radiology **213**(3): 647-662.

Buxton, R. B. (2002). Introduction to functional magnetic resonance imaging: principles and techniques, Cambridge Univ Pr.

Cassara, A., et al. (2008). "Realistic simulations of neuronal activity: A contribution to the debate on direct detection of neuronal currents by MRI." Neuroimage **39**(1): 87-106.

Cassarà, A. M. and B. Maraviglia (2008). "Microscopic investigation of the resonant mechanism for the implementation of nc-MRI at ultra-low field MRI." Neuroimage **41**(4): 1228-1241.

Chavhan, G. B. (2007). MRI made easy, Jaypee Brothers.

Chow, L. S. (2005). investigation of direct detection of nerve firing in the human visual system due to axonal field modulation of the magnetic resonance signal. Electronic and electrical engineering. Sheffield, The University of Sheffield. **PhD:** 187.

Chow, L. S., et al. (2004). "Attempting to detect firing of the optic nerve using GRACE MR and sequential averaging." Radiological Congress, UK, 24.

Chow, L. S., et al. (2006). "Investigating direct detection of axon firing in the adult human optic nerve using MRI." NeuroImage **30**(3): 835-846.

Chow, L. S., et al. (2006). "Investigation of MR signal modulation due to magnetic fields from neuronal currents in the adult human optic nerve and visual cortex." Magnetic resonance imaging **24**(6): 681-691.

Chow, L. S., et al. (2007). "Investigation of axonal magnetic fields in the human corpus callosum using visual stimulation based on MR signal modulation." Journal of Magnetic Resonance Imaging **26**(2): 265-273.

Chow, L. S., et al. (2007). "Investigation of axonal magnetic fields in the human corpus callosum using visual stimulation based on MR signal modulation." Journal of Magnetic Resonance Imaging **26**(2): 265-273.

Chow, L. S., et al. (2008). "Comparison of BOLD and direct-MR neuronal detection (DND) in the human visual cortex at 3T." Magn Reson Med **60**(5): 1147-1154.

Chu, R., et al. (2004). "Hunting for neuronal currents: absence of rapid MRI signal changes during visual-evoked response." NeuroImage **23**(3): 1059-1067.

Colonnier, M. and J. O'Kusky (1981). "[Number of neurons and synapses in the visual cortex of different species]." Revue canadienne de biologie/editee par l'Universite de Montreal **40**(1): 91-99.

Cook, I. A., et al. (1998). "Assessing the accuracy of topographic EEG mapping for determining local brain function." Electroencephalography and Clinical Neurophysiology **107**(6): 408-414.

Dale, A. M. and M. I. Sereno (1993). "Improved localizadon of cortical activity by combining eeg and meg with mri cortical surface reconstruction: A linear approach." Journal of cognitive neuroscience **5**(2): 162-176.

Dalen, K. and K. Hugdahl (1986). "Inhibitory versus facilitory interference for finger-tapping to verbal and nonverbal, motor, and sensory tasks." Journal of clinical and experimental neuropsychology **8**(6): 627-636.

Davis, K. D., et al. (1998). "Functional MRI study of thalamic and cortical activations evoked by cutaneous heat, cold, and tactile stimuli." Journal of Neurophysiology **80**(3): 1533-1546.

Debanne, D., et al. (2011). "Axon physiology." Physiological reviews **91**(2): 555-602.

Detre, J. A. and T. F. Floyd (2001). "Functional MRI and its applications to the clinical neurosciences." The Neuroscientist **7**(1): 64-79.

Ersland, L., et al. (1996). "Phantom limb imaginary fingertapping causes primary motor cortex activation: an fMRI study." Neuroreport **8**(1): 207-210.

Ethofer, T., et al. (2003). "Comparison of longitudinal metabolite relaxation times in different regions of the human brain at 1.5 and 3 Tesla." Magnetic resonance in medicine **50**(6): 1296-1301.

Faro, S. H., et al. (2011). Functional neuroradiology: principles and clinical applications, Springer, Science & Business Media.

Ferrari, M. and H. Zakon (1993). "Conductances contributing to the action potential of Sternopygus electrocytes." Journal of Comparative Physiology A **173**(3): 281-292.

Ferretti, A., et al. "A BOLD-fMRI study of the response in primary and secondary somatosensory cortices elicited by electric median nerve stimulation at different frequencies." IJBEM, Vol. 7, No. 1, 2005

Fukuyama, H., et al. (1997). "Brain functional activity during gait in normal subjects: a SPECT study." Neuroscience letters **228**(3): 183-186.

Gambarota, G. (2009). T2 relaxometry of human median nerve. Seminars in musculoskeletal radiology, (Vol. 13, No. 1, pp. 24-28).

George, J., et al. (1995). "Mapping function in the human brain with magnetoencephalography, anatomical magnetic resonance imaging, and functional

magnetic resonance imaging." Journal of clinical neurophysiology: official publication of the American Electroencephalographic Society **12**(5): 406.

Geva, T. (2006). "Magnetic resonance imaging: historical perspective." Journal of Cardiovascular Magnetic Resonance **8**(4): 573-580.

Gevins, A., et al. (1997). "High-resolution EEG mapping of cortical activation related to working memory: effects of task difficulty, type of processing, and practice." Cerebral Cortex **7**(4): 374-385.

Goldberg, S. (2007). "MRIs and the Perception of Risk." Am. JL & Med. **33**: 229.

Greicius, M. D., et al. (2007). "Resting-state functional connectivity in major depression: abnormally increased contributions from subgenual cingulate cortex and thalamus." Biological psychiatry **62**(5): 429-437.

Haacke, E. M., et al. (1999). Magnetic resonance imaging: physical principles and sequence design, Wiley-Liss New York:.

Haas, L. (2003). "Hans Berger (1873–1941), Richard Caton (1842–1926), and electroencephalography." Journal of Neurology, Neurosurgery & Psychiatry **74**(1): 9.

Hagberg, G. E., et al. (2008). "The effect of physiological noise in phase functional magnetic resonance imaging: from blood oxygen level-dependent effects to direct detection of neuronal currents." Magnetic resonance imaging **26**(7): 1026-1040.

Hatada, T., et al. (2004). "Detection of weak magnetic fields induced by electrical currents with MRI: theoretical and practical limits of sensitivity." Magnetic Resonance in Medical Sciences **3**(4): 159-163.

Hazlett, E. A., et al. (2001). "Thalamic activation during an attention-to-prepulse startle modification paradigm: a functional MRI study." Biological psychiatry **50**(4): 281-291.

Hill, D. and R. Keynes (1949). "Opacity changes in stimulated nerve." The Journal of physiology **108**(3): 278-281.

Hofner, N., et al. (2011). "Are brain currents detectable by means of low-field NMR? A phantom study." Magn Reson Imaging **29**(10): 1365-1373.

Huang, J. (2013). "Detecting neuronal currents with MRI: A human study." Magn Reson Med, 71(2), 756-762.

Jacks, A. and N. Miller (2003). "Spontaneous retinal venous pulsation: aetiology and significance." Journal of Neurology, Neurosurgery & Psychiatry **74**(1): 7-9.

Jasanoff, A. (2007). "Bloodless FMRI." Trends Neurosci **30**(11): 603-610.

Joseph, R. (2009). "Quantum physics and the multiplicity of mind: Split-brains, fragmented minds, dissociation, quantum consciousness." Journal of Cosmology **3**: 600-640.

Joy, M., et al. (1989). "In vivo detection of applied electric currents by magnetic resonance imaging." Magnetic resonance imaging **7**(1): 89-94.

Kamei, H., et al. (1999). "Neuronal current distribution imaging using magnetic resonance." Magnetics, IEEE Transactions on **35**(5): 4109-4111.

Kennan, R. P., et al. (1994). "Intravascular susceptibility contrast mechanisms in tissues." Magnetic resonance in medicine **31**(1): 9-21.

Konn, D., et al. (2003). "MRI detection of weak magnetic fields due to an extended current dipole in a conducting sphere: a model for direct detection of neuronal currents in the brain." Magn Reson Med **50**(1): 40-49.

Konn, D., et al. (2004). "Initial attempts at directly detecting alpha wave activity in the brain using MRI." Magnetic resonance imaging **22**(10): 1413-1427.

Kovacs, H., et al. (2005). "Cryogenically cooled probes—a leap in NMR technology." Progress in Nuclear Magnetic Resonance Spectroscopy **46**(2): 131-155.

Kraus Jr, R., et al. (2008). "Toward direct neural current imaging by resonant mechanisms at ultra-low field." NeuroImage **39**(1): 310-317.

Kunze, N. M. (2010). "Investigation of local deformation of the median nerve in magnetic resonance images of the carpal tunnel.", htt://ir.uiowa.edu/etd/534.

Kwong, K. K., et al. (1992). "Dynamic magnetic resonance imaging of human brain activity during primary sensory stimulation." Proceedings of the National Academy of Sciences **89**(12): 5675.

Lachaux, J. P., et al. (2005). "The many faces of the gamma band response to complex visual stimuli." Neuroimage **25**(2): 491-501.

Landini, L., et al. (2005). Advanced image processing in magnetic resonance imaging, CRC/Taylor & Francis.

Lauterbur, P. C. (1973). "Image formation by induced local interactions: examples employing nuclear magnetic resonance." Nature **242**(5394): 190-191.

Leuba, G. and L. Garey (1989). "Comparison of neuronal and glial numerical density in primary and secondary visual cortex of man." Experimental brain research **77**(1): 31-38.

Levit-Binnun, N., et al. (2007). "Transcranial magnetic stimulation in a finger-tapping task separates motor from timing mechanisms and induces frequency doubling." Journal of cognitive neuroscience **19**(5): 721-733.

Liston, A. D., et al. (2004). "The MR detection of neuronal depolarization during 3-Hz spike-and-wave complexes in generalized epilepsy." Magn Reson Imaging **22**(10): 1441-1444.

Liston, A. D., et al. (2004). "The MR detection of neuronal depolarization during 3-Hz spike-and-wave complexes in generalized epilepsy." Magn Reson Imaging **22**(10): 1441-1444.

Logothetis, N. K. and J. Pfeuffer (2004). "On the nature of the BOLD fMRI contrast mechanism." Magnetic resonance imaging **22**(10): 1517-1531.

Lotze, M., et al. (1999). "Activation of cortical and cerebellar motor areas during executed and imagined hand movements: an fMRI study." Journal of cognitive neuroscience **11**(5): 491-501.

Luo, Q. and J. H. Gao (2010). "Modeling magnitude and phase neuronal current MRI signal dependence on echo time." Magnetic Resonance in Medicine **64**(6): 1832-1837.

Luo, Q., et al. (2011). "Modeling neuronal current MRI signal with human neuron." Magnetic resonance in medicine **65**(6): 1680-1689.

Luo, Q., et al. (2011). "Detection of neuronal current MRI in human without BOLD contamination." Magn Reson Med **66**(2): 492-497.

Luo, Q., et al. (2009). "Physiologically evoked neuronal current MRI in a bloodless turtle brain: Detectable or not?" Neuroimage **47**(4): 1268-1276.

Mandelkow, H., et al. (2007). "Heart beats brain: The problem of detecting alpha waves by neuronal current imaging in joint EEG-MRI experiments." NeuroImage **37**(1): 149-163.

McClure, S. M., et al. (2004). "The neural substrates of reward processing in humans: the modern role of FMRI." The Neuroscientist **10**(3): 260-268.

McRobbie, D. W. (2003). MRI from picture to proton, Cambridge Univ Pr.

Mickiewicz, S. P. and A. Coombes (1986). Treatment pulse sequences for a transcutaneous nerve stimulation device, Patent No. 4,582,063.

Middleton, W., et al. (1987). "MR imaging of the carpal tunnel: normal anatomy and preliminary findings in the carpal tunnel syndrome." American Journal of Roentgenology **148**(2): 307-316.

Mintun, M., et al. (1984). "Brain oxygen utilization measured with O-15 radiotracers and positron emission tomography." Journal of nuclear medicine: official publication, Society of Nuclear Medicine **25**(2): 177-187.

Monagle, K., et al. (1999). "Quantitative MR imaging of carpal tunnel syndrome." AJR. American journal of roentgenology **172**(6): 1581-1586.

Moridani, M. K. (2009). "Functional brain imaging with use of a new and powerful neuroimaging technique." JBiSE: 173.

Movshon, J. A., et al. (1978). "Receptive field organization of complex cells in the cat's striate cortex." The Journal of physiology **283**(1): 79-99.

Mulert, C. and L. Lemieux (2010). EEG-fMRI: Physiological Basis, Technique and Applications, Springer Verlag.

Muthuswamy, J. and N. V. Thakor (1998). "Spectral analysis methods for neurological signals." Journal of Neuroscience Methods **83**(1): 1-14.

Niedermeyer, E. and F. H. L. Da Silva (2005). Electroencephalography: basic principles, clinical applications, and related fields, Lippincott Williams & Wilkins.

Nielsen, J. A., et al. (2013). "An evaluation of the left-brain vs. right-brain hypothesis with resting state functional connectivity magnetic resonance imaging." PloS one **8**(8): e71275.

Ogawa, S., et al. (1990). "Brain magnetic resonance imaging with contrast dependent on blood oxygenation." Proceedings of the National Academy of Sciences **87**(24): 9868.

Paley, M., et al. (2015). Advanced fMRI and the Brain Computer Interface. Brain-Computer Interfaces, Springer**:** 185-213.

Paley, M. N., et al. (2009). "Modelling of axonal fields in the optic nerve for direct MR detection studies." Image and Vision Computing **27**(4): 331-341.

Park, T. S. and S. Y. Lee (2007). "Effects of neuronal magnetic fields on MRI: numerical analysis with axon and dendrite models." NeuroImage **35**(2): 531-538.

Park, T. S., et al. (2004). "Effect of nerve cell currents on MRI images in snail ganglia." Neuroreport **15**(18): 2783-2786.

Parkes, L. M., et al. (2007). "Inability to directly detect magnetic field changes associated with neuronal activity." Magn Reson Med **57**(2): 411-416.

Pekar, J. J. (2006). "A brief introduction to functional MRI." Engineering in Medicine and Biology Magazine, IEEE **25**(2): 24-26.

Pell, G., et al. (2005). Neurogenic inhomogeneity localization for detection of activity (NILDA). Intl Soc Mag Reson Med, (Vol. 13, p. 123).

Phelps, M. E. (2000). "PET: the merging of biology and imaging into molecular imaging." Journal of Nuclear Medicine **41**(4): 661-681.

Poplawsky, A. J., et al. (2012). "Direct detection of a single evoked action potential with MRS in Lumbricus terrestris." NMR Biomed **25**(1): 123-130.

Rabi, I., et al. (1938). "The Molecular Beam Resonance Method for Measuring Nuclear Magnetic Moments." Phys. Rev **53**(495): 318.

Rajagopalan, P., et al. (1995). "Magnetic resonance imaging using deoxyhemoglobin contrast versus positron emission tomography in the assessment of brain function." Progress in Neuro-Psychopharmacology and Biological Psychiatry **19**(3): 351-366.

Rauch, S. L., et al. (1998). "Thalamic deactivation during early implicit sequence learning: a functional MRI study." Neuroreport **9**(5): 865-870.

Ridgway, J. P. (2010). "Cardiovascular magnetic resonance physics for clinicians: part I." J Cardiovasc Magn Reson **12**: 71.

Rodionov, R., et al. (2010). "Looking for neuronal currents using MRI: an EEG-fMRI investigation of fast MR signal changes time-locked to frequent focal epileptic discharges." NeuroImage **50**(3): 1109-1117.

Romo Vázquez, R., et al. (2011). "Blind source separation, wavelet denoising and discriminant analysis for EEG artefacts and noise cancelling." Biomedical Signal Processing and Control, 7(4), 389-400.

Salomon, R., et al. (2014). "Comparison of an 8-Channel and a 32-Channel Coil for High-Resolution fMRI at 7 T." Brain topography **27**(2): 209-212.

Schubert, T. and A. J. Szameitat (2003). "Functional neuroanatomy of interference in overlapping dual tasks: an fMRI study." Cognitive Brain Research **17**(3): 733-746.

Sharma, V., et al. (2002). "Molecular imaging of gene expression and protein function in vivo with PET and SPECT." Journal of Magnetic Resonance Imaging **16**(4): 336-351.

Sharon, D., et al. (2007). "The advantage of combining MEG and EEG: Comparison to fMRI in focally stimulated visual cortex." Neuroimage **36**(4): 1225-1235.

Shen, J., et al. (2008). "Magnetic resonance microneurography of rabbit sciatic nerve on a 1.5-T clinical MR system correlated with gross anatomy." Microsurgery **28**(1): 32-36.

Shimoyama, I., et al. (1990). "The finger-tapping test: a quantitative analysis." Archives of neurology **47**(6): 681-684.

Singh, M. (1994). "Sensitivity of MR phase shift to detect evoked neuromagnetic fields inside the head." Nuclear Science, IEEE Transactions on **41**(1): 349-351.

Song, A. W. and A. M. Takahashi (2001). "Lorentz effect imaging." Magnetic resonance imaging **19**(6): 763-767.

Stroman, P., et al. (2001). "Spin-echo versus gradient-echo fMRI with short echo times." Magnetic resonance imaging **19**(6): 827-831.

Swinney, K. and J. Wikswo Jr (1980). "A calculation of the magnetic field of a nerve action potential." Biophysical journal **32**(2): 719-731.

Tamura, M., et al. (1997). "Localized near–infrared spectroscopy and functional optical imaging of brain activity." Philosophical Transactions of the Royal Society of London. Series B: Biological Sciences **352**(1354): 737-742.

Tang, L., et al. (2008). "Failure to direct detect magnetic field dephasing corresponding to ERP generation." Magn Reson Imaging **26**(4): 484-489.

Teplan, M. (2002). "Fundamentals of EEG measurement." Measurement Science Review **2**(2): 1-11.

Triantafyllou, C., et al. (2011). "Echo-time and field strength dependence of BOLD reactivity in veins and parenchyma using flow-normalized hypercapnic manipulation." PloS one **6**(9): e24519.

Truong, T.-K., et al. (2006). "Synchronized detection of minute electrical currents with MRI using Lorentz effect imaging." Journal of Magnetic Resonance **179**(1): 85-91.

Tudor, M., et al. (2005). "Hans Berger (1873-1941)--the history of electroencephalography]." Acta medica Croatica: časopis Hravatske akademije medicinskih znanosti **59**(4): 307.

Uchiyama, S., et al. (2005). "Quantitative MRI of the wrist and nerve conduction studies in patients with idiopathic carpal tunnel syndrome." Journal of Neurology, Neurosurgery & Psychiatry **76**(8): 1103-1108.

Villringer, A. and B. Chance (1997). "Non-invasive optical spectroscopy and imaging of human brain function." Trends in Neurosciences **20**(10): 435-442.

Vinhas, V., et al. (2008). "Realtime dynamic multimedia storyline based on online audience biometric information." New Directions in Intelligent Interactive Multimedia: 545-554.

Vre, R. and M. Lemort (1995). "Biophysical properties and clinical applications of magnetic resonance imaging contrast agents." British journal of radiology **68**(807): 225.

Wandell, B. A., et al. (2007). "Visual field maps in human cortex." Neuron **56**(2): 366-383.

Wijesinghe, R. S. and B. J. Roth (2009). "Detection of peripheral nerve and skeletal muscle action currents using magnetic resonance imaging." Annals of biomedical engineering **37**(11): 2402-2406.

Wikswo, J. P., et al. (1989). Intraoperative recording of the magnetic field of a human nerve. Advances in biomagnetism, Springer**:** 137-140.

Witt, S. T., et al. (2008). "Functional neuroimaging correlates of finger-tapping task variations: an ALE meta-analysis." NeuroImage **42**(1): 343-356.

Wright, P., et al. (2008). "Water proton T 1 measurements in brain tissue at 7, 3, and 1.5 T using IR-EPI, IR-TSE, and MPRAGE: results and optimization." Magnetic Resonance Materials in Physics, Biology and Medicine **21**(1-2): 121-130.

Xiong, H.-C., et al. (2009). "Simulation study of the dendritic effect on direct MRI detection of neural electric event." Journal of Electronic Science and Technology of China **7**(1): 92-95.

Xiong, J., et al. (2003). "Directly mapping magnetic field effects of neuronal activity by magnetic resonance imaging." Hum Brain Mapp **20**(1): 41-49.

Xue, Y., et al. (2009). "Direct MRI mapping of neuronal activity evoked by electrical stimulation of the median nerve at the right wrist." Magnetic Resonance in Medicine **61**(5): 1073-1082.

Xue, Y., et al. (2009). "Direct MRI mapping of neuronal activity evoked by electrical stimulation of the median nerve at the right wrist." Magn Reson Med **61**(5): 1073-1082.

Xue, Y., et al. (2006). "Direct MRI detection of neuronal magnetic fields in the brain: theoretical modeling." NeuroImage **31**(2): 550-559.

Yang, H., et al. (2003). "Mapping of periodic waveforms using the ghost reconstructed alternating current estimation (GRACE) magnetic resonance imaging technique." Magnetic resonance in medicine **50**(3): 633-637.

Zifkin, B. G. and G. Avanzini (2009). "Clinical neurophysiology with special reference to the electroencephalogram." Epilepsia **50**: 30-38.

Zifkin, B. G. and G. Avanzini (2009). "Clinical neurophysiology with special reference to the electroencephalogram." Epilepsia **50**: 30-38.

Ethan et al. (2013) “Median Nerve Block “ http://www.medscape.com Mar 7, 2013.

http://emedicine.medscape.com/article/1369028-overview [04.08.2014]